Severe slugging

in gas-liquid two-phase pipe flow

Severe slugging
in gas-liquid two-phase pipe flow

PROEFSCHRIFT

ter verkrijging van de graad van doctor
aan de Technische Universiteit Delft,
op gezag van de Rector Magnificus Prof. ir. K.C.A.M. Luyben,
voorzitter van het College voor Promoties,
in het openbaar te verdedigen
op maandag 15 oktober 2012 om 10.00 uur

door

Reza MALEKZADEH

Master of Science in Applied Earth Sciences
geboren te Ghaemshahr, Iran.

Dit proefschrift is goedgekeurd door de promotor:

Prof. dr. R.F. Mudde

Samenstelling promotiecommissie:

Rector Magnificus	voorzitter
Prof. dr. R.F. Mudde	Technische Universiteit Delft, promotor
Prof. dr. ir. R.A.W.M. Henkes	Technische Universiteit Delft
Prof. dr. B.J. Azzopardi	University of Nottingham, UK
Prof. dr. O.J. Nydal	Norwegian University of Science and Technology
Prof. dr. ir. J.D. Jansen	Technische Universiteit Delft
Prof. dr. ir. H.W.M. Hoeijmakers	Universiteit Twente
Prof. dr. ir. H.E.A. van den Akker	Technische Universiteit Delft
Prof. dr. ir. C.R. Kleijn	Technische Universiteit Delft, reservelid

Author email: rezamalekzadeh@gmail.com

Human beings are members of a whole,
In creation of one essence and soul.
If one member is afflicted with pain,
Other members uneasy will remain.
If you've no sympathy for human pain,
The name of human you cannot retain!§

Saadi Shirazi
The 13th century Persian poet

To my country, my pride
IRAN

---

§Translated by M. Aryanpoor.

Contents

Summary

Gas-liquid two-phase flow occurs in both onshore and offshore crude oil and natural gas production and transportation facilities. In an offshore oil and gas production facility, pipeline-riser systems are required to transport two-phase hydrocarbons from subsurface oil and gas wells to a central production platform. Severe slugs reaching several thousands pipe diameters may occur when transporting gas and liquid in these pipeline-riser systems.

Severe slugging creates potential problems in the platform facilities, e.g. separators, pumps, and compressors. Severe slugging may cause flooding and overpressurization of the separator, rupture of the pipe, and an increased back pressure at the wellhead. All of these might lead to the complete shutdown of the production facility. Therefore, the accurate predictions of severe slugging characteristics, e.g. slug length, oscillatory period, are essential for the proper design and operation of two-phase flow in the pipeline-riser systems.

Pipelines used for the transportation of hydrocarbons in an offshore production facility, are laid out over the seafloor. The uneven seafloor topography forms different pipeline-riser configurations.

In this dissertation, we described the severe slugging characteristics in a long downward inclined pipeline-riser system. We carried out experiments in a relatively long pipeline-riser configuration, and also performed numerical simulations using a one-dimensional two-fluid model. It was found experimentally, as also reproduced numerically, that transient slugs were generated in the pipeline upstream of the riser base. These transient slugs effectively contributed to the initial blockage of the riser base. Furthermore, an existing analytical model for the prediction of the flow behaviour in the pipeline-riser system was modified. The modified model, which was tested against our experimental results, showed a better performance than previously published models.

We developed a transient drift flux model to simulate the severe slugging characteristics in a pipeline-riser system. The model was tested against experimental

data and interestingly, could predict the occurrence of severe slugging in a horizontal pipeline-riser system, which is a subject of debate in the open literature. That motivated us to conduct experiments in a horizontal pipeline-riser configuration. It was observed that severe slugging can develop even in the horizontal pipeline-riser configuration. Moreover, a new class of severe slugging was found and referred to as dual-frequency severe slugging, which corresponds to dual-frequency pressure and flow rate fluctuations. It was found that dual-frequency severe slugging evolves when the pipeline length exceeds a certain threshold.

In this dissertation, we also described the severe slugging characteristics in a hilly-terrain pipeline-riser configuration. A hilly-terrain pipeline consists of interconnected horizontal, downhill, and uphill sections. It was observed that, the existence of a hilly-terrain unit in a pipeline-riser system induces a more severe type of slugging, which exhibits longer slugs than that of a horizontal pipeline-riser system.

So far we have summarized our work on the characteristics of severe slugging in a pipeline-riser system. In this dissertation, we also discuss the occurrence of severe slugging in an extended reach well. In response to meet the world energy demand, the oil and gas industry has also moved towards development of resources in scattered, isolated oil and gas pockets. Snake wells and fish-hook wells are extended reach wells, which have been used to develop these small hydrocarbon deposits more efficiently than conventional vertical or horizontal wells. The extended reach well resembles the pipeline-riser configuration. The flow conditions, e.g. pressure, and the pipe specifications, e.g. diameter, at the bottom of a well are generally different than the pipeline laid out over the seafloor. It is expected that severe slugging at the bottom of the well is less likely to occur.

In this dissertation, we performed numerical simulations to study the possible formation of severe slugging at the bottom of an extended reach well. It was found that severe slugs were initiated at the bottom of the extended reach well. This teaches one to study the well hydrodynamics more carefully when designing an extended reach well.

Samenvatting

Twee fase gas-vloeistof stromingen komen zowel op land als op zee voor bij de productie en het transport van ruwe olie en aardgas. Om gas en olie vanuit ondergrondse bronnen naar een platform op zee te transporteren, is een systeem nodig van pijpleiding, die leidt naar een vertical pijpleiding naar een platform (pipeline-risers). In een dergelijk pijp-systeem, kunnen deze twee-fase koolwaterstoffen severe slugs vormen, die zich over enkele duizenden pijpdiameters uitstrekken.

Deze slugs kunnen heuige schade toebrengen op het platform, die in het ergste geval leiden tot het sluiten van een platform. Zo kan de scheider onder een te hoge druk of waterstand uitkomen, kunnen pijpen scheuren, en kan ook de druk in de bron te hoog worden. Daarom is het belangrijk om de eigenschappen van deze slugs, zoals lengte en periode, nauwkeurig te kunnen voorspellen. Deze gegevens zijn van groot belang bij het ontwerp en de uitvoering van dergelijke pipeline-riser-systemen.

De pijpleiding die worden gebruikt bij het transport van olie en gas op zee, liggen direct op deze zeebodem. De vorm van de zeebodem is van belang voor het ontwerp van de pipeline-riser.

In dit proefschrift hebben wij de eigenschappen van severe slugs in een berg-afwaarts georiënteerde pipeline-riser systeem beschreven. Wij hebben experimenten uitgevoerd op een relatief lange pipeline-riser systeem. Daarnaast hebben we numerieke simulatie uitgevoerd met behulp van een een-dimensionaal twee-fase model. Met beide methoden vonden we dat tijdsafhankelijke slugs ontstonden voor de onderkant van de riser, waardoor deze bijdroeg aan het ontstaan van een verstopping aan de onderkant van de riser. Daarnaast is een bestaand analytisch model, die beschrijft hoe de stroming zich gedraag in het systeem, aangepast, zodat deze zich beter gedraagt ten opzichte van de experimentele resultaten dan in eerder gepubliceerd werk.

Voor de simulatie van deze severe slugs hebben wij een transient drift flux model ontwikkeld. Het is interessant om te constateren dat dit model de aanwe-

zigheid van slugs in een horizontaal pipeline-riser systeem kan voorspellen. Deze uitkomsten komen overeen met de experimentele gegevens en zijn in de literatuur nog een punt van discussie. Dit was de motivatie om deze experimenten uit te voeren. Belangrijker nog is de ontdekking van severe slugs die met twee verschillende frequenties voorkomen (dual-frequency severe slugging), hetgeen overeenkomt met de twee frequenties in druk en debiet fluctuaties. Deze dubbele frequentie komt voor vanaf een minimale lengte van de pijpleidingen.

In dit proefschrift hebben we tevens een beschrijving gegeven van de severe slugs in een pipeline-riser systeem dat op een heuvelachtige zeebodem ligt. Deze pijpleiding bestaat dan uit dalende, stijgende en horizontale pijpleiding. Hierbij is gevonden dat de slugs die in een dergelijk systeem voorkomen sterker en langer zijn dan in een pipeline-riser met een horizontal aanloop.

Behalve de beschrijving van de karakteristieken van een pipeline-riser, komen we in dit proefschrift ook terug op severe slugs in een bron met een groot bereik. Om te voldoen aan de wereldwijde vraag naar olie en gas, wordt er nu ook geboord naar afgelegen en versnipperde velden. Bronnen in de vorm van een slang of vishaak worden nu ook aangeboord, en door het grote bereik, zijn de traditionele horizontale en verticale boringen niet meer efficient. De bronnen met groot bereik vertonen gelijkenissen met de pipeline-riser systemen, maar the stroomcondities, zoals druk, en de pijpeigenschappen, zoals diameter, zijn in hun algemeenheid anders in de bron dan in de pijpleiding op de oceaanbodem. Daarom wordt aangenomen dat severe slugs in dergelijke bronnen minder vaak voorkomen.

In dit proefschrift hebben zijn numerieke simulaties uitgevoerd om de mogelijke vorming van severe slugs in een bron met groot bereik te bestuderen. Daarbij werd gevonden dat deze severe slugs ontstaan op de bodem van een dergelijke bron. Dit leert ons dat de hydrodynamica in de bron met groot bereik bij de aanboring van een bron met nauwkeurig moet worden bekeken.

Chapter 1

Introduction

1.1 Pipeline-riser systems

Increasingly, oil and gas are produced from offshore hydrocarbon fields. According to the latest estimate by the International Energy Agency, about a third of the world's oil production comes from offshore oil fields, and it is expected to increase to about one-half by 2015[1]. Pipeline-riser systems in an offshore oil and gas production facility are required to transport hydrocarbons (plus often also some water) from subsurface oil and gas wells to a central production platform[2,3]. Here, both liquid and gas flow simultaneously, creating a two-phase flow in these pipeline-riser systems. The diameter of the pipeline and the riser ranges from typically 0.1 to 0.8 m. The length of the pipeline can vary from a few kilometres (for liquid dominated systems) to more than hundred kilometres (for gas dominated systems). The height of the riser depends on the water depth, which can range from a few tens of metres (in lakes) to more than two kilometres (in deepwater areas).

1.2 Severe slugging

Even at constant inlet and outlet boundary conditions represented by gas and liquid mass flow rates and separator pressure, respectively, unsteady state flow may occur in such two-phase pipeline-riser systems operating at relatively low gas and liquid flow rates. The cyclic unsteady state flow characterized by large-amplitude, relatively long-period pressure and flow rate fluctuations has been referred to as severe slugging.

At relatively low flow rates, liquid accumulates at the bottom of the riser, creating a blockage for the gas, until sufficient upstream pressure has been built up to flush the liquid slug out of the riser. After this liquid surge, and subsequent

gas surge, part of the liquid in the riser falls back to the riser base to create a new blockage and the cycle repeats. This transient cyclic phenomenon causes periods of no liquid and gas production at the riser top (production starvation) followed by very high liquid and gas surges, and is called severe slugging[4,5]. Fig. 1.1 illustrates different stages of a cycle of severe slugging. These stages are explained in more detail in Chapter 5.
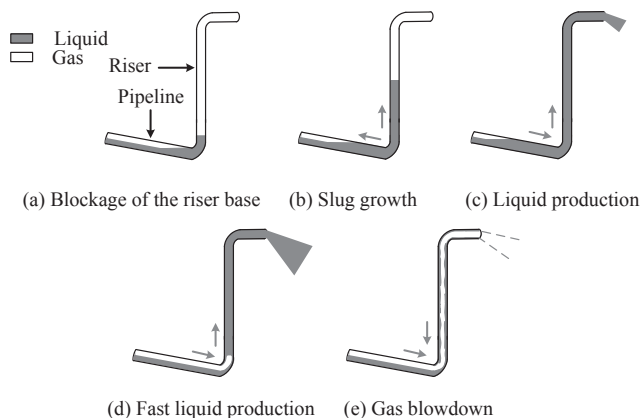
Figure 1.1: *Stages for severe slugging.*

Severe slugging creates potential problems in the platform facilities downstream of the riser top, which have been designed to operate under steady state conditions, e.g. separators, pumps, and compressors. For instance, the peak flow rates during the liquid and gas surges might cause flooding and overpressurization of the separator, which consequently might lead to the complete shutdown of a production facility[6]. Moreover, an increased back pressure at the wellhead may lead to the end of the production and abandonment of the well[7]. Furthermore, it can create violent impacts, with the flow with the velocity of the gas but with the density of the liquid passing especially through barriers such as orifices, partially closed valves and bends. These repeating impacts provoke a faster mechanical fatigue and can eventually lead to a rupture[8]. Therefore, the accurate prediction of severe slugging characteristics is essential for the proper design and operation of two-phase flow in these systems[9–12].

1.3   Extended reach wellbore

Total world energy consumption grows by 53 percent from 2008 to 2035, and oil and gas are expected to continue supplying much of the energy used worldwide

(about 50 percent in 2035)[13]. Conventional supplies of easily accessible oil and natural gas, the so-called "easy oil", will not meet this rising demand[14]. In response to meet the world energy demand, the oil and gas industry has also moved towards development of resources in scattered, isolated hydrocarbon pockets. As these deposits are small, it is not economically feasible to exploit them in a conventional way.

Snake wells and fish-hook wells are relatively new technologies and have been used to develop these hydrocarbon deposits more efficiently than conventional wells. Snake wells are laterally weaving ("snaking") extended reach near horizontal wells that penetrate a number of different reservoir pockets[15,16]. Fish-hook wells are extended reach wells that penetrate the deepest reservoir pockets first and the shallowest ones at the end of the wells[17]. A schematic of a fish-hook well is given in Fig. 1.2.
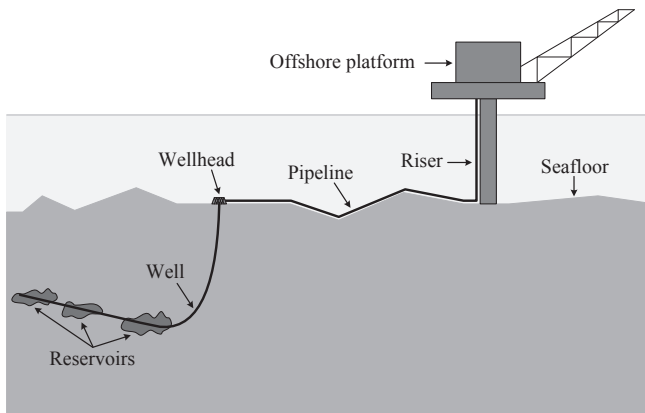
Figure 1.2: *Schematic of a fish-hook well connected to a pipeline-riser system in an offshore production facility.*

These extended reach wells resemble pipeline-riser configurations mentioned in the previous sections. Therefore, transient conditions of flow are expected, which consequently can play an important role in the well performance. Effective use of these technologies requires us to better understand the transient two-phase flow behaviour in extended reach wells.

1.4   Scientific questions

1.4.1   Bottom hole conditions

Yocum[18] observed that severe slugging in a pipeline-riser system could be eliminated by increasing the backpressure at the riser top or by reducing the pipeline

diameter upstream of the riser base. These findings were confirmed by various researchers, including Schmidt et al. [19], Taitel [20], and Jansen et al. [4].

The diameter of the tubing at the bottom of a wellbore is generally smaller than the diameter of a pipeline laid out over the seafloor. Furthermore, the average pressure at the bottom of a wellbore is higher than the average pressure of the surface pipeline. Thus, the severe slugging phenomenon at the bottom of a wellbore is expected to be less pronounced.

In this dissertation, we address the question *Considering the above-mentioned issues, could severe slugging happen in an extended reach wellbore?* We resolve this question by performing numerical simulations for the two-phase flow of oil and gas in an extended reach wellbore as well as experiments in a relatively large air-water two-phase flow facility.

1.4.2   Pipeline orientation

Severe slugging in a downward inclined pipeline-riser system (a pipe downward inclined by a few degrees from the horizontal connected to a vertical riser) had been studied both experimentally and numerically by several investigators [4,19–23], and among them, the laboratory experiments were conducted for relatively short pipeline-riser systems. The pipeline length was limited to a maximum of 57.4 m and the riser height has a maximum of 15 m. As mentioned in Section 1.1, in a real offshore pipeline-riser system the length of the near horizontal part will be much longer.

One of the questions we address in this dissertation is *What are the severe slugging characteristics in a long pipeline-riser system?* and associated with that *To what extend can they be reproduced by a numerical model?*

Moreover, the occurrence of severe slugging in a horizontal pipeline-riser system (a horizontal pipeline followed by a vertical riser) is a subject of debate in the open literature. So far only Fabre et al. [24] observed severe slugging in a relatively short horizontal pipeline-riser system. Their observed experimental data could not be reproduced by the numerical models developed by various researchers, including Sarica and Shoham [25], from which these authors concluded that the horizontal pipeline in the experiments by Fabre et al. [24] might have actually been slightly downward inclined. Furthermore, Fabre et al. [24] did not describe and analyze the process of severe slugging for the horizontal pipeline-riser configuration.

A second question we address is *Does severe slugging occur in a horizontal pipeline-riser configuration?* and associated with that *What are the characteristics of severe slugging in this system?* and *Does a numerical model reproduce them?*

The pipelines used for the transportation of oil and gas from the subsurface wellheads and through the vertical risers to a central production platform, are laid out over the seafloor. The uneven seafloor topography results in hilly-terrain

pipeline-riser systems. A hilly-terrain pipeline consists of interconnected horizontal, downhill, and uphill sections[26]. Despite all the research that has been done and published, there is still a lack of understanding of how flow characteristics change in a hilly-terrain pipeline-riser system. Because of the importance of flow oscillations in practical applications, the flow behaviour needs to be known for a hilly-terrain pipeline-riser configuration, as well.

A third question we address is *What are the characteristics of severe slugging in a hilly-terrain pipeline-riser system?* and associated with that *Do they differ from that of a downward inclined or a horizontal pipeline-riser system?*

We resolve these questions by conducting experiments for the two-phase flow of air and water in a relatively large flow facility and also by performing numerical simulations. Of course, the fundamental understanding of flow behaviour in a long downward inclined, horizontal, and a hilly-terrain pipeline-riser configuration is also relevant to the efficient design of an extended reach wellbore.

1.5   Outline

This dissertation is divided into two main parts. The first part, i.e. Chapters 1 - 4, is mainly aimed at providing the reader the necessary information required to better understand the second part of the dissertation. Chapter 2 gives an overview of the basic concepts of two-phase flow in pipes. The flow pattern delineation procedure and the calculation of the two-phase flow variables, e.g. liquid holdup and pressure drop, are also described. In Chapter 3, the physical and numerical background of the one-dimensional two-fluid model, in particular the OLGA flow model, is presented. Chapter 4 gives an overview of the modelling techniques for coupling of a wellbore flow model to a reservoir flow model.

The second part, i.e. Chapters 5 - 10, comprises a collection of papers produced during this Ph.D. study. Therefore, these chapters are self-contained, and are closely related to the research questions raised in this chapter.

Chapter 2

Two-phase-flow concepts

The purpose of this chapter is to explain briefly the concepts of two-phase flow and the relevant terms that will be referred to frequently in this dissertation. First the criteria that are used to delineate a specific flow pattern are discussed. Then estimation of the in-situ liquid volume fraction, i.e. liquid holdup, and the pressure drop for the predicted flow pattern is presented.

2.1   Introduction

Gas-liquid two-phase flows encountered in various industrial fields. Examples are the petroleum, chemical and process, nuclear reactor, geothermal energy, and space industries[27]. Two-phase flow occurs in the petroleum industry during the production and transportation of oil and gas in both the wellbore and the pipeline. The reservoir influx into the wellbore, may contain all three separate phases (gas, oil and water). However, gas often enters the wellbore in solution with oil and comes out as a separate phase when oil moves up enough along the wellbore for the pressure to drop below the bubble point pressure. Both cases leading to gas-liquid two-phase flow in the wellbore and subsequently in the pipeline[28,29].

This two-phase flow of gas and liquid can take many configurations or patterns. The term flow patten or flow regime refers to the geometrical distribution of the gas and the liquid phases in a pipe. The existing flow pattern in a given two-phase flow system depends on the relative magnitudes of the forces that act on the fluids, e.g. buoyancy, turbulence, inertia, and surface tension. These forces vary significantly with flow rates, pipe diameter, inclination angle, and fluid properties of the phases. The latter change as a result of large pressure and temperature variations the fluids encounter. Therefore, several different flow patterns can exist in a given wellbore or pipeline[30].

Empirical models for two-phase flow calculations can give inaccurate results,

when applied to situations different from the database from which they are derived[29]. Mechanistic models, on the other hand, are based on mathematical formulations consistent with the observed physical phenomena and thus can predict two-phase flow behaviour more accurately. Most mechanistic models presented in the open literature are for an isolated mechanism, such as film thickness, bubble rise velocity, or flow-pattern delineation[31,32]. Ansari et al.[33] developed a comprehensive mechanistic model for upward, vertical two-phase flow. Xiao et al.[34] also presented a comprehensive mechanistic model for gas-liquid two-phase flow in horizontal and near horizontal pipelines. These comprehensive mechanistic models are able first to delineate the existing flow pattern, and then to predict the flow characteristics, such as liquid holdup and pressure drop. However, they are applicable to only some pipe inclinations. Hasan and Kabir[35–37] presented a comprehensive mechanistic model to predict two-phase-flow behaviour in wellbores. Petalas and Aziz[38] also developed a comprehensive mechanistic model which is applicable to all pipe inclinations. A brief overview of this model is given in this chapter. Like other comprehensive mechanistic models, it requires determining the existing flow pattern beforehand. Its approach to predict the flow pattern is to examine each pattern transition based on developed criteria valid for that specific transition.

The mechanistic models are widely used in transient two-phase flow simulators, e.g. see Chapter 3, and also in the two-phase flow calculations, e.g. see Chapter 7.

2.2   Two-phase flow in pipes

Fig. 2.1 shows the flow patterns existing in horizontal and near-horizontal pipes. These flow patterns are dispersed bubble flow, stratified flow (smooth and wavy), annular-mist flow, slug flow, and elongated bubble flow. Dispersed bubble flow

Direction of flow ⟶
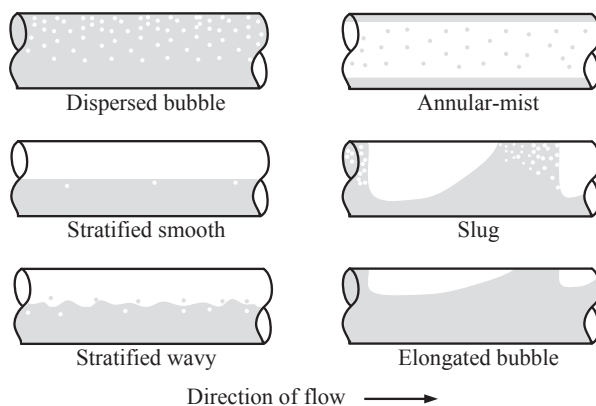
Figure 2.1: *Flow patterns in horizontal pipes.*

occurs at very high liquid flow rates. The liquid phase is the continuous phase
and the gas phase is dispersed as discrete bubbles. Stratified flow occurs at
relatively low flow rates. Liquid flows through the bottom portion of the pipe
and gas flows at the top. At somewhat higher gas flow rates, the two phases
are still stratified but the interface becomes wavy. The former flow pattern is
called stratified smooth, whereas the latter flow pattern is referred to as stratified
wavy. Annular-mist flow occurs at higher gas flow rates. Here, the gas phase flows
through the centre of the pipe, which may contain entrained liquid droplets. The
liquid flows as a thin film through the annulus formed by the pipe wall and the
gas core. At relatively high flow rates, the slug flow regime occurs and exhibits
a series of liquid slugs separated by gas pockets. The liquid slugs often contain
smaller entrained gas bubbles. Elongated bubble flow is considered the limiting
case of slug flow, when the liquid slug is free of entrained gas bubbles.

Fig. 2.2 shows the flow patterns existing in vertical and sharply inclined pipes.
These flow patterns are dispersed bubble flow, annular-mist flow, bubble flow,
slug flow, and churn flow. Bubble flow occurs at relatively low liquid flow rates.
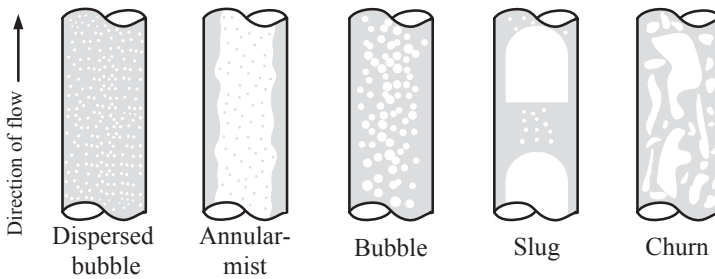
Figure 2.2: *Flow patterns in vertical pipes.*

The liquid phase is the continuous phase and the gas phase is dispersed as discrete
bubbles, moving upward in a zigzag motion. Slug flow in vertical pipe is symmet-
ric around the pipe axis. The gas pockets become relatively large bullet-shape
bubbles known as Taylor bubbles. Churn flow occurs at higher gas flow rates, and
is characterized by a chaotic flow of gas and liquid in which the shape of both the
gas pockets and the liquid slugs are distorted.

2.3   Flow-pattern delineation

The procedure for flow-pattern delineation is as follows. A particular flow pattern
is assumed, and its stability under various criteria is examined. If the flow pattern
turns out to be unstable, a new flow pattern is assumed and the procedure is
repeated. This procedure continues until a stable flow pattern is reached. The
flow patterns are examined in the following order: dispersed bubble flow, stratified
flow, annular-mist flow, bubble flow and intermittent flow.

2.3.1   Dispersed bubble flow

The dispersed bubble flow region in the flow pattern map is bounded by two criteria. The first criterion is based on the transition to slug flow proposed by Barnea [39]. A transition from intermittent flow occurs when the liquid volume fraction in the slug, V_{Ls} (-), is less than the value associated with the maximum volumetric packing density of the dispersed gas bubbles (0.52):

$$V_{Ls} < (1 - 0.52) \quad \text{or} \quad V_{Ls} < 0.48. \tag{2.1}$$

The liquid volume fraction in the slug is obtained from the correlation proposed by Gregory et al. [40], which is given by:

$$V_{Ls} = \frac{1}{1 + (v_{\text{mix}}/8.66)^{1.39}}, \tag{2.2}$$

where $v_{\text{mix}} = v_{sg} + v_{sL}$ is the mixture velocity (ms^{-1}), and v_{sg} and v_{sL} denote superficial gas and liquid velocity, respectively (ms^{-1}).

A transition from dispersed bubble flow to churn flow can also occur when the maximum volumetric packing density of the dispersed gas bubbles is exceeded [38]:

$$C_G = \frac{v_{sg}}{v_{\text{mix}}} > 0.52. \tag{2.3}$$

If the criteria given by Eq. 2.1 and Eq. 2.3 are satisfied, i.e. $V_{Ls} < 0.48$ & $C_G \leq 0.52$, dispersed bubble flow exists. Otherwise, the stability of stratified flow is examined next.

2.3.2   Stratified flow

A sketch of the equilibrium-stratified-flow geometry is given in Fig. 2.3. Here, θ denotes the inclination angle from the horizontal (rad). d is the pipe internal diameter (m). v_g and v_L are the gas and liquid average velocities, respectively (ms^{-1}). A_g, S_g, A_L, and S_L represent the area for flow (m^2) and the wetted perimeter (m) of the gas and the liquid phases, respectively. S_i is the interface length (m), and h_L denotes the liquid height (m). Examining the stability of the stratified flow requires the determination of the equilibrium liquid height in the pipe (h_L), which can be obtained by applying momentum balances on the gas and the liquid phases [32].

The momentum balance equations for the gas and the liquid phases are given, respectively, by:

$$-A_L \left(\frac{dp}{dL} \right) - \tau_{wL} S_L + \tau_i S_i - \rho_L A_L g \sin\theta = 0, \tag{2.4}$$

and

$$-A_g \left(\frac{dp}{dL} \right) - \tau_{wg} S_g - \tau_i S_i - \rho_g A_g g \sin\theta = 0, \tag{2.5}$$
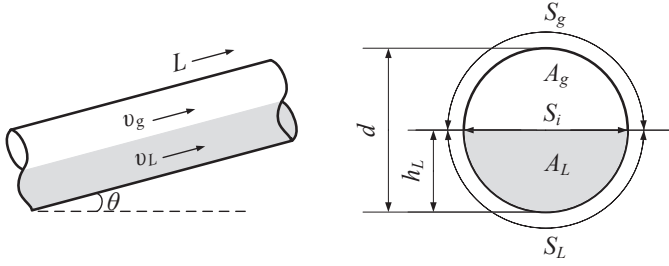
Figure 2.3: *Stratified flow representation.*

where, dp/dL denotes the pressure gradient (Nm^{-3}). ρ_L and ρ_g are the liquid and gas densities, respectively (kgm^{-3}). g is the gravitational acceleration (ms^{-2}). τ_{wL} and τ_{wg} represent the shear stress of the liquid and the gas phases at the wall, respectively, and τ_i represents the shear stress at the interface (Nm^{-2}). Eq. 2.4 and Eq. 2.5 can be combined to eliminate the pressure gradient terms as shown below[32]:

$$\tau_{wg}\frac{S_g}{A_g} - \tau_{wL}\frac{S_L}{A_L} + \tau_i S_i \left(\frac{1}{A_L} + \frac{1}{A_g}\right) - (\rho_L - \rho_g)\, g \,\sin\theta = 0. \qquad (2.6)$$

Eq. 2.6 is an implicit equation for h_L, and can be expressed in terms of the dimensionless liquid height, $\tilde{h}_L = h_L/d$, using the geometric relationships outlined by Taitel and Dukler [32]. The geometric relationships are given by the following equations:

$$
\begin{aligned}
A_L &= 0.25d^2 \left[\pi - \cos^{-1}\left(2\tilde{h}_L - 1\right) + \left(2\tilde{h}_L - 1\right)\sqrt{1 - \left(2\tilde{h}_L - 1\right)^2}\right], \\
A_g &= 0.25d^2 \left[\cos^{-1}\left(2\tilde{h}_L - 1\right) - \left(2\tilde{h}_L - 1\right)\sqrt{1 - \left(2\tilde{h}_L - 1\right)^2}\right], \\
S_L &= d\left[\pi - \cos^{-1}\left(2\tilde{h}_L - 1\right)\right], \\
S_g &= d\cos^{-1}\left(2\tilde{h}_L - 1\right), \\
S_i &= d\sqrt{1 - \left(2\tilde{h}_L - 1\right)^2}.
\end{aligned}
\qquad (2.7)
$$

The shear stresses are given by the following equations[38]:

$$\tau_{wg} = \frac{\lambda_g \rho_g \upsilon_g^2}{2}, \qquad (2.8)$$

$$\tau_{wL} = \frac{\lambda_L \rho_L \upsilon_L^2}{2}, \qquad (2.9)$$

$$\tau_{wi} = \frac{\lambda_i \rho_g \left(v_g - v_L\right) \left| \left(v_g - v_L\right) \right|}{2}. \tag{2.10}$$

The friction factor at the gas/wall interface, λ_g, in Eq. 2.8 is obtained from standard methods[41] using the pipe roughness and the following definition of Reynolds number[38]:

$$\text{Re}_g = \frac{d_g \rho_g v_g}{\mu_g}, \tag{2.11}$$

where $d_g = 4A_g/(S_g + S_i)$ is the hydraulic diameter of the gas phase (m), and μ_g denotes the viscosity of the gas phase (Pas). The friction factor at the liquid/wall interface, λ_L, in Eq. 2.9 is determined from the following empirical relationship[38]:

$$\lambda_L = 0.452 \lambda_{sL}^{0.731}, \tag{2.12}$$

where the friction factor based on superficial liquid velocity, λ_{sL}, is obtained from standard methods[41] using the pipe roughness and the following definition of Reynolds number[38]:

$$\text{Re}_{sL} = \frac{d \rho_L v_{sL}}{\mu_L}, \tag{2.13}$$

where μ_L denotes the viscosity of the liquid phase (Pas). The interfacial friction factor, λ_i, in Eq. 2.10 is calculated from the following empirical relationship[38]:

$$\lambda_i = \left(0.004 + 0.5 \times 10^{-6} \text{Re}_{sL}\right) \text{Fr}_L^{1.335} \left[\frac{\rho_L d_g}{\rho_g v_g^2}\right], \tag{2.14}$$

where the Froude number is defined as $\text{Fr}_L = v_L/\sqrt{gh_L}$.

Having determined the liquid height, it is now possible to examine the stability of the stratified flow. A transition from stratified flow occurs when the gas velocity is just sufficient to create large enough waves on the liquid surface for bridging the pipe[32]:

$$v_g = \left(1 - \frac{h_L}{d}\right) \left[\frac{\left(\rho_L - \rho_g\right) g A_g \cos\theta}{\rho_g \ dA_L/dh_L}\right]^{0.5}. \tag{2.15}$$

At steep downward inclination, a transition from stratified flow to annular flow can occur even at relatively low gas velocity. The following criterion is proposed by Barnea[39] for this type of transition:

$$v_L > \left[\frac{g\left(d - h_L\right) \ \cos\theta}{\lambda_L}\right]^{0.5}, \tag{2.16}$$

where λ_L is calculated from Eq. 2.12. It is assumed that stratified flow is limited to horizontal and downward inclinations only.

If $\theta \leq 0$, and the criteria given by Eq. 2.15 and Eq. 2.16 are satisfied, i.e. the gas velocity is less than the transitional value given by Eq. 2.15 & the liquid velocity is less than the value given by Eq. 2.16, stratified flow exists. Otherwise, the stability of annular-mist flow is examined next.

It should be mentioned that in the model proposed by Petalas and Aziz [38] no distinction is made between stratified smooth and stratified wavy flow for the purpose of determining liquid holdup and pressure drop. Therefor, the transition between these two flow regimes is not discussed here.

2.3.3 Annular-mist flow

Examining the stability of annular-mist flow is based on the work of Taitel and Dukler [32] and Oliemans et al. [42], which is similar to the approach used for stratified flow. A schematic of annular-mist flow is given in Fig. 2.4.
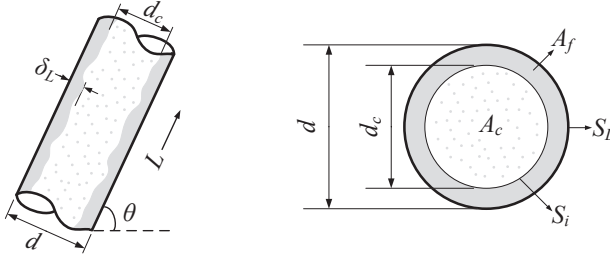
Figure 2.4: *Annular-mist flow representation.*

The momentum balance equations for the liquid film and the gas core with liquid droplets are given, respectively, by:

$$-A_f \left(\frac{dp}{dL} \right) - \tau_{wL} S_L + \tau_i S_i - \rho_L A_f g \, \sin\theta = 0, \qquad (2.17)$$

and

$$-A_c \left(\frac{dp}{dL} \right) - \tau_i S_i - \rho_c A_c g \, \sin\theta = 0, \qquad (2.18)$$

where, A_f and A_c denote the area for flow of the liquid film and the core, respectively (m^2). ρ_c represents the core density (kgm^{-3}). For fully developed flow, the pressure gradient in the film and core are equal. Thus, Eq. 2.17 and Eq. 2.18 can be combined to eliminate the pressure gradient terms as shown below [42]:

$$-\tau_{wL} \frac{S_L}{A_f} + \tau_i S_i \left(\frac{1}{A_f} + \frac{1}{A_c} \right) - (\rho_L - \rho_c) g \, \sin\theta = 0. \qquad (2.19)$$

Eq. 2.19 can be expressed in terms of the dimensionless liquid film thickness, $\tilde{\delta}_L = \delta_L/d$, and the liquid fraction entrained, FE, using geometric relationships. The geometric relationships are given by the following equations [42]:

$$A_f \quad = \quad \pi \delta_L \left(d - \delta_L \right),$$

$$
\begin{aligned}
A_c &= \frac{\pi\left(d - 2\delta_L\right)^2}{4}, \\
S_L &= \pi d, \\
S_i &= \pi\left(d - 2\delta_L\right).
\end{aligned}
\tag{2.20}
$$

The shear stresses are given by the following equations[42]:

$$
\tau_{wL} = \frac{\lambda_f \rho_L \upsilon_f^2}{2},
\tag{2.21}
$$

$$
\tau_i = \frac{\lambda_i \rho_c \left(\upsilon_c - \upsilon_f\right)\left|\left(\upsilon_c - \upsilon_f\right)\right|}{2},
\tag{2.22}
$$

where, υ_f and υ_c are the liquid film and core velocities, respectively (ms^{-1}). The friction factor for the liquid film, λ_f, in Eq. 2.21 is obtained from standard methods[41] using the pipe roughness and the following definition of the film Reynolds number[42]:

$$
\mathrm{Re}_f = \frac{d_f \rho_L \upsilon_f}{\mu_L},
\tag{2.23}
$$

where $d_f = 4\delta_L(d - \delta_L)/d$ is the hydraulic diameter of the liquid film (m). The interfacial friction factor, λ_i, and the liquid fraction entrained, FE, are calculated from the following empirical relationships, respectively[42]:

$$
\frac{\lambda_i}{\lambda_c} = 0.24 \left(\frac{\sigma}{\rho_c \upsilon_c^2 d_c}\right)^{0.085} \mathrm{Re}_f^{0.305},
\tag{2.24}
$$

and

$$
\frac{FE}{1 - FE} = 0.735 N_B^{0.074} \left(\frac{\upsilon_{sg}}{\upsilon_{sL}}\right)^{0.2},
\tag{2.25}
$$

where the dimensionless number, N_B, is defined as[42]:

$$
N_B = \frac{\mu_L^2 \upsilon_{sg}^2 \rho_g}{\sigma^2 \rho_L}.
\tag{2.26}
$$

Once the liquid film thickness is calculated, the stability of the annular-mist flow can be examined. Barnea[39] proposed two mechanisms for the transition from annular flow. The first mechanism is based on the observation that the minimum interfacial shear stress is associated with a change in the direction of the velocity profile in the liquid film. When the velocity profile in the liquid film becomes negative, liquid accumulation cause blockage of the core and the transition to intermittent flow occurs. The minimum shear stress condition is obtained from:

$$
2\lambda_f \frac{\rho_L}{\rho_L - \rho_c} \frac{\upsilon_{sg}^2 \left(1 - FE\right)^2}{gd\,\sin\theta} - \frac{V_f^3 \left(1 - \frac{3}{2}V_f\right)}{2 - \frac{3}{2}V_f} = 0,
\tag{2.27}
$$

where, the liquid fraction in the film, V_f, is:

$$V_f = \frac{A_f}{A} = 4\tilde{\delta}_L \left(1 - \tilde{\delta}_L\right). \tag{2.28}$$

Eq. 2.27 can be solved by applying an iterative scheme to calculate the film thickness at which the minimum shear stress occurs, $\tilde{\delta}_{L,\min}$. The second mechanism occurs at relatively high liquid flow rate, when the liquid film is thick enough to supply sufficient liquid for wave growth. The resulting waves may cause blockage of the gas core by bridging the pipe cross-sectional area. This happens when the in-situ liquid volume fraction exceeds 50% of the value associated with the maximum volumetric packing density of gas bubbles (0.52):

$$V_L \geq \frac{1}{2}\left(1 - 0.52\right) \quad \text{or} \quad V_L \geq 0.24. \tag{2.29}$$

If the criteria given by Eq. 2.27 and Eq. 2.29 are satisfied, i.e. $\tilde{\delta}_L < \tilde{\delta}_{L,\min}$ & $V_L \leq 0.24$, annular-mist flow exists. Otherwise, the stability of bubble flow is examined next.

2.3.4   Bubble flow

Bubble flow is encountered in vertical and steeply inclined pipes. It can exist if the following conditions are satisfied. First, the Taylor bubble velocity exceeds the bubble velocity. This may happen when the pipe diameter is large enough[43]:

$$d > 19 \left[\frac{(\rho_L - \rho_g)\sigma}{\rho_L^2 g}\right]^{0.5}. \tag{2.30}$$

Second, the migration of bubbles to the top wall of the pipe is prevented. This may happen when the inclination angle is large enough[39]:

$$\cos\theta \leq \frac{3}{4\sqrt{2}}v_b^2 \left(\frac{C_l\gamma^2}{gd_b}\right), \tag{2.31}$$

where $C_l = 0.8$ denotes the lift coefficient, $\gamma = 1.3$ represents the bubble distortion coefficient, and $d_b = 0.007$ (m) is the recommended bubble diameter. v_b denotes the bubble rise velocity in a stagnant liquid (m), and is given by[44]:

$$v_b = 1.41 \left[\frac{g\left(\rho_L - \rho_g\right)\sigma}{\rho_L^2}\right]^{0.25} \sin\theta. \tag{2.32}$$

Third, a transition from intermittent flow to bubble flow occurs when the liquid volume fraction calculated for slug flow, V_L, becomes higher than the critical value of 0.75 (see Taitel et al. [43]).

If the above mentioned criteria are satisfied, i.e. the pipe diameter is greater than the value obtained by Eq. 2.30 & $\cos\theta$ is less than or equal to the value given by Eq. 2.31 & $V_L > 0.75$, bubble flow exists. Otherwise, the stability of intermittent flow is examined next.

2.3.5   Intermittent flow

The slug and elongated bubble flow patterns can be classified as the intermittent flow pattern. A transition from intermittent flow occurs when sufficient liquid is not available for slug formation[38]:

$$V_L \leq 0.24. \tag{2.33}$$

The liquid volume fraction during intermittent flow can be obtained from[45]:

$$V_L = \frac{V_{Ls} v_t + v_{db} (1 - V_{Ls}) - v_{sg}}{v_t}, \tag{2.34}$$

where, the liquid volume fraction in the slug, V_{Ls}, is obtained from Eq. 2.2. v_t denotes the translational velocity of the slug, and v_{db} is the velocity of the dispersed bubbles. The translational velocity of the slug is calculated from[46]:

$$v_t = C_0 v_{\mathrm{mix}} + v_d, \tag{2.35}$$

where, C_0 is a distribution coefficient related to the velocity and concentration profiles and is determined from the following empirical correlation[38]:

$$C_0 = (1.64 + 0.12 \sin\theta) \left[\frac{\rho_L v_{\mathrm{mix}} d}{\mu_L} \right]^{-0.031}. \tag{2.36}$$

The drift velocity, v_d, in Eq. 2.35 can be obtained from[47]:

$$v_d = \min\left(0.316 \sqrt{\frac{\rho_L v_{d_\infty} d}{2\mu_L}}, 1 \right) \times v_{d_\infty}, \tag{2.37}$$

where, v_{d_∞} is given by[46]:

$$v_{d_\infty} = v_{dh_\infty} \cos\theta + v_{dv_\infty} \sin\theta. \tag{2.38}$$

v_{dh_∞} in Eq. 2.38 is given by[48]:

$$v_{dh_\infty} = \left(0.54 - \frac{1.76}{\mathrm{Bo}^{0.56}} \right) \left[\frac{gd (\rho_L - \rho_g)}{\rho_L} \right]^{0.5}, \tag{2.39}$$

where, the Bond number is obtained from:

$$\mathrm{Bo} = \frac{(\rho_L - \rho_g) gd^2}{\sigma}. \tag{2.40}$$

v_{dv_∞} in Eq. 2.38 is obtained from a modified form of the Wallis[49] correlation:

$$v_{dv_\infty} = 0.345 \left(1 - e^{-\beta} \right) \left[\frac{gd (\rho_L - \rho_g)}{\rho_L} \right]^{0.5}, \tag{2.41}$$

where, the coefficient, β, is:

$$\beta = \text{Bo} \times e^{\left[3.278 - 1.424 \ln(\text{Bo})\right]}. \tag{2.42}$$

The velocity of the dispersed bubbles, v_{db}, in Eq. 2.34 is obtained from[45]:

$$v_{db} = C_0 v_{\text{mix}} + v_b, \tag{2.43}$$

where, C_0 is calculated from Eq. 2.36 and the riser velocity of the dispersed bubbles, v_b, is determined from[50]:

$$v_b = 1.53 \left[\frac{g\left(\rho_L - \rho_g\right)\sigma}{\rho_L^2}\right]^{0.25} \sin\theta. \tag{2.44}$$

If the criterion given by Eq. 2.33 is satisfied, i.e. $V_L > 0.24$, intermittent flow exists. When none of the transition criteria mentioned above are satisfied, the flow pattern is referred to as churn flow. This flow pattern represents a transition zone between dispersed bubble flow and annular-mist flow and between intermittent flow and annular-mist flow.

2.4　Calculation of holdup and pressure drop

Following the flow-pattern delineation, the in-situ volume fractions and the pressure drop can be calculated as described below.

2.4.1　Dispersed bubble flow

The in-situ liquid volume fraction, i.e. liquid holdup, in dispersed bubble flow is calculated by following the procedure described in Section 2.3.5 for the dispersed bubbles in the liquid slug[38].

$$v_{db} = C_0 v_{\text{mix}} + v_b, \tag{2.45}$$

where, C_0 is calculated from Eq. 2.36, and v_b is determined from Eq. 2.44. The liquid holdup is obtained from[38]:

$$V_L = 1 - \frac{v_{sg}}{v_{db}}. \tag{2.46}$$

If $v_{db} \leq 0$, the liquid holdup is then obtained from[38]:

$$V_L = 1 - \frac{v_{sg}}{C_0 v_{\text{mix}}}. \tag{2.47}$$

Following the liquid holdup calculation, the pressure gradient is obtained from[38]:

$$-\left(\frac{dp}{dL}\right) = \frac{2\lambda_{\text{mix}}\rho_{\text{mix}}v_{\text{mix}}^2}{d} + \rho_{\text{mix}}g\,\sin\theta, \tag{2.48}$$

where, λ_{mix} is obtained from standard methods[41] using the pipe roughness and the following definition of the Reynolds number[38]:

$$\mathrm{Re}_{\mathrm{mix}} = \frac{d\rho_{\mathrm{mix}} v_{\mathrm{mix}}}{\mu_{\mathrm{mix}}}. \tag{2.49}$$

The mixture density and viscosity in Eq. 2.49 are obtained from[38]:

$$\rho_{\mathrm{mix}} = V_L \rho_L + (1 - V_L) \rho_g, \tag{2.50}$$

and

$$\mu_{\mathrm{mix}} = V_L \mu_L + (1 - V_L) \mu_g. \tag{2.51}$$

2.4.2   Stratified flow

The liquid holdup in stratified flow is obtained from[38]:

$$V_L = \frac{A_L}{A}. \tag{2.52}$$

The pressure gradient is calculated from either Eq. 2.4 or Eq. 2.5.

2.4.3   Annular-mist flow

The liquid holdup in annular-mist flow is determined from[38]:

$$V_L = 1 - \left(1 - 2\tilde{\delta}_L\right)^2 \frac{v_{sg}}{v_{sg} + FE v_{sL}}. \tag{2.53}$$

The pressure gradient is calculated from either Eq. 2.17 or Eq. 2.18.

2.4.4   Bubble flow

The in-situ gas volume fraction, $V_g = 1 - V_L$, in bubble flow is obtained from[38]:

$$V_g = \frac{v_{sg}}{v_t}, \tag{2.54}$$

where, v_t denotes the translational bubble velocity (ms^{-1}), and is defined as[51]:

$$v_t = C_0 v_{\mathrm{mix}} + v_b, \tag{2.55}$$

where, C_0 is taken as 1.2, and v_b is determined from Eq. 2.32. The value of V_g is limited to the following range[38]:

$$0 \le V_g \le \frac{v_{sg}}{v_{\mathrm{mix}}}. \tag{2.56}$$

The pressure gradient is calculated from[38]:

$$-\left(\frac{dp}{dL}\right) = \frac{2\lambda_{\mathrm{mix}L}\rho_{\mathrm{mix}}v_{\mathrm{mix}}^2}{d} + \rho_{\mathrm{mix}}g\ \sin\theta, \tag{2.57}$$

where, $\lambda_{\mathrm{mix}L}$ is obtained from standard methods[41] using the pipe roughness and the following definition of the Reynolds number[38]:

$$\mathrm{Re}_{\mathrm{mix}L} = \frac{d\rho_L v_{\mathrm{mix}}}{\mu_L}. \tag{2.58}$$

2.4.5   Intermittent flow

The liquid holdup in intermittent flow is calculated from Eq. 2.34. The pressure gradient is estimated from[38]:

$$-\left(\frac{dp}{dL}\right) = \rho_{\mathrm{mix}}g\ \sin\theta + \eta\left(\frac{dp}{dL}\right)_{fr_{SL}} + (1-\eta)\left(\frac{dp}{dL}\right)_{fr_{AM}}. \tag{2.59}$$

Here, η is an empirically determined weighting factor and is given by[38]:

$$\eta = \left[\frac{v_{sL}}{v_{\mathrm{mix}}}\right]^{(0.75-V_L)}, \tag{2.60}$$

with the condition that $\eta \le 1$. In Eq. 2.59, the frictional pressure gradient for the slug portion, $\left(\frac{dp}{dL}\right)_{fr_{SL}}$, is determined from[38]:

$$\left(\frac{dp}{dL}\right)_{fr_{SL}} = \frac{2\lambda_{\mathrm{mix}L}\rho_{\mathrm{mix}}v_{\mathrm{mix}}^2}{d}, \tag{2.61}$$

where, the friction factor, $\lambda_{\mathrm{mix}L}$, is obtained from standard methods[41] using the pipe roughness and the Reynolds number given by Eq. 2.58. The frictional pressure gradient calculated for annular-mist flow, $\left(\frac{dp}{dL}\right)_{fr_{AM}}$, is determined from[38]:

$$\left(\frac{dp}{dL}\right)_{fr_{AM}} = \frac{4\tau_{wL}}{d}, \tag{2.62}$$

where, the shear stress, τ_{wL}, is obtained from Eq. 2.21.

Churn flow represents a transition zone between dispersed bubble flow and annular-mist flow and between intermittent flow and annular-mist flow. An interpolation between the appropriate boundary regimes is made to determine the liquid holdup and pressure drop values in churn flow.

Chapter 3

The OLGA model

In this chapter the physical background of the OLGA model is discussed based on documents published in the open literature. The OLGA model was used to perform numerical simulations to support that the flow instabilities found in our experiments are not artefacts of the experimental set-ups. Moreover, the numerical simulations could help to better understand the physics behind the observed flow instabilities.

3.1 Introduction

OLGA (OiL & GAs) is a transient one-dimensional commercial multiphase flow simulator, which is used by the oil and gas industry for the multiphase flow design of wells and pipelines. OLGA was jointly been developed by SINTEF and IFE in Norway. SINTEF carried out experiments in large scale, high pressure two-phase laboratory flow loop, and IFE developed the multiphase flow simulator[52]. This software was commercialised in 1990, and is available from Scandpower Petroleum Technology in Norway. This computer code can be used as a steady-state point model (OLGAS), and as a complete transient flow simulator (OLGA).

Through the years the performance of the model was verified against both laboratory and field data as shown by Nossen et al.[53]. The latest improvements in the model by replacing empirical correlations with mechanistic closures are discussed by Biberg et al.[52].

Nowadays the program is a three-fluid model, which is able to treat water as a separate third phase in addition to oil and gas phases, compared with the early version (two-fluid model) given by Bendiksen et al.[54]. However, in this research the two-phase module was used for the air-water flow simulations in our experimental test loops. Hence, a description of the two-fluid model is given here[54].

3.2   Transport equations

The two-fluid model contains three separate mass balance equations for the gas, liquid droplets and liquid film, which are coupled through interfacial mass transfer terms. Two momentum balance equations are applied: one combined equation for the gas flow with liquid droplets, and one equation for the liquid film flow. Furthermore, a single mixture energy balance equation is applied.

3.2.1   Conservation of mass

The conservation of total mass is described by the following three equations[54].

For the gas phase:

$$\frac{\partial}{\partial t}\left(V_g\rho_g\right) = -\frac{1}{A}\frac{\partial}{\partial z}\left(AV_g\rho_g\upsilon_g\right) + \psi_g + G_g. \tag{3.1}$$

For the liquid droplets:

$$\frac{\partial}{\partial t}\left(V_D\rho_L\right) = -\frac{1}{A}\frac{\partial}{\partial z}\left(AV_D\rho_L\upsilon_D\right) - \psi_g\frac{V_D}{V_L+V_D} + \psi_e - \psi_d + G_D. \tag{3.2}$$

For the liquid film:

$$\frac{\partial}{\partial t}\left(V_L\rho_L\right) = -\frac{1}{A}\frac{\partial}{\partial z}\left(AV_L\rho_L\upsilon_L\right) - \psi_g\frac{V_L}{V_L+V_D} - \psi_e + \psi_d + G_L. \tag{3.3}$$

In Eqs. 3.1 - 3.3 subscripts g, D and L represent the gas, liquid droplet and liquid film phases, respectively. V denotes the volume fraction (-), υ is the velocity (ms^{-1}), ρ is the density (kgm^{-3}), and A is the cross-sectional area of the pipe (m^2). ψ_g denotes the mass transfer rate between the phases (kgm^{-3}s^{-1}), ψ_e is the entrainment rate of liquid droplets (kgm^{-3}s^{-1}), and ψ_d is the deposition rate of liquid droplets (kgm^{-3}s^{-1}). G denotes the possible mass source of a particular phase (kgs^{-1}m^{-3}).

3.2.2   Conservation of momentum

The conservation of momentum is also described by three separate equations for the gas, liquid droplets and liquid film[54]. However, the equations for the gas and liquid droplets phases are combined to yield a combined momentum equation, where the drag terms, F_D (Nm^{-3}), between them cancel out.

For the gas phase:

$$\begin{aligned}
\frac{\partial}{\partial t}\left(V_g\rho_g\upsilon_g\right) = {} & -V_g\left(\frac{\partial p}{\partial z}\right) - \frac{1}{A}\frac{\partial}{\partial z}\left(AV_g\rho_g\upsilon_g{}^2\right) - \lambda_g\frac{1}{2}\rho_g|\upsilon_g|\upsilon_g\frac{S_g}{4A} \\
& -\lambda_i\frac{1}{2}\rho_g|\upsilon_r|\upsilon_r\frac{S_i}{4A} + V_g\rho_g g\,\cos\alpha + \psi_g\upsilon_a - F_D.
\end{aligned} \tag{3.4}$$

For the liquid droplets:

$$\frac{\partial}{\partial t}\left(V_D \rho_L v_D\right) = -V_D \left(\frac{\partial p}{\partial z}\right) - \frac{1}{A}\frac{\partial}{\partial z}\left(AV_D \rho_L v_D{}^2\right) + V_D \rho_L g \cos\alpha$$
$$-\psi_g \frac{V_D}{V_L + V_D} v_a + \psi_e v_i - \psi_d v_D + F_D. \tag{3.5}$$

As mentioned above, Eqs. 3.4 and 3.5 are combined to yield the following equation.

$$\frac{\partial}{\partial t}\left(V_g \rho_g v_g + V_D \rho_L v_D\right) = -\left(V_g + V_D\right)\left(\frac{\partial p}{\partial z}\right)$$
$$-\frac{1}{A}\frac{\partial}{\partial z}\left(AV_g \rho_g v_g{}^2 + AV_D \rho_L v_D{}^2\right) - \lambda_g \frac{1}{2}\rho_g |v_g| v_g \frac{S_g}{4A}$$
$$-\lambda_i \frac{1}{2}\rho_g |v_r| v_r \frac{S_i}{4A} + \left(V_g \rho_g + V_D \rho_L\right) g \cos\alpha$$
$$+\psi_g \frac{V_D}{V_L + V_D} v_a + \psi_e v_i - \psi_d v_D. \tag{3.6}$$

For the liquid film:

$$\frac{\partial}{\partial t}\left(V_L \rho_L v_L\right) = -V_L \left(\frac{\partial p}{\partial z}\right) - \frac{1}{A}\frac{\partial}{\partial z}\left(AV_L \rho_L v_L{}^2\right) - \lambda_L \frac{1}{2}\rho_L |v_L| v_L \frac{S_L}{4A}$$
$$+\lambda_i \frac{1}{2}\rho_g |v_r| v_r \frac{S_i}{4A} + V_L \rho_L g \cos\alpha - \psi_g \frac{V_L}{V_L + V_D} v_a$$
$$-\psi_e v_i + \psi_d v_D - V_L d\left(\rho_L - \rho_g\right) g \frac{\partial V_L}{\partial z}\sin\alpha, \tag{3.7}$$

where,

$$\begin{aligned} v_a &= v_L \quad \text{for} \quad \psi_g > 0 \quad \text{(and evaporation from the liquid film)}\\ v_a &= v_D \quad \text{for} \quad \psi_g > 0 \quad \text{(and evaporation from the liquid droplets)}\\ v_a &= v_g \quad \text{for} \quad \psi_g < 0 \quad \text{(condensation)}. \end{aligned}$$

In Eqs. 3.4 - 3.7, α represents the pipe inclination from the vertical (rad). S_g, S_L and S_i are the wetted perimeters of the gas, liquid and interface, respectively (m). p represents the pressure (Nm^{-2}), and v_r denotes the relative velocity (ms^{-1}). The internal mass source, G, is assumed to enter perpendicular to the pipe wall, carrying no net momentum. The above conservation equations can be applied for all flow regimes, however, certain terms may drop out for certain flow regimes.

The relative velocity is given by the following equation[54].

$$v_g = R_D \left(v_L + v_r\right), \tag{3.8}$$

where, R_D is a distribution slip ratio (-), which is a flow-regime dependent coefficient and is discussed in section 3.3. The droplet velocity is defined by[54]

$$v_D = v_g - v_{0D} \ \cos\alpha. \tag{3.9}$$

Here, v_{0D} is the terminal velocity of droplets (ms^{-1}). Furthermore, the interphase velocity, v_i (ms^{-1}), is approximated by v_L.

3.2.3 Conservation of energy

For the conservation of energy a single mixture energy balance equation is applied[54].

$$\frac{\partial}{\partial t}\left[m_g\left(E_g + \tfrac{1}{2}v_g^2 + gh\right) + m_L\left(E_L + \tfrac{1}{2}v_L^2 + gh\right) + m_D\left(E_D + \tfrac{1}{2}v_D^2 + gh\right)\right]$$
$$= -\frac{\partial}{\partial z}\left[m_g v_g\left(H_g + \tfrac{1}{2}v_g^2 + gh\right) + m_L v_L\left(H_L + \tfrac{1}{2}v_L^2 + gh\right)\right.$$
$$\left. + m_D v_D\left(H_D + \tfrac{1}{2}v_D^2 + gh\right)\right] + H_S + U, \tag{3.10}$$

where, m_f is equal to $V_f \rho_f$ for phase f, E denotes the internal energy per unit mass (Jkg^{-1}), h is the elevation (m), H_S represents the enthalpy from the mass sources (Jkg^{-1}), and U is the heat transfer per unit volume from the pipe walls (Jm^{-3}). Work between the gas and liquid phases are usually negligible when compared to the heat transfer from the pipe walls. Thus, in Eq. 3.10 the term representing work between the gas and liquid phases is neglected.

3.3   Flow-regime description

The friction factors and wetted perimeters depend on the flow regime. Two basic flow regimes are considered: separated flow, which consists of stratified and annular-mist flow, and distributed flow, which consists of bubble and slug flow.

3.3.1 Separated flow

The distributions of phases across the respective phase areas are assumed constant. Therefore, the distribution slip ratio, R_D, in Eq. 3.8 is equal to 1.

Stratified flow is subdivided into stratified smooth and wavy. The following expression is used to obtain the average wave height, h_w (m)[54]:

$$\frac{1}{2}\rho_g\left(v_g - v_L\right)^2 = h_w\left(\rho_L - \rho_g\right)g \ \sin\alpha + \left(\frac{\sigma}{h_w}\right), \tag{3.11}$$

where, σ denotes the surface tension (Nm^{-1}). The wall friction factor, λ_f (-), of phase f for laminar or turbulent flow is given by

$$\lambda_f = \begin{cases} \frac{64}{N_{\text{Re}}} & \text{for laminar flow.} \\ 0.0055\left[1 + \left(\frac{2\times10^4\epsilon}{d_h} + \frac{10^6}{N_{\text{Re}}}\right)^{\frac{1}{3}}\right] & \text{for turbulent flow.} \end{cases} \tag{3.12}$$

Here, ϵ denotes the absolute pipe roughness (m), d_h is the hydraulic diameter (m), and N_{Re} is the Reynolds number (-).

The interfacial friction factor for annular flow proposed by Wallis, Eq. 3.13, has been applied for vertical pipes.

$$\lambda_i = 0.02 \left[1 + 75 \left(1 - V_g\right)\right], \tag{3.13}$$

and for inclined pipes the following equation is used for annular-mist flow[54].

$$\lambda_i = 0.02 \left(1 + KV_L\right), \tag{3.14}$$

where, K is an empirically determined coefficient.

For stratified smooth flow, Eq. 3.12 with zero pipe roughness is used to obtain the interfacial friction factor, and for stratified wavy flow the minimum value of Eq. 3.14 and the following equation is used[54].

$$\lambda_i = \frac{h_w}{d_{hi}}. \tag{3.15}$$

3.3.2　Distributed flow

For pure bubble flow, Eq. 3.8 becomes[54]

$$v_g = R \left(v_L + v_{0S}\right), \tag{3.16}$$

where, R is given by

$$R = \frac{1 - V_g}{\frac{1}{C_0} - V_{gS}}. \tag{3.17}$$

Here, C_0 is a distribution slip parameter (-), which is given by Eq. 3.21. In Eq. 3.16, v_{0S} denotes the average bubble-rise velocity (ms^{-1}) and is obtained by the following equation[54].

$$v_{0S} = 1.18 \left[\frac{g\sigma \left(\rho_L - \rho_g\right)}{\rho_L^2}\right]^{0.25} \left[(1 - V_g) \left|\cos\alpha\right|\right]^{0.5}. \tag{3.18}$$

In Eq. 3.17, V_{gS} represents the void fraction in liquid slugs (-) and can be obtained by[54]

$$V_{gS} = \frac{v_{sg} + v_{sL}}{C + v_{sg} + v_{sL}}, \tag{3.19}$$

where, C is an empirically determined constant. v_{sg} and v_{sL} denote superficial gas and liquid velocity, respectively (ms^{-1}).

For pure slug flow, $V_{gS} = 0$ and Eq. 3.8 becomes[54]

$$v_g = \frac{1 - V_g}{\frac{1}{C_0} - V_g} \left[v_L + \frac{v_{0b}}{C_0 \left(1 - V_g\right)}\right], \tag{3.20}$$

where, C_0 is given by [54]

$$C_0 = \begin{cases} 1.05 + 0.15 \; \cos^2\alpha & \text{for } N_{\text{Fr}} < 3.5. \\ 1.20 & \text{for } N_{\text{Fr}} > 3.5. \end{cases} \tag{3.21}$$

Here, N_{Fr} is the Froude number (-). In Eq. 3.20, v_{0b} is the bubble velocity in stagnant liquid (ms^{-1}) and is obtained by [54]

$$v_{0b} = \begin{cases} 0.35\sqrt{gd} \; \cos\alpha + 0.54\sqrt{gd} \; \sin\alpha & \text{for } N_{\text{Fr}} < 3.5. \\ 0.35\sqrt{gd} \; \cos\alpha & \text{for } N_{\text{Fr}} > 3.5. \end{cases} \tag{3.22}$$

The velocity of slug bubbles can be approximated by [54]

$$v_B = C_0 \left(v_{sL} + v_{sg} \right) + v_{0b}. \tag{3.23}$$

3.4 Fluid properties

All fluid properties, e.g. densities, compressibilities, viscosities, surface tension, enthalpies, heat capacities, and thermal conductivies, can be provided to OLGA by a file that contains a table in which these fluid properties of the phases are given for a number of thermodynamic conditions, i.e. pressure and temperature. The fluid properties during a simulation are found by interpolating in this table.

3.5 Numerical scheme

The two-fluid model, as formulated above, provides a set of coupled first-order, nonlinear, one-dimensional partial differential equations. OLGA uses a finite difference scheme on a staggered grid for the spatial discretization. A semi-implicit time integration method is used. The time step, Δt (s), is limited by the average phase velocities based on the mass-transfer criterion [54].

$$\Delta t \le \min_j \left(\frac{\Delta z_j}{|v_{fj}|} \right), \tag{3.24}$$

where, Δz, denotes the length of a gird cell (m), and v_f is the velocity of phase f. Index j is used to identify a grid cell.

Chapter 4

Reservoir-wellbore flow-model coupling

In this dissertation the two-phase flow code OLGA was also applied to simulate the characteristics of severe slugging generated at the bottom of an extended reach wellbore, see Chapter 5. This wellbore flow model was coupled to a reservoir flow model, which describes the flow of oil and gas from the reservoir into the wellbore, and vice versa. The purpose of this chapter is to give an overview of the modelling techniques that are commonly used to couple a wellbore flow model to a reservoir flow model.

4.1 Introduction

A comprehensive reservoir management modelling system can be described as comprising four interacting subsystems: the reservoir model, the near-wellbore reservoir model, the wellbore model, and the surface model[55]. Fig. 4.1 depicts the relationship between these models. It is worth mentioning that a reservoir simulator generally includes both a reservoir model and a near-wellbore reservoir model[56].

The reservoir model describes the flow of fluids within a porous petroleum reservoir, see e.g. Aziz and Settari [57]. The near-wellbore reservoir model represents the inflow of fluids from the reservoir into the wellbore or the injection of fluids from the wellbore into the reservoir. The wellbore model describes fluid flow from the bottom of the wellbore to the surface and the surface model represents the flow of fluids within surface facilities. The mathematical models associated with each subsystem depends on physical conservation laws and closure relationships, e.g. see Chapter 3.
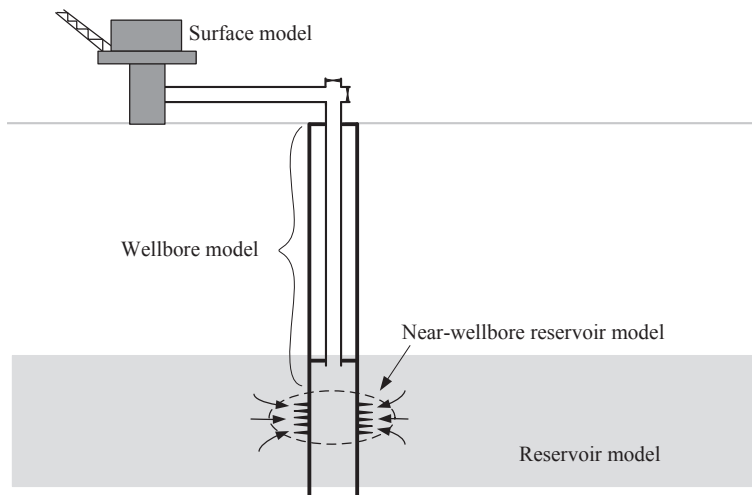
Figure 4.1: *Reservoir management modelling system comprises four interacting subsystems.*

The wellbore flow model represents outflow to the surface from the wellbore-reservoir system. Thus, fluid flow into the wellbore from the reservoir should be considered. The modelling techniques that are commonly applied to couple a wellbore flow model (static or dynamic) to a reservoir flow model (static or dynamic) are as follows.

4.2   Wellbore simulator with productivity index

The difference between the reservoir pressure, p_r, and the flowing pressure at the bottom of a wellbore, p_{wf}, is the driving force for the inflow of fluids from the reservoir into the wellbore[58]. The Productivity Index (PI) is used to measure the ability of a well to produce the hydrocarbon fluid from a reservoir. For a single phase oil production, the PI ($m^3s^{-1}Pa^{-1}$) is given by[58]:

$$PI = \frac{Q_o}{p_r - p_{wf}},$$ (4.1)

where Q_o is the oil flow rate (m^3s^{-1}), p_r denotes the volumetric-average drainage area pressure (Pa), and p_{wf} is the flowing pressure at the bottom of the wellbore (Pa). The productivity index is generally measured during a production test, i.e. by flowing the well through a test separator located at the surface and measuring the fluid flow rate as a function of the flowing bottom hole pressure, see e.g. Golan and Whitson [59]. The flowing pressure at the bottom of the wellbore can be measured with a permanent downhole gauge or a dedicated wire line tool.

The productivity index is a valid measure of the well productivity potential if the well is flowing at steady state or semi-steady state conditions. Therefore, during a production test, the well is allowed to flow at a constant flow rate for a sufficient amount of time to reach the semi-steady state conditions[60].

Resistance to the inflow of fluids from a reservoir into a wellbore depends on reservoir rock and fluid properties, details of the completion of the wellbore, and the effect of drilling on the near-wellbore reservoir[59]. The productivity index can be calculated using analytical methods. Applying mass conservation equations and Darcy's law for radial fluid flow into a vertical well at semi-steady state conditions, PI can be calculated as[58]:

$$\text{PI} = \frac{2\pi kh}{\log\frac{r_e}{r_w} - 0.75 + s} \left(\frac{k_{ro}}{\mu_o B_o} \right),$$

(4.2)

where k denotes the reservoir absolute permeability (m^2), h is the reservoir thickness (m), r_e represents the drainage radius (m), r_w denotes the wellbore radius (m), s is the skin factor (-), k_{ro} is the oil relative permeability (-), μ_o is the oil viscosity (Pas), and B_o is the oil formation volume factor (-).

The plot of p_{wf} versus Q_o is a straight line with a slope of $-1/\text{PI}$. This graphical representation is called the Inflow Performance Relationship (IPR). However, when the pressure drops below the bubble point pressure, the IPR deviates from the simple straight line. Several empirical methods are designed to predict the non-linear behaviour of the IPR, for instance Vogel's method[61] and Fetkovich's method[62]. The following relationship is proposed by Vogel[61] to generate the IPR for a saturated-oil reservoir:

$$\frac{Q_o}{Q_{o\max}} = 1 - 0.2 \left(\frac{p_{wf}}{p_r} \right) - 0.8 \left(\frac{p_{wf}}{p_r} \right)^2,$$

(4.3)

where $Q_{o\max}$ denotes the maximum oil flow rate a well could theoretically deliver at zero p_{wf}.

In this coupling method, a wellbore simulator uses the static pressure-rate equations, e.g. the semi-steady state IPR, to describe the influx of fluids from the reservoir, which ignore the flow dynamics, e.g. gas coning, in the near-wellbore reservoir.

4.3   Reservoir simulator with lift curves

Most reservoir simulators use lift curves to represent fluid flow in the wellbore. Lift curves are obtained using a separate wellbore modelling program and are included in the reservoir simulator as an input file. Lift curves, also often called Vertical Flow Performance (VFP) tables, consist of an array of flowing bottom hole pressure for a given wellbore diameter, inclination angle, roughness and fluid properties at different combinations of flow parameters, e.g. flow rate, wellhead

pressure, water cut and gas oil ratio. A reservoir simulator calculates the operating point, i.e. the actual well flow rate and flowing bottom hole pressure, by intersecting the lift curves with a calculated inflow performance relationship, as illustrated in Fig. 4.2.
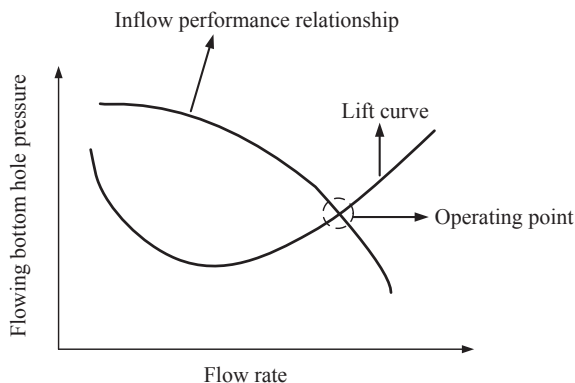

Figure 4.2: *Graphical representation of the operating point, which is the intersection between the IPR and the lift curve.*

In this coupling method, a reservoir simulator uses steady state lift curves for modelling of the fluid flow in a wellbore, which ignore the flow dynamics, e.g. severe slugging, in the wellbore.

4.4   Integrated dynamic reservoir-wellbore simulator

In some practical scenarios, e.g. gas coning, the near-wellbore reservoir dynamics can have a considerable impact on the flow dynamics in the wellbore[63–65]. Sturm et al.[63] developed an integrated dynamic reservoir-wellbore model to simulate the transient flow of oil and gas from thin oil rims subject to gas and water coning. They assumed a steady state reservoir model at the outside of the transient radial near-wellbore reservoir model. Hu et al.[66] developed an integrated dynamic reservoir-wellbore model by implicitly coupling an existing transient wellbore flow model with an existing near-wellbore reservoir flow model. Here, the wellbore model provides the pressure boundary, p_{wf}, to the reservoir model and then the reservoir model calculates the flow rate of each phase at the bottom of the wellbore. At each time step of the simulation, the reservoir model also calculates a sensitivity coefficient for the production rate with respect to the wellbore pressure. At the next simulation time step, the wellbore model uses this sensitivity coefficient to predict the pressure at the bottom of the wellbore.

The integrated dynamic reservoir-wellbore model chooses the smaller integra-

tion time step of the two models, i.e. wellbore and reservoir models, which slows down the simulation speed compared with running the two models in a separate mode. Thus, an integrated dynamic reservoir-wellbore simulator is computationally expensive.

In this dissertation, the characteristics of severe slugging generated in a pipeline-riser system downstream of a wellbore and also in an extended reach wellbore are the focus of investigation. Therefore, a semi-steady state IPR can be used to describe the influx of oil and gas from a reservoir, which is computationally less expensive.

Bibliography

[1] International Energy Agency. World energy outlook 2010. Technical Report OECD/IEA, Paris, 2010.

[2] J.Ø. Tengesdal, C. Sarica, and L. Thompson. Severe slugging attenuation for deepwater multiphase pipeline and riser systems. *SPE Production & Facilities J.*, 18(4):269–279, 2003.

[3] D. Denney. "self-lifting" method to eliminate severe slugging in offshore production systems. *J. of Petroleum Tech.*, 55(12):36–37, 2003.

[4] F.E. Jansen, O. Shoham, and Y. Taitel. The elimination of severe slugging-experiment and modeling. *Int. J. Multiphase Flow*, 22(6):1055–1072, 1996.

[5] K. Kovalev, A. Cruickshank, and J. Purvis. The slug suppression system in operation. Paper SPE 84947 presented at Offshore Europe, Aberdeen, United Kingdom, 2 - 5 September 2003.

[6] S. Mokhatab. *Severe Slugging in Offshore Production Systems*. Petroleum science and technology. Nova Science Publishers, New York, USA, 2010.

[7] J.E. Seim, V.L. van Beusekom, R.A.W.M. Henkes, and O.J. Nydal. Experiments and modelling for the control of riser instabilities with gas lift. Presented at 15th International Conference on Multiphase Production Technology, Cannes, France, 15-17 June, 2011.

[8] B.W. Santana, D.J. Fetzner, N.W. Edwards, and R.W. Haupt. Program for improving multiphase flow slug force resistance at kuparuk river unit processing facilities. Paper SPE 26104 presented at the SPE Western Regional Meeting, Anchorage, Alaska, 26 - 28 May 1993.

[9] V. Henriot, A. Courbot, E. Heintze, and L. Moyeux. Simulation of process to control severe slugging: Application to the dunbar pipeline. Paper SPE

56461 presented at the SPE Annual Technical Conference and Exhibition, Houston, Texas, 3 - 6 October 1999.

[10] C. Sarica and J.Ø. Tengesdal. A new technique to eliminate severe slugging in pipeline/riser systems. Paper SPE 63185 presented at the SPE Annual Technical Conference and Exhibition, Dallas, Texas, 1 - 4 October 2000.

[11] K. Havre and M. Dalsmo. Active feedback control as a solution to severe slugging. *SPE Production & Facilities J.*, 17(3):138–148, 2002.

[12] S. Mokhatab, B.F. Towler, and S. Purewal. A review of current technologies for severe slugging remediation. *Petroleum Science & Tech. J.*, 25(10):1235–1245, 2007.

[13] U.S. Energy Information Administration. International energy outlook 2011. Technical Report DOE/EIA-0484(2011), Washington, DC 20585, 2011.

[14] J.L. Bravo. Energy security and diversity - the role of a technology strategy for an integrated oil company. Paper IPTC 12375 presented at the International Petroleum Technology Conference, Kuala Lumpur, Malaysia, 3 - 5 December 2008.

[15] W. Obendrauf, K. Schrader, N. Al-Farsi, and A. White. Smart snake wells in champion west-expected and unexpected benefits from smart completions. Paper SPE 100880 presented at the SPE Asia Pacific Oil & Gas Conference and Exhibition, Adelaide, Australia, 11 - 13 September 2006.

[16] L. Bacarreza, C. Hornabrook, C.C. Khoo, H. Nevøy, and N.-J. Japar. The snaking wells in champion west, offshore brunei. best practices for erd well construction. Paper IADC/SPE 114550 presented at the IADC/SPE Asia Pacific Drilling Technology Conference and Exhibition, Jakarta, Indonesia, 25 - 27 August 2008.

[17] B.N. Rao, A.M. Amin, R. Van Petegeg, and J. Broussard. On the hydraulics of inverted flow path gravel pack operations. Paper SPE 151803 presented at the SPE International Symposium and Exhibition on Formation Damage Control, Lafayette, Louisiana, USA, 15 - 17 February 2012.

[18] B.T. Yocum. Offshore riser slug flow avoidance, mathematical model for design and optimization. Paper SPE 4312 presented at SPE Annual European Meeting, London, April 1973.

[19] Z. Schmidt, J.P. Brill, and H.D. Beggs. Experimental study of severe slugging in a two-phase-flow pipeline-riser pipe system. *SPE J.*, 20(5):407–414, 1980.

[20] Y. Taitel. Stability of severe slugging. *Int. J. Multiphase Flow*, 12(2):203–217, 1986.

[21] B.F.M. Pots, I.G. Bromilow, and M.J.W.F. Konijn. Severe slug flow in off-shore flowline/riser systems. *SPE Production Eng. J.*, 2(4):319–324, 1987.

[22] Y. Taitel, S. Vierkandt, O. Shoham, and J.P. Brill. Severe slugging in a riser system: experiments and modeling. *Int. J. Multiphase Flow*, 16(1):57–68, 1990.

[23] J. L. Baliño, K. P. Burr, and R. H. Nemoto. Modeling and simulation of severe slugging in air-water pipeline-riser systems. *Int. J. Multiphase Flow*, 36(8):643–660, 2010.

[24] J. Fabre, L.L. Peresson, J. Corteville, R. Odello, and T. Bourgeols. Severe slugging in pipeline/riser systems. *SPE Production Eng. J.*, 5(3):299–305, 1990.

[25] C. Sarica and O. Shoham. A simplified transient model for pipeline-riser systems. *Chemical Engineering Science*, 46:2167–2179, 1991.

[26] H.-Q. Zhang, E.M. Al-Safran, S.S. Jayawardena, C.L. Redus, C. Sarica, and J.P. Brill. Modeling of slug dissipation and generation in gas-liquid hilly-terrain pipe flow. *ASME J. Energy Resour. Technol.*, 125(3):161–168, 2003.

[27] O. Shoham. *Mechanistic Modeling of Gas-Liquid Two-Phase Flow in Pipes*. Society of Petroleum Engineers, Richardson, Texas, 2006.

[28] K.E. Brown, P. Sukarno, J. Lea, Z. Schmidt, D.R. Doty, C. Granger, L. Ledlow, J. Mach, E. Proaño, A.P. Szilas, B. Agena, B. Tighe, R. Aguilera, and L. Acevedo. *Production Optimization of Oil and Gas Wells by Nodal Systems Analysis*, volume 4 of *The Technology of Artificial Lift Methods*. PennWell Publishing Co., Tulsa, Oklahoma, 1984.

[29] A.R. Hasan and C.S. Kabir. *Fluid Flow and Heat Transfer in Wellbores*. Society of Petroleum Engineers, Richardson, Texas, 2002.

[30] J.P. Brill and H. Mukherjee. *Multiphase Flow in Wells*, volume 17 of *SPE monograph series*. Society of Petroleum Engineers, Richardson, Texas, 1999.

[31] D. Barnea. A unified model for predicting flow-pattern transitions for the whole range of pipe inclinations. *Int. J. Multiphase Flow*, 13(1):1–12, 1987.

[32] Y. Taitel and A.E. Dukler. A model for predicting flow regime transitions in horizontal and near horizontal gas-liquid flow. *AIChe Journal*, 22(1):47–55, 1976.

[33] A.M. Ansari, N.D. Sylvester, C. Sarica, O. Shoham, and J.P. Brill. A comprehensive mechanistic model for upward two-phase flow in wellbores. *SPE Production & Facilities J.*, 9(2):143–151, 1994.

[34] J.J. Xiao, O. Shoham, and J.P. Brill. A comprehensive mechanistic model for two-phase flow in pipelines. Paper SPE 20631 presented at SPE Annual Technical Conference and Exhibition, New Orleans, Louisiana, 23-26 September 1990.

[35] A.R. Hasan and C.S. Kabir. A study of multiphase flow behavior in vertical wells. *SPE Production Eng. J.*, 3(2):263–272, 1988.

[36] A.R. Hasan and C.S. Kabir. Predicting multiphase flow behavior in a deviated well. *SPE Production Eng. J.*, 3(4):474–482, 1988.

[37] C.S. Kabir and A.R. Hasan. Performance of a two-phase gas/liquid model in vertical wells. *J. Pet. Sci. & Eng.*, 4(3):273–289, 1990.

[38] N. Petalas and K. Aziz. A mechanistic model for multiphase flow in pipes. *Journal of Canadian Petroleum Technology*, 39(6):43–55, 2000.

[39] D. Barnea. A unified model for predicting flow-pattern transitions for the whole range of pipe inclinations. *Int. J. Multiphase Flow*, 13(1):1–12, 1987.

[40] G.A. Gregory, M.K. Nicholson, and K. Aziz. Correlation of liquid volume fraction in slug for horizontal gas-liquid slug flow. *Int. J. Multiphase Flow*, 4(1):33–39, 1978.

[41] S.W. Churchill. Friction-factor equation spans all fluid-flow regimes. *Chemical Engineering*, 84(24):91–92, 1977.

[42] R.V.A. Oliemans, B.F.M. Pots, and N. Trompe. Modeling of annular dispersed 2-phase flow in vertical pipes. *Int. J. Multiphase Flow*, 12(5):711–732, 1986.

[43] Y. Taitel, D.Barnea, and A.E. Dukler. Modeling flow pattern transitions for steady upward gas-liquid flow in vertical tubes. *AIChe Journal*, 26(3): 345–354, 1980.

[44] N. Zuber, F.W. Staub, G. Bijwaard, and P.G. Kroeger. Steady state and transient void fraction in two-phase flow systems. Technical Report EURAEC-GEAP-5417, General Electric Co., San Jose, CA, January 1967.

[45] G.W. Govier and K. Aziz. *The Flow of Complex Mixtures in Pipes*. Van Nostrand, Reinhold, 1972. Reprinted by Robert E. Kriger Publishing Co., Huntington, New York, NY, 1977.

[46] K.H. Bendiksen. An experimental investigation of the motion of long bubbles in inclined tubes. *Int. J. Multiphase Flow*, 10(4):467–483, 1984.

[47] E.E. Zukoski. Influence of viscosity surface tension and inclination angle on motion of long bubbles in closed tubes. *J. Fluid Mech.*, 25(4):821–837, 1966.

[48] M.E. Weber. Drift in intermittent two-phase flow in horizontal pipes. *Canadian J. Chem. Eng.*, 59(3):398–399, 1981.

[49] G.B. Wallis. *One-dimensional Two-Phase Flow*. McGraw-Hill, New York, 1969.

[50] T.Z. Harmathy. Velocity of large drops and bubbles in media of infinite or restricted extent. *AIChe Journal*, 6(2):281–288, 1960.

[51] N. Zuber and J.A. Findlay. Average volumetric concentration in two-phase flow systems. *J. Heat Transfer*, 87(4):453–467, 1965.

[52] D. Biberg, H. Holmås, G. Staff, T. Sira, J. Nossen, P. Andersson, C. Lawrence, B. Hu, and K. Holmås. Basic flow modelling for long distance transport of wellstream fluids. 14th International Conference on Multiphase Production Technology, Cannes, France, 17-19 June, 2009.

[53] J. Nossen, R. Shea, and J. Rasmussen. New developments in flow modeling and field data verification. 2nd North American Conference on Multiphase Technology, Banff, Canada, 21-23 June, 2000.

[54] K.H. Bendiksen, D. Malnes, R. Moe, and S. Nuland. The dynamic two-fluid model OLGA: Theory and application. *SPE Production Eng. J.*, 6(2): 171–180, 1991.

[55] J.R. Fanchi. *Principles of Applied Reservoir Simulation*. Gulf Professional Publishing, Burlington, MA 01803, USA, 2006.

[56] D.W. Peaceman. *Fundamentals of numerical reservoir simulation*, volume 6 of *Development in petroleum science*. Elsevier Scientific Publishing Company, Amsterdam, The Netherlands, 1977.

[57] K. Aziz and A. Settari. *Petroleum Reservoir Simulation*. Applied Science Publications, London, UK, 1979.

[58] M.J. Economides, A.D. Hill, and C. Ehlig-Economides. *Petroleum production systems*. Prentice Hall petroleum engineering series. PTR Prentice Hall, Englewood Cliffs, N.J., 1994.

[59] M. Golan and C.H. Whitson. *Well performance*. Prentice Hall, Englewood Cliffs, N.J., 2nd edition, 1991.

[60] T. Ahmed. *Reservoir engineering handbook*. Gulf Professional Publishing, Burlington, MA 01803, USA, 3rd edition, 2006.

[61] J.V. Vogel. Inflow performance relationships for solution-gas drive wells. *Journal of Petroleum Technology*, 20(1):83–92, 1968.

[62] M.J. Fetkovich. The isochronal testing of oil wells. Paper SPE 4529 presented at fall meeting of the Society of Petroleum Engineers of AIME, Las Vegas, Nevada, 30 September - 3 October 1973.

[63] W.L. Sturm, S.P.C. Belfroid, O. van Wolfswinkel, M.C.A.M. Peters, and F.J.P.C.M.G. Verhelst. Dynamic reservoir well interaction. Paper SPE 90108 presented at SPE Annual Technical Conference and Exhibition, Houston, Texas, USA, 26 - 29 September 2004.

[64] E.D. Nennie, G.J.N. Alberts, S.P.C. Belfroid, E. Peters, and G.J.P. Joosten. An investigation into the need of a dynamic coupled well-reservoir simulator. Paper SPE 110316 presented at SPE Annual Technical Conference and Exhibition, Anaheim, California, USA, 11 - 14 November 2007.

[65] J. Sagen, M. Østenstad, B. Hu, K.E.I. Henanger, S.K. Lien, Z. Xu, S. Groland, and T. Sira. A dynamic model for simulation of integrated reservoir, well and pipeline system. Paper SPE 147053 presented at SPE Annual Technical Conference and Exhibition, Denver, Colorado, USA, 30 October - 2 November 2011.

[66] B. Hu, J. Sagen, G. Chupin, T. Haugset, A. Ek, T. Sommersel, Z.G. Xu, and J.C. Mantecon. Integrated wellbore-reservoir dynamic simulation. Paper SPE 109162 presented at SPE Asia Pacific Oil and Gas Conference and Exhibition, Jakarta, Indonesia, 30 October - 1 November 2007.

Chapter 5

A Modelling Study of Severe Slugging in Wellbore§

Abstract

Developments in extended reach drilling and completion technologies allow to economically access a number of scattered small hydrocarbon pockets and will open up further opportunities for maximizing recovery from these fields. Effective use of these developments requires us to better understand the transient multiphase flow behaviour. Undulation is associated to horizontal wells with some degrees of deviation from the horizontal. The inclination angle could be a result of a lack of sufficient drilling control or could be designed on purpose, for instance, fish-hook wells, snake wells and undulating wells. A complicated and undulating trajectory may initiate severe slugging at the bottom of a wellbore. In this paper, OLGA, a commercial transient two-fluid multiphase flow simulator, and Cheng's inflow performance relationship were coupled together to characterize severe slugging. Simulation shows that severe slugging is formed at the bottom of the wellbore and moved up to the surface. Furthermore, it creates pressure pulsation at the bottom of the wellbore that can influence the reservoir performance.

5.1   Introduction

Fish-hook wells, snake wells and undulating wells are relatively new technologies and have been used to develop hydrocarbon fields more efficiently than conventional wells. Much of the world's oil exists in scattered and isolated pockets. As these deposits are small, it is not economically feasible to exploit them in a conventional way. Based on their geological settings, the optimal well trajectory could be a fish-hook well, where its geometry is in the shape of a fish-hook with the deepest reservoirs drilled first and the shallowest reservoirs at the end of the wellbore. It could also be a snake well that follows a complex undulating path and snakes back and forth to reach a number of different reservoir pockets. Another example is an undulated horizontal well for an extremely anisotropic formation, when vertical permeability is much smaller than horizontal permeability. In that case an undulating well may be drilled to overcome the low vertical permeability and increase the well productivity.

As a horizontal well gets longer and follows a more complicated and undulating trajectory, wellbore hydrodynamics plays an important role in well performance, especially when two-phase gas-liquid flow is involved.

In this paper we address a phenomenon named severe slugging, happening at the bottom of a wellbore close to hydrocarbon reservoirs. At relatively low gas and liquid flow rates, liquid will have the tendency to accumulate at a low spot in the wellbore, blocking over time a free passage of the gas phase. However, as production at the well continuous, the compressed upstream gas will flush out the liquid phase that has been accumulated in this lower part of the wellbore. Thereby, it creates a relatively long liquid slug that is pushed out of the wellbore. After this liquid surge, and subsequent gas surge, part of the liquid in the wellbore falls back to this low spot to create a new blockage and the cycle repeats. These slugs create potential problems for the receiving surface facilities like separators, pumps, and compressors, which are designed to operate under steady state conditions. Moreover, they create pressure oscillations at the bottom of the wellbore that can influence the production rates at the oil and gas well.

Severe slugging was first reported in offshore oilfield production systems by Yocum (1973). In an offshore oil and gas production facility, pipeline-riser systems are required to transport multiphase hydrocarbons from wellheads to a central production platform. Severe slugging in pipeline-riser systems has been studied by several investigators. In Fig. 5.1 different stages of a cycle of severe slugging are illustrated.

Accumulation of a sufficient amount of liquid at the riser base creates a full blockage. Therefore, a free gas passage is blocked. This stage is called blockage of the riser base (Fig. 5.1a). As both phases continue to flow into the pipeline, while the gas passage is blocked, the liquid level in the riser increases. As a consequence, the pressure at the riser base increases, pushing the liquid-gas interface in the pipeline further away from the riser base and compressing the accumulated gas in the pipeline. This stage is known as slug growth (Fig. 5.1b). When the liquid
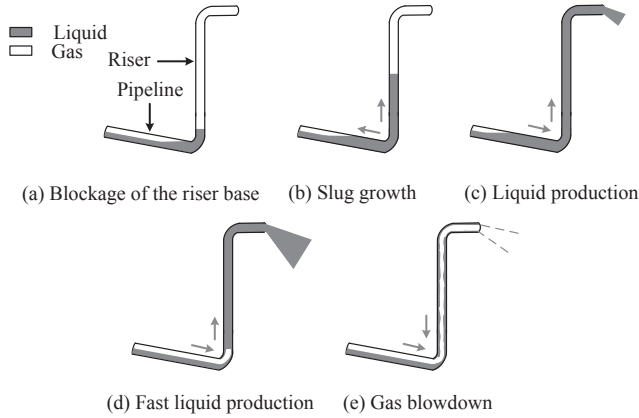
(a) Blockage of the riser base   (b) Slug growth   (c) Liquid production

(d) Fast liquid production   (e) Gas blowdown

Figure 5.1: *Stages for severe slugging (from Malekzadeh et al. 2012).*

level reaches the riser top, the pressure at the riser base reaches its maximum and, subsequently, the pressure of the compressed gas in the pipeline becomes higher than the hydrostatic head of the liquid-filled riser. Liquid starts to flow out at the riser top and simultaneously the slug tail in the pipeline will be pushed towards the riser base. This is the liquid production stage (Fig. 5.1c). When the gas phase penetrates into the riser, the hydrostatic head of the riser decreases. The gas will expand and flush the liquid column out of the riser. This stage is known as fast liquid production (Fig. 5.1d). After that, gas will be produced at a high rate, causing a quick depressurization of the system. This is the gas blowdown stage (Fig. 5.1e). Once the gas is expelled, the pressure reaches its minimum leading to the fallback of the remaining liquid and accumulation at the riser base, and the cycle repeats (Malekzadeh et al. 2012).

Yocum (1973) recognized that the reduction of the pipeline diameter and backpressure increase can eliminate severe slugging. The diameter of the tubing at the bottom of a wellbore, which is about 0.1 m, is smaller than the diameter of a pipeline laid out over the seafloor, which is up to 0.8 m. Furthermore, the average pressure at the bottom of a wellbore is higher than the average pressure of the surface pipeline. Therefore, the severe slugging phenomenon at the bottom of a wellbore is expected to be less pronounced. The objective of this study is to investigate numerically the characteristics of flow instabilities at the bottom of a wellbore close to hydrocarbon reservoirs.

Belfroid et al. (2005) used a simplified transient drift flux wellbore flow model coupled to a radial single phase reservoir model to investigate the wellbore-reservoir interaction during a range of flow instabilities such as severe slugging and water coning. However, as the topography of the wellbore gets complicated,

a more accurate description of the multiphase flow is necessary.

In this paper, OLGA, a commercial transient two-fluid multiphase flow simulator, is used to analyze the severe slugging at the bottom of a wellbore. To represent the extraction of fluids from the reservoir into the horizontal oil well under solution gas drive mechanism, the Cheng's method is used. The solution gas drive mechanism is a drive mechanism in which the principal drive mechanism is the expansion of the oil and its originally dissolved gas. A drop in pressure below the bubble point pressure releases the originally dissolved gas from the oil. The increase in fluid volumes during this process drives the oil towards the wellbore (Dake 1978). Cheng et al. (1990) proposed an inflow model to represent the extraction of fluids from a reservoir or the injection of fluids into a reservoir for a horizontal well. A hypothetical example demonstrates the occurrence of severe slugging at the bottom of an extended reach well.

5.2 Wellbore flow model

The multiphase flow simulations in the wellbore were performed using the multiphase flow simulator OLGA. This is a transient one-dimensional, commercial computer code based on a two-fluid flow model. The three-dimensional velocity profile in the wellbore is averaged over the cross section, which simplifies the flow equations from three-dimensional to one-dimensional. This simplification requires using empirical closure relations in the model for the wall friction and for the interfacial stress between the liquid and the gas. The one-dimensional model contains three separate mass balance equations for the gas, liquid droplets and liquid film, which are coupled through interfacial mass transfer terms. Two momentum balance equations are applied: one combined equation for the gas flow with liquid droplets, and one equation for the liquid film flow (Bendiksen 1991).

5.3 Inflow model

In this study, the reservoir model is restricted to a near-wellbore reservoir model. However, that is a valid assumption since the time scale of the flow instabilities caused by severe slugging in the wellbore is so small that it will not be felt by the reservoir itself and the reservoir observes the time-average of the instabilities occurring in the wellbore. The Productivity Index (PI) is used to measure the ability of a well to produce. For a single phase oil production, the PI $(\text{m}^3\text{s}^{-1}\text{Pa}^{-1})$ is given by

$$\text{PI} = \frac{Q_o}{p_r - p_{wf}}, \tag{5.1}$$

where Q_o is the oil flow rate $(\text{m}^3\text{s}^{-1})$, p_r denotes the volumetric-average drainage area pressure (Pa), and p_{wf} is the flowing pressure at the bottom of the wellbore (Pa). The productivity index is generally measured during a production test

and would be a valid measure if the reservoir fluid in the near-wellbore area is flowing at steady state or semi-steady state condition. Reservoir fluid flow may be modelled using analytical methods. Pressure support in a reservoir often is not sufficient and as a consequence of oil production from the wells, the drainage area pressure gradually drops over time, a situation known as semi-steady state condition. At semi-steady state conditions, a Neumann boundary condition $\frac{dp}{dr}|_{r=r_e} = 0$, which implies that there is no pressure gradient for fluid flow at the external boundary (r_e), can be used to represent a gradual pressure depletion of the drainage area of a reservoir. Applying mass conservation equations and Darcy's law for radial fluid flow into a vertical well at semi-steady state conditions, PI can be calculated as

$$\text{PI} = \frac{Q_o}{p_r - p_{wf}} = \frac{2\pi k h}{\log\frac{r_e}{r_w} - 0.75 + s} \left(\frac{k_{ro}}{\mu_o B_o}\right), \tag{5.2}$$

where k denotes the reservoir absolute permeability (m^2), h is the reservoir thickness (m), r_e represents the drainage radius (m), r_w denotes the wellbore radius (m), s is the skin factor (-), k_{ro} is the oil relative permeability (-), μ_o is the oil viscosity (Pas), and B_o is the oil formation volume factor (-). The plot of p_{wf} versus Q_o is a straight line with a slope of $-\frac{1}{\text{PI}}$. This graphical representation is called the Inflow Performance Relationship (IPR). However, when the pressure drops below the bubble point pressure, the IPR deviates from the simple straight line. Several empirical methods are designed to predict the non-linearity behaviour of the IPR, for instance Vogel's method (1968). Cheng et al. (1990) proposed a form of Vogel's method for horizontal wells.

In this paper, the characteristics of severe slugging formed in a long extended undulating well have been the focus of investigation. Therefore, a semi-steady state IPR has been used to describe the influx of oil and gas from the reservoir, which ignores the flow transient in the near-wellbore area. For most practical situations, the source of the accumulated gas in the wellbore is a gas cap in the reservoir as well as solution gas which comes out of solution when the pressure drops below the bubble point pressure. Therefore, the IPR is a non-linear function of the flow rate and cannot be represented with a straight line anymore. For that reason, in this work Cheng's method for the horizontal well has been used in the following form

$$\frac{Q_o}{Q_{o\max}} = 0.9885 + 0.2055 \left(\frac{p_{wf}}{p_r}\right) - 1.1818 \left(\frac{p_{wf}}{p_r}\right)^2, \tag{5.3}$$

where $Q_{o\max}$ denotes the maximum oil flow rate a well could theoretically deliver at zero p_{wf}.

5.4   Test case

The well under consideration consists of eight inflow points which are distributed along the slightly downward-inclined section of the well, see Fig. 5.2. The flow from all inflow points enters the tubing. The total length of the well is 6670 m. The downward-inclined section of the well is approximately 3000 m long with 1.3 degree downward inclination. The inner diameter of the tubing is 0.089 m. At the top side of the vertical section of the well a separator is located with a constant back pressure of 20 barg. The transient wellbore flow model, OLGA, uses a PI calculated by Cheng's method for each inflow point, which represents the reservoir.
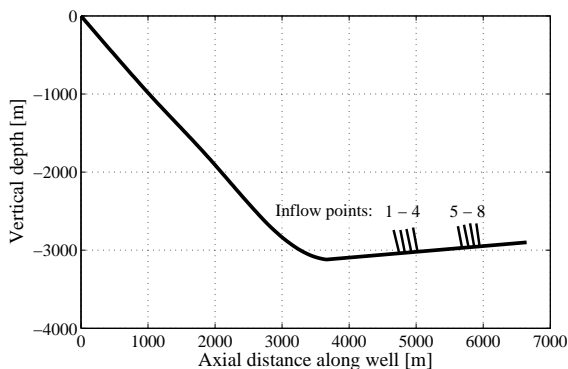

Figure 5.2: *Geometry description of the well. x=0 corresponds to the wellhead.*

Table 5.1 presents the basic reservoir properties and well data.

Table 5.1: *Reservoir and well data*

Initial reservoir pressure	251 bara
Wellhead pressure	21 bara
Oil specific gravity	0.85
Gas specific gravity	0.65
Gas-oil ratio	150 Sm^3/ Sm^3
Tubing inner diameter	0.089 m

It is assumed that PI for all inflow points is the same and is given by Cheng's model. Fig. 5.3 depicts the PI used in this study.

The numerical model, with a total of 281 grid cells in the well, is used to simulate this test case. The maximum and minimum simulation time steps were 5 s and 0.01 s, respectively. We carried out a sensitivity analysis to verify that
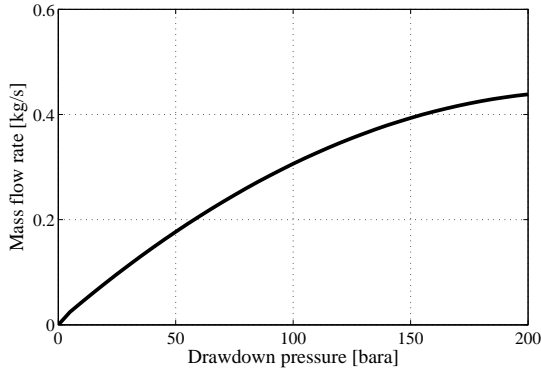
Figure 5.3: *IPR model based on Cheng's formulation.*

the number of grid cells is such that the results are numerically accurate. This was accomplished by meshing the computation domain with 140 and 281 numbers of grid cells. Severe slugging was predicted by both numbers of grid cells. The simulation has been done using a Dell Latitude D830 laptop which has one Intel Core 2 Duo T9300 processor clocked at 2.5 GHz and 3.5 GB of RAM. It takes about 5 hours of CPU time to simulate 30 hours of flow time using the model with 281 grid cells.
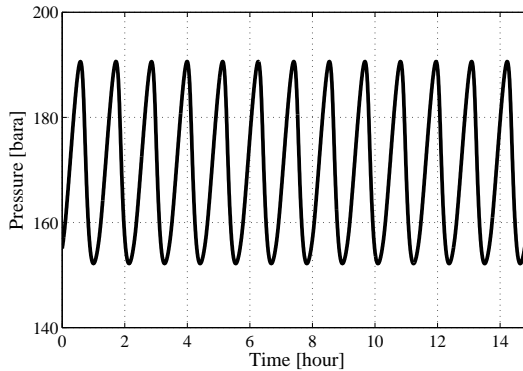
Figure 5.4: *Transient behaviour of pressure at the bottom of the wellbore, x=3670 m.*

Accumulation of a sufficient amount of oil at the lowest point in the well (axial distance along the well equals to 3670 m) creates a blockage. Therefore, a free gas passage is blocked. Oil fallback from the vertical section of the well will contribute to this initial blockage. Then the slug grows mainly in the slightly downward-inclined section and also partly in the vertical section of the well and eventually

is blown out via the vertical section of the well into the separator. In Fig. 5.4, the pressure trend at the lowest point in the wellbore, corresponding to 3670 m axial distance along the well, is plotted.
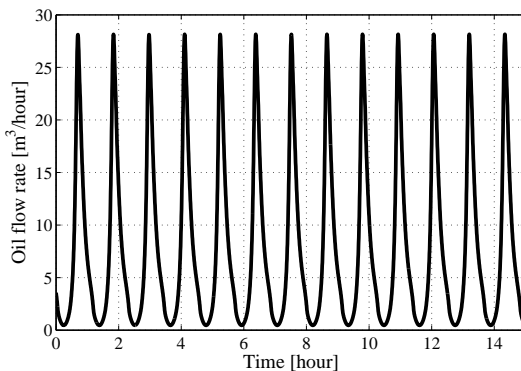
Figure 5.5: *Oil flow rate at the wellhead.*
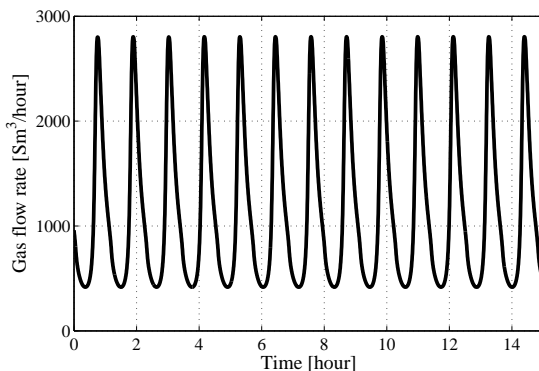
Figure 5.6: *Gas flow rate at the wellhead.*

As already discussed, this instability in the bottom hole pressure is associated with the severe slugging. The period and amplitude of oscillations are approximately 68 minutes and 38 bar respectively. The oil and gas productions as functions of time are plotted in Figs. 5.5 and 5.6, respectively. They show the same pattern as observed for the bottom hole pressure. It is not surprising that the predicted periods of oscillations in the oil and gas flow rates at the wellhead are equal to the one predicted in Fig. 5.4 (68 minutes). The amplitude of the fluctuations in the predicted oil flow rate at the wellhead is approximately 27 $m^3 h^{-1}$. As can be seen from Fig. 5.6, the amplitude of the fluctuations in the predicted gas flow rate at

the wellhead is approximately 2400 Sm^3h^{-1} (the S refers to standard conditions which are 1.01325 bara and 15.56 °C).

When considering a system consisting of only the slightly downward-inclined section, at average flow conditions (pressure = 171 bara, oil flow rate = 14 m^3h^{-1} and gas flow rate = 1610 Sm^3h^{-1}) the predicted flow regime is stratified flow. For a system consisting of only the vertical section, the flow regime in the lower part of the vertical section is predicted to be bubbly flow and in the upper section the hydrodynamic slug flow is predicted. However, the interaction between the downward-inclined section and the vertical section of the well can create a stable blockage, which consequently might lead to the formation of severe slugging.

It should be noted that, a horizontal or an upward-inclined section instead of the slightly downward-inclined section of the well, can prevent the formation of a stable blockage at the lowest point in the well (just before the vertical section of the well) and consequently can eliminate severe slugging. Furthermore, a higher PI can also prevent the formation of severe slugging and a steady flow will occur.

5.5 Concluding remarks

Severe slugging generally occurs in an offshore pipeline-riser system which transports oil and gas from a wellhead placed at the seafloor to a central production platform located at surface. However, it was shown that this phenomenon may also happen at the bottom of a wellbore.

The primary difference between severe slugging occurring at the bottom of the wellbore and that of happening at the surface is the average pressure. Furthermore, the capacity of the tubing at the bottom hole, which depends on the length and diameter of the tubing, is generally smaller than the capacity of the pipeline laid out over the seafloor. Therefore, it is expected that severe slugging at the bottom of the wellbore is less likely to occur. However, it was numerically shown that in the case of an extended reach well, the flow instabilities at the bottom of the wellbore, such as severe slugging, may occur. Thus, the wellbore hydrodynamics should be carefully studied when designing a well with a complicated trajectory such as an extended reach well.

Acknowledgements

Nomenclature

Q_o = volumetric oil flow rate, m^3s^{-1}
p_r = volumetric-average drainage area pressure, Pa
p_{wf} = bottom-hole flowing pressure, Pa
k = reservoir permeability, m^2
h = reservoir thickness, m
r_e = reservoir external boundary, m
r_w = wellbore radius, m
s = skin factor, -
k_{ro} = oil relative permeability, -
μ_o = oil viscosity, Pas
B_o = oil formation volume factor, -
$Q_{o\max}$ = absolute open flow

Abbreviations

PI = Productivity Index
IPR = Inflow Performance Relationship

References

Belfroid, S.P.C., Sturm, W.L., Alberts, G.J.N. et al. 2005. Prediction of Well Performance Instability in Thin Layered Reservoirs. Paper SPE 95835 presented at the SPE Annual Technical Conference and Exhibition, Dallas, Texas, 9-12 October. http://dx.doi.org/10.2118/95835-MS.

Bendiksen, K.H., Malnes, D., Moe, R. et al. 1991. The Dynamic Two-Fluid Model OLGA: Theory and Application. *SPE Prod Eng* **6** (2): 171-180. SPE-19451. http://dx.doi.org/10.2118/19451-PA.

Cheng, A.M. 1990. Inflow Performance Relationships for Solution-Gas-Drive Slanted/Horizontal Wells. Paper SPE 20720 presented at the SPE Annual Technical Conference and Exhibition, New Orleans, Louisiana, 23-26 September. http://dx.doi.org/10.2118/20720-MS.

Dake, L.P. 1978. *Fundamentals of reservoir engineering*. Elsevier Science.

Malekzadeh, R., Mudde, R.F., Henkes, R. A. W. M. *In press*. Severe Slugging in Large-Scale Pipeline-Riser Systems: Experiments and Modelling. *International Journal of Multiphase Flow* (submitted December 23, 2011).

Vogel, J.V. 1968. Inflow Performance Relationships for Solution-Gas Drive Wells.
J. Pet. Tech. **20** (1): 83-92. SPE-1476. http://dx.doi.org/10.2118/1476-PA.

Yocum, B. 1973. Offshore Riser Slug Flow Avoidance: Mathematical Models
for Design and Optimization. Paper SPE 4312 presented at the SPE European
Meeting, London, United Kingdom, 2-3 April. http://dx.doi.org/10.2118/4312-
MS.

Chapter 6

Transient drift flux modelling of severe slugging in pipeline-riser systems[§]

Abstract

A large number of pipelines in the petroleum industry simultaneously transport gas and liquid. Transient behaviour of multiphase flow is frequently encountered in these pipelines. A common example is severe slugging that can occur in multiphase flow systems where a pipeline segment with a downward or even horizontal inclination is followed by a riser segment with an upward inclination. Transient flow conditions associated with severe slugging are relatively slow. Therefore, a transient drift flux model consisting of one momentum balance equation might suffice to express the dynamics of severe slugging. We present a transient drift flux model to simulate severe slugging phenomenon in pipeline-riser systems. The present model contains recently published correlations by Shi et al. for the drift flux slip model which cover the complete range of flow conditions without introducing any discontinuities in the calculated flow parameters. Thus, the transient simulations are converging rapidly and efficiently without applying any form of smoothing. The present model is tested against experimental data for severe slugging showing a better performance than previously published models.

6.1   Introduction

In two-phase flow systems where a pipeline segment with a downward or even horizontal inclination is followed by a riser segment with an upward inclination already at relatively low gas and liquid flow rates, liquid will have the tendency to accumulate at the riser base, blocking over time a free passage of the gas phase. This will result in an increasing liquid level in the riser. As production continues, gas in the pipeline will be accumulated and compressed. At some point as the gas pressure in the pipeline has increased high enough to counter the hydrostatic head of the liquid column in the riser, gas will expand and flush the liquid column out of the riser (see e.g. Malekzadeh et al., 2012).

Severe slugging corresponds to large-amplitude, relatively long-period pressure and flow rates fluctuations compared with hydrodynamic slug flow. This phenomenon creates potential problems at the downstream end of the pipe which has been designed to operate under steady state condition. Moreover, the high pressure fluctuations can reduce the ultimate recovery from the hydrocarbon field.

Severe slugging in a pipeline-riser system was first reported by Yocum (1973). Yocum proposed a minimum mixture velocity as a function of the square of the Froude number to maintain a stable flow. Schmidt et al. (1980) proposed the first model to predict the dynamic slug characteristics of severe slugging. The model required empirical correlations for the liquid holdup in the pipeline and the liquid fallback in the riser. Their results were in reasonable agreement with their experimental data for downward inclination pipelines. However, the model is limited in its application to severe slugging occurring in the portion of the flow pattern map indicated as Region I by the authors. Bøe (1981) proposed a mathematical criterion for the severe slugging region defined by the ratio between the pipeline pressure buildup rate and the riser hydrostatic pressure increase rate. Taitel (1986) investigated the conditions in which an unstable process occurs. The criteria proposed by Bøe (1981) and Taitel (1986) generate a severe slugging envelop in the flow pattern map. Fabre et al. (1990) observed severe slugging not only with a downward inclined pipeline, but also with a horizontal pipeline followed by a vertical riser albeit with a smaller amplitude of pressure fluctuations compared to that of the downward inclined pipeline-riser configuration. Their proposed model was not able to simulate accurately some of their own experimental data. Sarica and Shoham (1991) adapted Fabre's model and presented a simplified transient model. Their simulations showed better accuracy than above mentioned models. However, they assumed gravity-dominant flow in both the pipeline and the riser. When the friction and acceleration terms become important in the momentum equation, the model would suffer from non-convergence as has been observed by the authors. Many researchers have used OLGA, a commercial transient two-fluid multiphase simulator, to simulate the severe slugging phenomenon and study the effects of possible elimination techniques.

In this paper, a general and simple transient drift flux model is proposed to simulate severe slugging. The model contains recently published correlations, for

the profile parameter and drift velocity for the complete range of flow regimes. These correlations were presented by Shi et al. (2005) and have been implemented in the Multi-Segment Well calculations in ECLIPSE, a reservoir simulator developed by Schlumberger. For the model validation we used experimental data of severe slugging in a laboratory scale pipeline-riser system that has been published by Fabre et al. (1990) and we also compared our results with the OLGA version 5.3.2 predictions. The model predicts all the major features of the data and is in good agreement as well. Another advantage of the model is that it offers rapid calculations, because of the following reasons: first, correlations used for the drift flux parameters are functions of in situ gas volume fraction and mixture velocity, so they are not explicit functions of flow regimes. Therefore, the model does not introduce any discontinuities in the calculated parameters as flow regime changes from one to another. These discontinuities would reduce the convergence speed. Second, the transient drift flux model consists of one mixture momentum balance equation instead of two momentum balance equations as in the two-fluid model, like in OLGA.

6.2   The drift flux model

In gas and liquid transport the transient conditions of flow parameters, especially those associated with severe slugging, are relatively slow. Therefore, it is reasonable to express the dynamics of two-phase flow by the drift flux model which is based on one mixture momentum balance equation and an algebraic slip closure equation. The present model is based on one-dimensional, isothermal flow in a pipeline-riser system with a constant cross-sectional area. The liquid phase is assumed to be incompressible. Mass transfer between the phases is neglected.

Note that in real offshore pipeline-riser systems, thermal insulation coating may be applied to the piping systems to maintain the operating temperature of the conduit. This is for instance used when the oil and gas mixture contains waxes that may deposit on the cold pipe wall. If the temperature due to cooling changes substantially, the fluid properties may change appreciably along the pipeline. In those cases, energy balance equations should be added to the transport equations.

6.2.1   Transport equations

The drift flux model is governed by a set of partial differential equations: two mass balance equations, a mixture momentum balance equation and an algebraic slip closure equation. The liquid phase is assumed to be incompressible, thus the mass balance equation of the liquid phase can be written as follows:

$$\frac{\partial \alpha_l}{\partial t} = -\frac{1}{A}\frac{\partial q_l}{\partial x} + \frac{\phi_l}{A\rho_l}, \tag{6.1}$$

where α_l denotes the in situ liquid volume fraction (-), A is the cross-sectional area normal to flow (m^2), q_l is the liquid volume flow rate (m^{3}s^{-1}), ϕ_l represents

liquid inflow $(\text{kgs}^{-1}\text{m}^{-1})$ from side branches and ρ_l is the liquid density (kgm^{-3}). The mass balance equation of the gas phase can be written as:

$$\alpha_g \frac{\partial \rho_g}{\partial t} = \rho_g \frac{\partial \alpha_l}{\partial t} - \frac{1}{A} \frac{\partial (\rho_g q_g)}{\partial x} + \frac{\phi_g}{A}, \tag{6.2}$$

where α_g is the in situ gas volume fraction (-), ρ_g denotes the gas density (kgm^{-3}), q_g is the gas volume flow rate $(\text{m}^3\text{s}^{-1})$, and ϕ_g represents gas inflow $(\text{kgs}^{-1}\text{m}^{-1})$ from side branches. The equation of state for the gas phase can be written as:

$$p = \frac{ZRT}{M} \rho_g, \tag{6.3}$$

where p denotes pressure (Nm^{-2}), Z is the gas compressibility factor (-), R is the universal gas constant $(\text{Jmol}^{-1}\text{K}^{-1})$, T denotes temperature (K), and M is the gas molecular weight (Kgmol^{-1}). We assume that the additional liquid and gas inflow mentioned in Eq. (6.1) and Eq. (6.2) (ϕ_l and ϕ_g) are constant. They flow in radially and do not contribute to the momentum balance equation. The mixture momentum balance equation can be written as:

$$\rho_l \frac{\partial q_l}{\partial t} + \rho_g \frac{\partial q_g}{\partial t} + q_g \frac{\partial \rho_g}{\partial t} = -\frac{\partial \left(\rho_g q_g^2/\alpha_g + \rho_l q_l^2/\alpha_l \right)}{A \partial x} - A \frac{\partial p}{\partial x}$$
$$- A \rho_{\text{mix}} g \sin(\varphi) - A \frac{1}{2} \frac{f}{D} \rho_{\text{mix}} u_{\text{mix}} |u_{\text{mix}}|, \tag{6.4}$$

where $\rho_{\text{mix}} = \alpha_g \rho_g + \alpha_l \rho_l$ (kgm^{-3}), $u_{\text{mix}} = \alpha_g u_g + \alpha_l u_l = \frac{1}{A}(q_g + q_l)$ (ms^{-1}), g is the gravitational acceleration (ms^{-2}), φ is the deviation angle from horizontal (rad), f denotes Moody's friction factor (-), and D is the pipe internal diameter (m).

The drift flux model is used as an algebraic closure equation to express the slip between gas and liquid phases. The drift flux model is formulated as:

$$u_g = C_o u_{\text{mix}} + u_d, \tag{6.5}$$

where C_o (-), and u_d (ms^{-1}) are the profile parameter and drift velocity, respectively. u_g is the gas velocity (ms^{-1}). Eq. (6.5) can be rewritten as:

$$q_g = \frac{\alpha_g}{1 - C_o \alpha_g} (C_o q_l + A u_d). \tag{6.6}$$

Consequently, three partial differential equations, Eq. (6.1), Eq. (6.2) and Eq. (6.4) together with an algebraic closure equation Eq. (6.6), define a system of non-linear partial differential equations for transient modelling of multiphase flow in a pipe and are solved for four unknowns, α_l, p, q_l and q_g.

6.2.2   The slip model

The drift flux model was first proposed by Zuber and Findlay (1965). It expresses the slip between gas and liquid as a combination of two mechanisms. The first mechanism results from the non-uniform distribution of the gas phase and the velocity profile across the cross-section of the pipe. For instance, the concentration of gas in the vertical gas-liquid flow tends to be greater around the centre of the pipe and smaller near the pipe wall. The local mixture velocity is also fastest at the centre of the pipe. Therefore, the velocity of the gas phase averaged across the cross-section of the pipe tends to be greater than that of the liquid phase. The second mechanism results from the tendency of gas to rise vertically through the liquid due to buoyancy. Eq. (6.5) combines the two mechanisms, where C_o describes the effect of the first mechanism and u_d describes the second mechanism.

Many researchers derived relationships for C_o and u_d as functions of flow regimes. In our model we used relationships that have been developed by Shi et al. (2005). These relationships are functions of continuous variables (e.g., in situ gas volume fraction, mixture velocity and inclination angle) and are not functions of discrete variables such as flow regime. Thus they are continuous.

The profile parameter C_o is calculated from the following expression:

$$C_o = \frac{A_e}{1 + (A_e - 1)\,\gamma^2}, \tag{6.7}$$

where A_e is a constant parameter (-). The parameter γ (-) is given by:

$$\gamma = \frac{\beta - B}{1 - B}, \tag{6.8}$$

and the expression for β (-) is:

$$\beta = \max\left(\alpha_g, F_v \frac{\alpha_g |u_{\mathrm{mix}}|}{u_{sgf}}\right), \tag{6.9}$$

where B and F_v are constant parameters (-). $u_{sgf} = \alpha_g u_{gf}$ and u_{gf} (ms^{-1}) represents the flooding velocity which is the minimum gas velocity to prevent a thin annular film of liquid from falling back against the gas flow. Wallis and Makkenchery (1974) obtained the following relation for the flooding velocity:

$$u_{gf} = K_u \left(\frac{\rho_l}{\rho_g}\right)^{1/2} u_c. \tag{6.10}$$

In Eq. (6.10), K_u denotes the critical Kutateladze number (-), which is a function of dimensionless pipe diameter:

$$\hat{D} = \left[\frac{g\,(\rho_l - \rho_g)}{\sigma_{gl}}\right]^{1/2} D, \tag{6.11}$$

and is given in Table 6.1. σ_{gl} is the surface tension of a liquid-gas interface (Nm^{-1}). The characteristic velocity u_c (ms^{-1}) is given by:

$$u_c = \left[\frac{\sigma_{gl} g \left(\rho_l - \rho_g \right)}{\rho_l^2} \right]^{1/4}. \tag{6.12}$$

Table 6.1: *The relationship between the dimensionless pipe diameter and the critical Kutateladze number*

$\hat{D}$	K_u
≤ 2	0
4	1.0
10	2.1
14	2.5
20	2.8
28	3.0
≥ 50	3.2

The drift velocity u_d (ms^{-1}) is evaluated from:

$$u_d = \frac{\left(1 - \alpha_g\right) C_o K(\alpha_g) u_c}{\sqrt{\frac{\rho_g}{\rho_l}} \alpha_g C_o + 1 - \alpha_g C_o}, \tag{6.13}$$

where

$$\begin{aligned}
K(\alpha_g) &= \frac{1.53}{C_o} &&\text{when} \quad \alpha_g \leq a_1, \\
K(\alpha_g) &= K_u &&\text{when} \quad \alpha_g \geq a_2,
\end{aligned} \tag{6.14}$$

and a linear interpolation between these values when $a_1 < \alpha_g < a_2$. a_1 and a_2 are constant parameters (-). Eq. (6.13) is valid for vertical flow. To scale the drift velocity for inclined flow the following relation is applied by Shi et al. (2005):

$$u_d(\theta) = n_1 (\cos\theta)^{n_2} (1 + \sin\theta)^{n_3} \ u_d, \tag{6.15}$$

where θ is the deviation angle from vertical (rad), and $u_d(\theta)$ represents the drift velocity for inclined flow (ms^{-1}). The parameters A_e, B, F_v, a_1, a_2, n_1, n_2 and n_3 in the equations Eq. (6.7), Eq. (6.8), Eq. (6.9), Eq. (6.13) and Eq. (6.15) are user-definable constants (-). These parameters can be tuned to fit observations. Shi et al. (2005) proposed optimized parameters which fit a series of experiments performed in a 6 in. diameter pipe. The corresponding optimized values for the parameters mentioned above are: 1, 0.3, 1, 0.06, 0.21, 1.85, 0.21 and 0.95, respectively.

6.2.3   Numerical scheme

The system of non-linear partial differential equations (PDE's) presented in the previous section for modelling of the transient behaviour of multiphase flow in a pipe cannot be solved analytically. Therefore, numerical methods should be applied to obtain an approximate solution. To solve it numerically, we have to use discretization methods both in space and time to approximate the differential equations by a system of algebraic equations.

Spatial discretization

The first step in obtaining a numerical solution is to discretize the spatial domain and reduce a system of PDE's to a system of ordinary differential equations (ODE's). The finite difference discretization methods are one of the most effective techniques and widely employed to discretize the spatial domain. In our problem, the continuous one-dimensional domain is subdivided into a discrete set of grid nodes. Each node is identified by an index and the size of each grid cell is denoted by Δx. Each node has four unknown variable values α_l, p, q_l and q_g associated with it and must provide four algebraic equations. Spatial derivatives are replaced by finite-difference approximations.

The first spatial derivative in the liquid mass balance, Eq. (6.1), is approximated using backward-difference scheme (BDS) as follows:

$$\frac{\partial q_l}{\partial x} = \frac{q_l^i - q_l^{i-1}}{\Delta x},\tag{6.16}$$

where the superscripts i and $i-1$ represent spatial indices. The first spatial derivative in the gas mass balance, Eq. (6.2), is also approximated by BDS:

$$\frac{\partial (\rho_g q_g)}{\partial x} = \frac{\rho_g^i q_g^i - \rho_g^{i-1} q_g^{i-1}}{\Delta x}.\tag{6.17}$$

The first spatial derivative of pressure $\frac{\partial p}{\partial x}$ in the mixture momentum balance, Eq. (6.4), is approximated by forward-difference scheme (FDS) and the other first spatial derivatives by BDS:

$$\frac{\partial p}{\partial x} = \frac{p^{i+1} - p^i}{\Delta x},\tag{6.18}$$

where the superscript $i+1$ represents the spatial index.

Temporal discretization

In transient flow problems, time is a second coordinate direction that we have to consider. We applied a MATLAB built-in function which uses an algorithm based on fourth and fifth order Runge-Kutta formulas.

Initial condition

Initial conditions are implemented by specifying at time zero the unknown variable values α_l, p, q_l and q_g distributions in the pipe. The steady-state solution can be used as the initial condition.

Boundary condition

In the present study, gas and liquid mass flow rates are specified at the inlet of the pipe and pressure is specified at the outlet of the pipe. At boundary nodes where variable values are given, Dirichlet conditions, no equation is needed. When the boundary conditions involve derivatives, Neumann conditions, the boundary condition must be discretized to add an equation to the set of algebraic equations. At the inlet, flow boundary conditions are implemented as follows:

$$\frac{\partial \alpha_l}{\partial x} = 0, \quad \frac{\partial q_l}{\partial x} = 0, \quad \frac{\partial q_g}{\partial x} = 0 \quad \text{and}$$
$$\frac{\partial \rho_g}{\partial x} = 0. \tag{6.19}$$

At the outlet the following specifies a prescribed pressure:

$$p^{N+1} = p_{\text{specified}}, \tag{6.20}$$

where the outlet is identified by index N.

6.3 Model performance

The following is a comparison of the present model with a severe slugging test case defined by Masella et al. (1998). We also compare the response of the present model with the experimental data of Fabre et al. (1990) and with the predictions of OLGA version 5.3.2 with and without Slugtracking Module.

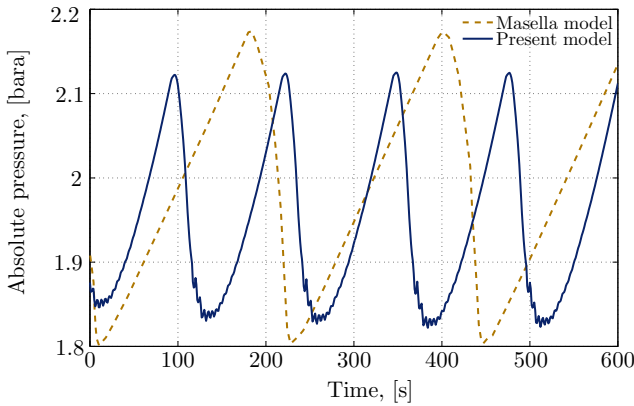### 6.3.1 Comparison with Masella et al. (1998) model

The Masella model is a drift flux model using a different slip model which takes into account the different flow regimes. Therefore, the slip model is a function of the flow regime.[§] We compare the present model and the Masella model on a severe slugging test case which has been defined by Masella. The test loop consists of a 60 m horizontal pipe connected to a 14 m vertical riser. The diameter of the pipe is 0.0508 m. Air and kerosene are the fluids used, and the test loop operates under the atmospheric end pressure. Table 6.2 presents this severe slugging test case.

[§]For more information, see Masella et al. (1998). They used mechanistic models to describe the slip between gas and liquid phases, and their approach is similar to the one described in Chapter 2.

Table 6.2: *Severe slugging test case defined by Masella et al. (1998)*

Pipe geometry	Configuration	Horizontal and vertical
	Length	60 m (hor.) and 14 m (vert.)
	Diameter	0.0508 m
Transient scenario	Inlet gas flowrate	0.000196 kg/s
	Inlet liquid flowrate	0.07854 kg/s
	Outlet pressure	1 bar
Fluid definition and properties	Composition	Air and kerosene
	Gas density	1 kg/m^3
	Liquid density	1000 kg/m^3
	Gas viscosity	1.5 10^{-5} Pa.s
	Liquid viscosity	1.5 10^{-3} Pa.s
	Surface tension	0.07 N/m

Fig. 6.1 shows the comparison between the predicted pressure trends at the bottom of the riser by both models. Both models predict the large amplitude pressure oscillations at the bottom of the riser for the severe slugging test case. Fig. 6.2 compares the transient response of the present model with the transient response of the Masella model on outlet liquid flow rate.

Figure 6.1: *Comparison between the present model and the Masella et al. (1998) model on pressure at the bottom of the riser for the severe slugging test case.*

It is clear that the period of our simulations is roughly twice as small as the period of Masella's simulations. The reason that our model predicts these oscillations with a higher frequency is the different slip model that we used. As will be shown in the following section, this slip model is more realistic than the one has been used by Masella et al. (1998).
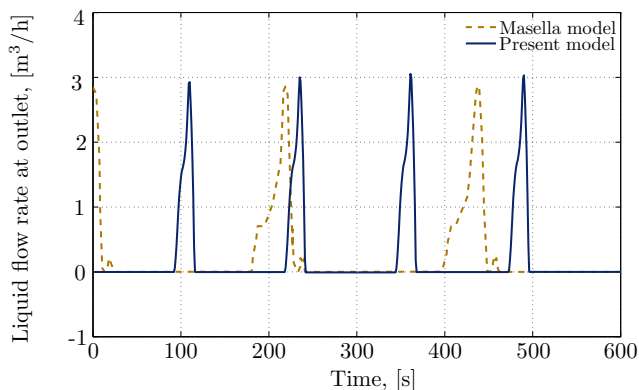
Figure 6.2: *Comparison between the present model and the Masella et al. (1998) model on outlet liquid flow rate for the severe slugging test case.*

A sensitivity analysis was carried out to evaluate the influence of the drift velocity, u_d, mentioned in Eq. (6.13) on the performance of the present model. It was found that an increase by a factor of 2 in the value of u_d decreases the predicted period by the present model from 127 s to 78 s, and the predicted amplitude of the pressure oscillations at the bottom of the riser decreases from about 0.3 bar to 0.2 bar.

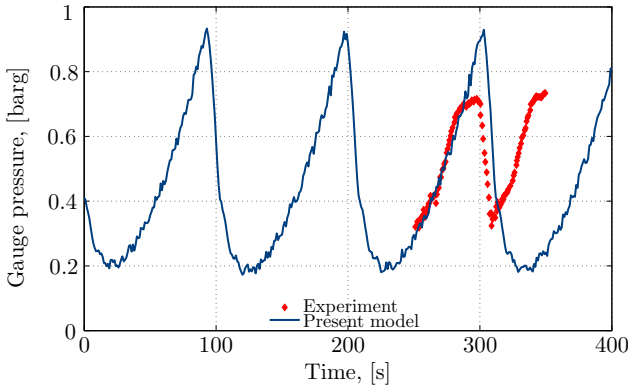### 6.3.2   Comparison with Fabre et al. (1990) experimental data

Next we compare the response of the present model with the experimental data published by Fabre et al. (1990). The test loop consists of a 25 m horizontal pipe connected to a 13.5 m vertical riser. The diameter of the pipe is 0.053 m. Air and water are the fluids used, and the test loop operates under the atmospheric end pressure. The conditions and geometry data are given in Table 6.3.

Fig. 6.3 shows the comparison between the predicted pressure trend at the bottom of the riser by the present model and the Fabre et al. (1990) experimental data. The data from Fabre et al. (1990) are taken as they are in their paper. In their work they start plotting the data from $t = 250$ s. No data are reported before $t = 250$ s. The data that we simulated are shifted in time such that the first rising part of Fabre et al. (1990) data coincides with the rising part of one of the peaks we computed. Note that in our simulation $t = 0$ s is arbitrary. It comes from adjusting the time axis such that the Fabre et al. (1990) curve reproduces at $t = 250$ s. In our simulation we started with initial conditions different from the regular severe slugging shown in Fig. 6.3. Then, the system goes through an initially developing flow before the regular severe slugging region is reached.

The present model is able to predict the cyclic flow behaviour occurring as a result of severe slugging phenomenon and is in reasonable agreement. However,

Table 6.3: *Definition of Fabre et al. (1990) experimental setup*

Pipe geometry	Configuration	Horizontal and vertical
	Length	25 m (hor.) and 13.5 m (vert.)
	Diameter	0.053 m
Transient scenario	Inlet gas flowrate	0.001173 kg/s
	Inlet liquid flowrate	0.1412 kg/s
	Outlet pressure	1 bar
Fluid definition and properties	Composition	Air and water
	Gas density	1.189 kg/m^3
	Liquid density	1000 kg/m^3
	Gas viscosity	1.983 10^{-5} Pa.s
	Liquid viscosity	1.0 10^{-3} Pa.s
	Surface tension	0.073 N/m

Figure 6.3: *Comparison between the present model and the Fabre et al. (1990) experimental data on pressure at the bottom of the riser.*

the predicted period is longer and the predicted pressure amplitude is higher. This suggests firstly, the period predicted by the Masella model in the previous section is too long in comparison with the prediction of the present model and secondly, the slip model used in the present model still does not accurately predict the flow behaviour of the pipeline-riser system.

A sensitivity analysis was carried out to evaluate the influence of the parameters a_1 and a_2 mentioned in Eq. (6.14) on the performance of the present model. It was found that a variation of about 20% in the value of a_1 does not change the predicted period and amplitude of the pressure oscillations. However, 20% increase in the value of a_2 slightly decreases the predicted period by the present model from 110 s to 108 s, and the predicted amplitude of the pressure oscillations at the bottom of the riser slightly decreases from 0.74 bar to 0.71 bar. Also, 20%

decrease in the value of a_2 increases the predicted period by the present model from 110 s to 114 s, and the predicted amplitude of the pressure oscillations at the bottom of the riser slightly increases from 0.74 bar to 0.75 bar. It was also found that 70% increase in the value of u_d decreases the predicted period and amplitude of the pressure oscillations by 21% and 5%, respectively.

As already mentioned in section 6.2.2, the parameters proposed by Shi et al. (2005) are tuned to fit a series of experimental data. It was shown that the performance of the present model is sensitive in particular to variation in a_2. Hence, future experiments are recommended.

6.3.3   Comparison with OLGA version 5.3.2

OLGA is a commercial transient one-dimensional program developed by SINTEF and IFE in Norway, and is based on a two-fluid flow model. It contains three separate mass balance equations for gas, liquid droplets and liquid bulk, which are coupled through interfacial mass transfer terms. Two momentum balance equations are applied; one combined equation for the gas flow with liquid droplets, and one equation for the liquid film flow. Furthermore, a single mixture energy equation is applied (see Bendiksen et al., 1991).

Fig. 6.4 shows the comparison between the present model and OLGA in predicting the Fabre et al. (1990) experimental data. As can be seen, OLGA inaccurately predicts a steady-state solution. Next we use OLGA with Slugtracking Module to simulate the same Fabre et al. (1990) experimental data. This is demonstrated in Fig. 6.5. OLGA with Slugtracking Module generates a transient solution. However, the period seems to be much longer than the period of our simulation and of the experimental data. Moreover, it does not show the constant-amplitude cyclic behaviour as observed by experimental data and simulated by our drift flux model.

6.3.4   Sensitivity analysis

In this section, sensitivity analyses are performed for the period and the amplitude of the pressure oscillations at the bottom of the riser with respect to the variation of the downward angle. Figs. 6.6 and 6.7 illustrate these analyses which are based on the simulations of our drift flux model and OLGA. We use the same input data as given in Table 6.3.

It is expected that small changes in the downward angle would not drastically change the period and the amplitude of the pressure oscillations. As can be seen from Fig. 6.6 to 6.7 for small downward angles, e.g. less than 1°, OLGA's predictions of the period and the amplitude of the pressure oscillations are very sensitive to the variation of the downward angle. However, the present model does not show this (unphysical) sensitivity to the variation of the downward angle. It can be seen that for large downward angle the predictions of two models are converging almost to the same values.
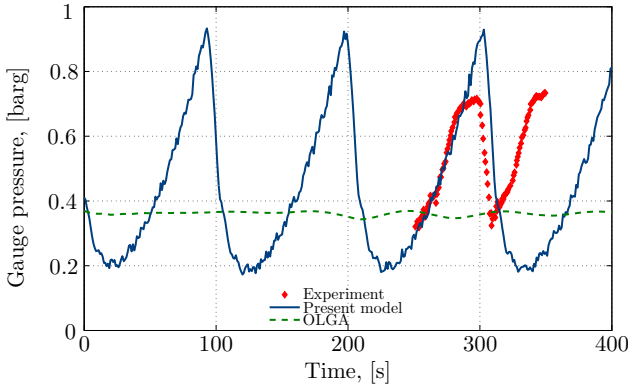
Figure 6.4: *Comparison between the present model, OLGA and the Fabre et al. (1990) experimental data on pressure at the bottom of the riser.*
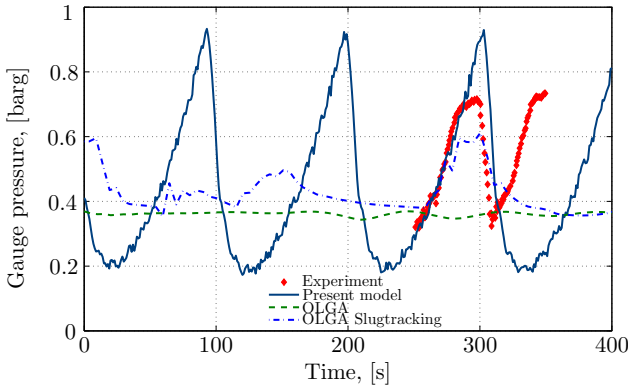
Figure 6.5: *Comparison between the present model, OLGA, OLGA with Slugtracking Module and the Fabre et al. (1990) experimental data on pressure at the bottom of the riser.*

6.4   Conclusions

(1) A general transient drift flux model is presented which contains recently published correlations for the slip model. These correlations make the algebraic slip model to be a function of continuous variables and not a function of discrete variables such as the flow regime.

(2) It has been shown that the model is able to predict the cyclic flow behaviour on a severe slugging test case.
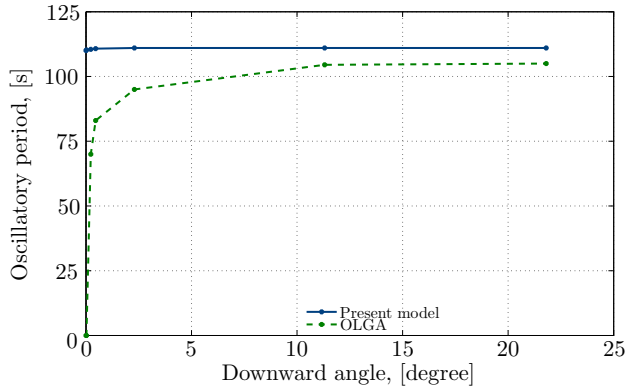
Figure 6.6: *Comparison between the sensitivity of the present model and OLGA on the periods of oscillations with respect to the downward angle.*
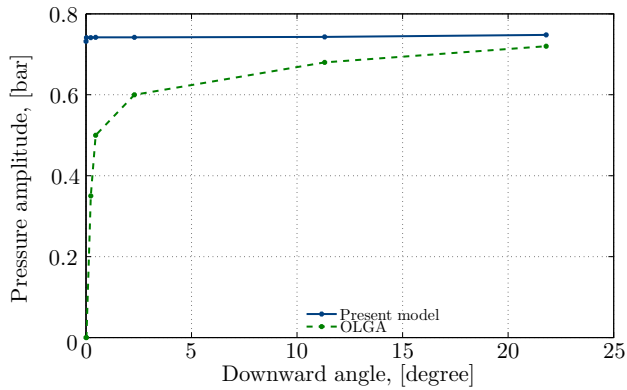
Figure 6.7: *Comparison between the sensitivity of the present model and OLGA on the amplitudes of the pressure oscillations at the bottom of the riser with respect to the downward angle.*

(3) The model has been tested against the Fabre et al. (1990) experimental data in a laboratory scale horizontal pipeline-vertical riser system. The model predicts all the major features of the data and is in reasonable agreement as well.

Acknowledgements

References

Bendiksen, K., Malnes, D., Moe, R., Nuland, S., 1991. The dynamic two-fluid model OLGA: Theory and application. SPE Production Eng. J. 6, 171-180.

Bøe, A., 1981. Severe slugging characteristics; part 1: Flow regime for severe slugging; part 2: Point model simulation study. Presented at Selected Topics in Two-Phase Flow, Trondheim, Norway.

Fabre, J., Peresson, L., Corteville, J., Odello, R., Bourgeols, T., 1990. Severe slugging in pipeline/riser systems. SPE Production Eng. J. 5, 299-305.

Malekzadeh, R., Henkes, R.A.W.M., Mudde, R.F. Severe slugging in a long pipelineriser system: Experiments and predictions. Int. J. Multiphase Flow (2012), http://dx.doi.org/10.1016/j.ijmultiphaseflow.2012.06.004

Masella, J., Tran, Q., Ferre, D., Pauchon, C., 1998. Transient simulation of two-phase flows in pipes. Int. J. Multiphase Flow 24, 739-755.

Sarica, C., Shoham, O., 1991. A simplied transient model for pipeline-riser systems. Chemical Engineering Science 46, 2167-2179.

Schmidt, Z., Brill, J., Beggs, H., 1980. Experimental study of severe slugging in a two-phase-flow pipeline-riser pipe system. SPE J. 20, 407-414.

Shi, H., Holmes, J., Durlofsky, L., Aziz, K., Diaz, L., Alkaya, B., Oddie, G., 2005. Drift-flux modeling of two-phase flow in wellbores. SPE J. 10, 24-33.

Taitel, Y., 1986. Stability of severe slugging. Int. J. Multiphase Flow 12, 203-217.

Wallis, G., Makkenchery, S., 1974. The hanging film phenomenon in vertical annular two-phase flow. J. Fluids Engineering 96, 297-298.

Yocum, B., 1973. Offshore riser slug flow avoidance, mathematical model for design and optimization. paper SPE 4312 presented at SPE Annual European Meeting, London.

Zuber, N., Findlay, J., 1965. Average volumetric concentration in two-phase flow systems. J. Heat Transfer 87, 453-467.

Severe slugging in a long pipeline-riser system: Experiments and predictions§

Abstract

At constant inflow conditions, large-amplitude pressure and flow rate fluctuations may occur in a pipeline-riser system operating at relatively low liquid and gas flow rates. This cyclic flow instability has been referred to as severe slugging. This study is an experimental, theoretical and numerical investigation of severe slugging in a relatively long pipeline-riser system. The experiments were carried out in a 65 m long, 50.8 mm diameter horizontal steel pipeline connected to a 35 m long, 50.8 mm diameter Perspex pipeline which is inclined to -2.54° from the horizontal, followed by a 15.5 m high, 45 mm vertical PVC riser operating at atmospheric end pressure. The experimental facility also included a 250 l gas buffer vessel, placed upstream of the pipeline, to obtain extra pipeline compressibility. Air and water were used as the experimental fluids. Five types of flow regimes were found and characterized based on visual observation and on the measured pressure drop over the riser. It was found that transient slugs were generated in the pipeline upstream of the riser base and they effectively contributed to the initial blockage of the riser base. An existing model for the prediction of the flow behaviour in the pipeline-riser system was modified. The modified model, which was tested against new experimental results obtained in this study, showed

a better performance than previously published models. Numerical simulations were also performed using a one-dimensional two-fluid model. A good agreement between the numerical simulations and the experimental data was found.

7.1   Introduction

Many of the world's giant oil fields have entered into a later stage of their production life, which is characterized by low oil production rates. As also the amount of easily accessible oil is decreasing, production from more difficult fields, like in deepwater locations, will play a larger role to contribute to meeting the world's energy challenges. Based on the current definition of deepwater used by the United States Bureau of Ocean Energy Management, Regulation and Enforcement, all fields in water depths of 300 m and greater are identified as deepwater fields. Multiphase hydrocarbons (plus often also formation water) are produced from subsurface deepwater oil fields and transported through longer delivery systems (pipeline and riser) to central production platforms. The diameter of the pipeline and the riser typically ranges from 0.1 to 0.8 m. The length of the pipeline can vary from a few kilometers to more than hundred kilometers. The height of the riser depends on the water depth, which can range from 300 m (the minimum water depth at which a deepwater field starts) to more than two kilometers. One of the challenging flow-assurance problems in the production from deepwater oil fields is slugging. This can be riser base slugging or severe slugging at end-of-field-life conditions, or density wave instabilities that can occur in a long riser when the gas is expanding due to the decreasing pressure when going up into the riser. Knowing under what conditions these unstable flows occur, and how this can be prevented, is of key importance when designing and operating such large systems.

Severe slugging is a transient cyclic phenomenon which may occur in multiphase pipeline-riser systems. At relatively low flow rates, liquid accumulates at the riser base, creating a blockage for the gas, until sufficient upstream pressure has been built up to flush the liquid slug out of the riser. After this liquid surge, and subsequent gas surge, the remaining liquid in the riser falls back to the riser base to create a new blockage and the cycle is repeated. Severe slugging causes large-amplitude pressure and flow rate fluctuations. Therefore, it creates potential problems in the platform facilities downstream of the riser top, which have been designed to operate under steady state conditions (such as separators, pumps, and compressors). For example, the peak flow rates during the liquid and gas surges might cause flooding and overpressurization of the separator, which consequently might lead to the complete shutdown of a production facility. Moreover, an increased back pressure at the well head may lead to the end of the production and abandonment of the well.

Severe slugging has been studied both experimentally and numerically by several investigators (see Schmidt et al., 1980; Pots et al., 1987; Taitel et al., 1990;

Fabre et al., 1990; Sarica and Shoham, 1991; Baliño et al., 2010). However, most of the existing laboratory experiments for severe slugging were conducted for relatively short pipeline-riser systems. The pipeline length was limited to a maximum of 57.4 m and the riser height has a maximum of 15 m. Because of the importance of flow instability in practical applications, severe slugging characteristics in long pipeline-riser systems should be studied further. Therefore, we have carried out experiments for the two-phase flow of air and water in a relatively long pipeline-riser system (a 123 m long pipeline represented by a gas buffer vessel connected to a 100 m long pipeline followed by a 15.5 m high riser).

Bøe (1981) and Taitel (1986) investigated the conditions in which an unstable process occurs. Their proposed analytical criteria generate a severe slugging envelop in the flow pattern map. Jansen et al. (1996) studied both theoretically and experimentally the effect of choking on severe slugging characteristics in a relatively short pipeline-riser system (a 10 m long pipeline represented by a gas buffer vessel connected to a 9.1 m long pipeline followed by a 3 m high riser). They modified the Taitel (1986) stability criteria to include the effect of the back pressure imposed by choke which was placed at the riser top. However, the two-phase time averaged pressure drop across the choke was assumed to be a function of single-phase liquid flow.

The main objective of the present study is to obtain a better understanding of the severe slugging characteristics in a long pipeline-riser system. To accomplish this objective, experiments were conducted to identify and characterize any possible flow instability in a flow pattern map of a relatively long pipeline-riser system. Numerical simulations were also performed to find out to what extent the experimental results can be reproduced. A final objective is to assess the applicability of the existing stability criteria for predictions of the boundary between stable (steady state) and unstable (severe slugging) flow in a long pipeline-riser system equipped with a choke at the riser top, and modify them if necessary.

This paper is organized as follows: in Section 7.2 the experimental facility is described; in Section 7.3 the experimentally observed flow regimes and also the flow pattern map are presented; in Section 7.4 stability maps are obtained by using the existing and modified stability criteria and are compared with experimental results; in Section 7.5 numerical simulations are performed and a comparison is made with the experimental data; in the last section the conclusions of the study are presented.

7.2 Experimental facility

The existing two-phase, air and water flow facility of the Shell Technology Centre in Amsterdam (STCA), see Fig. 7.1, was used to conduct the experiments. This facility was also used by Malekzadeh et al. (submitted for publication) to study the flow instabilities in a horizontal pipeline-riser system. The test facility comprises four main parts: the fluid supply, test loop (pipeline and riser), separation

area and measurement and control devices. This facility is powered and controlled by the Fieldpoint 2000 system of National Instruments and by Labview, which are the control hardware and software, respectively. The full experimental procedures, including startup, control, shutdown and data logging are done remotely through dedicated control and data acquisition systems.
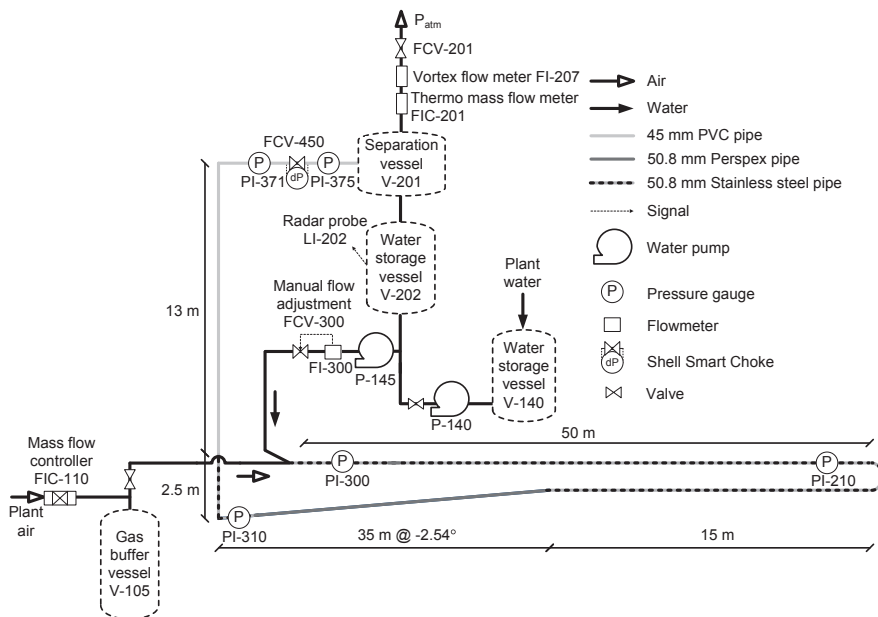
Figure 7.1: *Schematic of the experimental facility.*

Dry air at a pressure of 6 barg is delivered via a connection with the main air supply at the STCA. The air is supplied to a thermal mass flow meter and controller of model 5853E by Brooks, which automatically provides an almost constant mass flow rate into the test loop. The gas mass inflow rate varies by less than 0.1%. A maximum air flow rate of 30 $\mathrm{Sm^3\,h^{-1}}$ can be supplied (the S refers to standard conditions which are 1.00 bara and 15.56 °C). The water supply is city tap water connected to the first water storage tank (V-140), see Fig. 7.1. A worm pump connected to V-140 brings water to the second water storage tank situated right below the separator. Then water is supplied to the pipeline by a variable speed centrifugal pump. A relatively constant water volumetric flow rate can be achieved by manually adjusting the pump speed and by adjusting the opening of a control valve, which is located directly downstream of the pump. The liquid inflow rate varies by less than 4%. A maximum water flow rate of 5 $\mathrm{m^3\,h^{-1}}$ can be supplied. The water flow rate into the test loop is measured with an electromagnetic flow meter of type Promag 50W by Endress & Hauser.

The test loop consists of a 65 m long, 50.8 mm diameter horizontal steel pipeline connected to a 35 m long, 50.8 mm diameter Perspex pipeline which is inclined to -2.54° from the horizontal, followed by a 15.5 m high, 45 mm vertical PVC riser. The Perspex pipeline and the PVC riser are transparent, allowing visual observation of the flow behaviour in the system. The riser discharges the fluid into the two-phase separator, operating at atmospheric pressure. The separator pressure varies by less than 3%. Air and water are separated by gravity. The upper section of the separator has a mist mat and dry air is vented to the open air, monitored by one vortex and one thermo mass flow indicators. The lower section of the separator drains the water, which flows down and returns to the second water storage tank. The water level in this tank is measured with a continuous level transmitter of type Levelflex M-FMP40 by Endress & Hauser, which can provide an estimation of the water outflow. A variable-volume gas buffer vessel is located between the gas mass flow controller and the gas inlet, upstream of the pipeline. The air volume of the buffer vessel can be adjusted by partly filling it with water. The function of the gas buffer vessel is to create a virtually longer pipeline. In the current study, the air volume of the buffer vessel is set at 250 l, which corresponds to an additional pipeline length of 123 m. It should be noted that the facility also included a choke at the riser top, which has a K_v value (flow factor) of 10 $m^3 h^{-1} bar^{-1/2}$. During all experiments this choke was left fully open. Pressure transducers are located at the inlet of the pipeline, approximately at the middle of the pipeline, at the riser base and at the top of the riser before and after the choke. These pressure transducers are manufactured by Endress & Hauser and are of type Cerebar M-PMC41 and Cerebar S-PMP71. Additional pressure devices are also used to measure and monitor the pressure in the gas buffer vessel, the inlet of the gas line, the outlet of the liquid pump and in the two-phase separator. The temperatures of the fluids are measured with temperature transmitters that are located at various locations in the test loop.

7.3   Riser-induced instabilities

Based on preliminary numerical simulations an experimental matrix is defined to cover all possible flow regimes occurring in the test loop. Later, by obtaining further experimental results this experimental matrix was refined to establish both the characteristics of each flow regime and the transition boundaries between the flow regimes. The water flow rate ranges from 0.14 $m^3 h^{-1}$ to 4.38 $m^3 h^{-1}$ and the air flow rate from 2.49 $Sm^3 h^{-1}$ to 29.98 $Sm^3 h^{-1}$. The corresponding superficial water velocity ranges from U_{SL}= 0.02 - 0.60 $m s^{-1}$ and the superficial air velocity at standard conditions (1.00 bara, 15.56 °C) ranges from U_{SG0}= 0.34 - 4.11 $m s^{-1}$. Different flow patterns have been obtained by fixing the water flow rate and by changing the air flow rate. The observed flow patterns are classified into five categories: stable flow (STB), unstable oscillations (USO), severe slugging of type 1 (SS1), severe slugging of type 2 (SS2), and severe slugging of type 3 (SS3). A

classification of severe slugging is given by Baliño et al. (2010), who distinguished the types 1, 2, and 3. In this paper, the same abbreviations were used for the classification of the flow regimes. The flow patterns were identified based on visual observations and on the analysis of the pressure drop over the riser (riser ΔP). The riser ΔP is also used for defining different stages of a severe slugging cycle; the riser ΔP is defined as the difference between the pressure at the riser base and the riser top. Typical riser ΔP traces of these five flow patterns are shown in Fig. 7.2. The above mentioned, experimentally observed, flow patterns are described below.
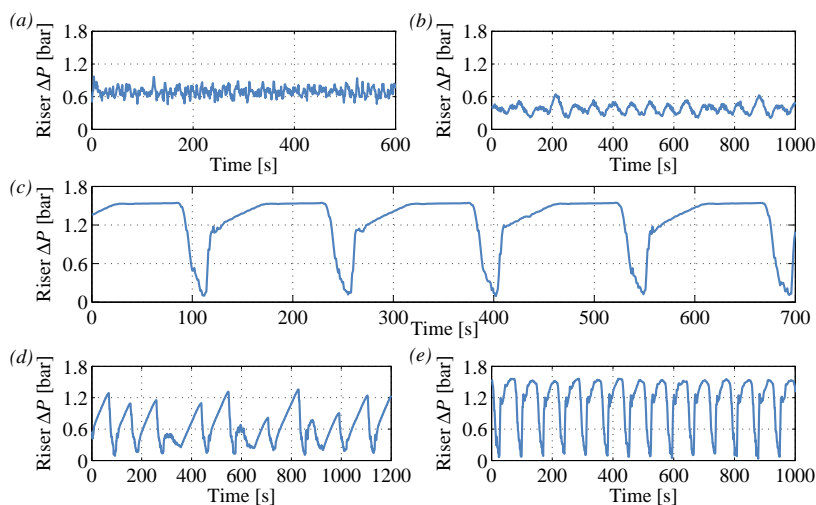
Figure 7.2: *Experimental riser ΔP traces of the five mentioned flow patterns corresponding to (a) STB (U_{SL}=0.50 $m\,s^{-1}$ & U_{SG0}=4.00 $m\,s^{-1}$), (b) USO (U_{SL}=0.10 $m\,s^{-1}$ & U_{SG0}=3.75 $m\,s^{-1}$), (c) SS1 (U_{SL}=0.24 $m\,s^{-1}$ & U_{SG0}=0.90 $m\,s^{-1}$), (d) SS2 (U_{SL}=0.10 $m\,s^{-1}$ & U_{SG0}=2.00 $m\,s^{-1}$) and (e) SS3 (U_{SL}=0.50 $m\,s^{-1}$ & U_{SG0}=2.00 $m\,s^{-1}$).*

7.3.1   Stable flow

At relatively high liquid and gas flow rates, short hydrodynamic slugs are generated in the pipeline and they are moving up into the riser. Therefore, the flow patterns in the pipeline and in the riser are mainly hydrodynamic slug flow. The riser ΔP exhibits fluctuations with a small amplitude (less than approximately 0.4 bar in our experiments) and a relatively high frequency. Thus, hydrodynamic slug flow is considered to be stable flow as compared to other types of flow regime mentioned in this study.

7.3.2   Unstable oscillations

This flow regime is characterized by an oscillating gas void fraction in the riser and also in the pipeline. The gas and liquid phases flow continuously through the riser base into the riser. The amplitude of the pressure oscillations is much smaller compared to other types of severe slugging. The flow pattern in the riser changes from hydrodynamic slug flow to churn flow and in the pipeline from hydrodynamic slug flow to stratified flow. This process exhibits a cyclic behaviour.

7.3.3   Severe slugging of type 1

Various researchers, including Schmidt et al. (1980) and Taitel (1986) described a cycle of SS1 in four stages: (1) slug formation; (2) slug movement into the separator; (3) blowout; (4) liquid fallback. However, to highlight the differences between all types of severe slugging, we can better describe a cycle of SS1 in five stages: (1) blockage of the riser base; (2) slug growth; (3) liquid production; (4) fast liquid production; (5) gas blowdown. In Fig. 7.3a these five stages are illustrated. They are also marked on a measured cycle of the riser ΔP for SS1 corresponding to $U_{SL}=0.20$ m s^{-1} and $U_{SG0}=1.00$ m s^{-1}, as shown in Fig. 7.3b. The process of SS1 can be described as follows (Seim et al. (2011)).

Figure 7.3: *Stages for severe slugging of type 1 (a) a graphical illustration (b) marked on a cycle of an experimental riser ΔP trace ($U_{SL}=0.20$ m s^{-1} & $U_{SG0}=1.00$ m s^{-1}).*

Accumulation of a sufficient amount of liquid at the riser base creates a full blockage. Therefore, a free gas passage is blocked. Liquid fallback from the riser and also transient slugs generated in the pipeline will contribute to this initial blockage. This stage is called blockage of the riser base. As both phases continue to flow into the pipeline while the gas passage is blocked, the liquid level in the riser increases. As a consequence, the pressure at the riser base increases, pushing the liquid-gas interface in the pipeline further away from the riser base and compressing the accumulated gas in the pipeline. This stage is known as

slug growth. When the liquid level reaches the riser top, the pressure at the riser base reaches its maximum and the pressure of the compressed gas in the pipeline becomes higher than the hydrostatic head of the liquid-filled riser. Liquid starts to flow out at the riser top and simultaneously the slug tail in the pipeline will be pushed towards the riser base. This is the liquid production stage. When the gas phase penetrates into the riser, the hydrostatic head of the riser decreases. The gas will expand and flush the liquid column out of the riser. This stage is known as fast liquid production. After that, gas will be produced at a high rate, causing a quick depressurization of the system. This is the gas blowdown stage. Once the gas is expelled, the pressure reaches its minimum leading to the fallback of the remaining liquid and accumulation at the riser base, and the cycle repeats.

The following features can be concluded from Fig. 7.3b.

- The pressure drop for the initial liquid fallback is 0.11 bar.

- As a direct consequence of the quick depressurization of the pipeline in each cycle, the gas velocity in the pipeline increases, which in turn generates transient slugs. The transient slugs increase the liquid volume fraction in the riser by 57%. It should be noted that, part of the transient slugs remains in the pipeline and contributes to the formation of the slug in the pipeline.

- The maximum riser ΔP is 1.53 bar. This corresponds to 100% of liquid volume fraction in the riser. Also the riser ΔP remains at its maximum for a certain period of time (about 40 s).

It should be noted that the above mentioned comments are based on two assumptions: first, the air density is negligible compared to the water density, and second, frictional and accelerational pressure drops in the riser are negligible compared to gravitational pressure drop. Therefore, the riser ΔP is considered to be equal to the hydrostatic head of the liquid in the riser.

7.3.4   Severe slugging of type 2

The transitional severe slugging of type 2 is qualitatively similar to SS1, but the slug length is shorter than the height of the riser and it often has intermittent unstable oscillations. In Fig. 7.4a four stages of SS2 are illustrated. They are also marked on the experimental cycle for the riser ΔP of SS2 corresponding to U_{SL}=0.10 m s^{-1} and U_{SG0}=2.00 m s^{-1}, as shown in Fig. 7.4b.

During the process of SS2 the riser base is generally penetrated by gas prior to the liquid filling the whole riser. Therefore, the maximum riser ΔP is lower than that of SS1, i.e. less than 1.53 bar in our experiments. It should be noted that contrary to SS1, the liquid-gas interface remains close to the riser base. Thus, slugs only grow in the riser and they also differ in length.
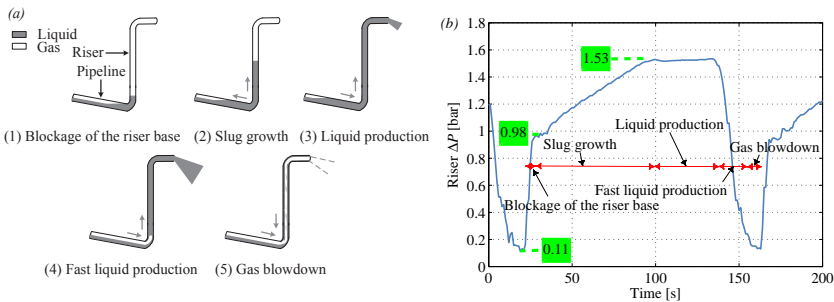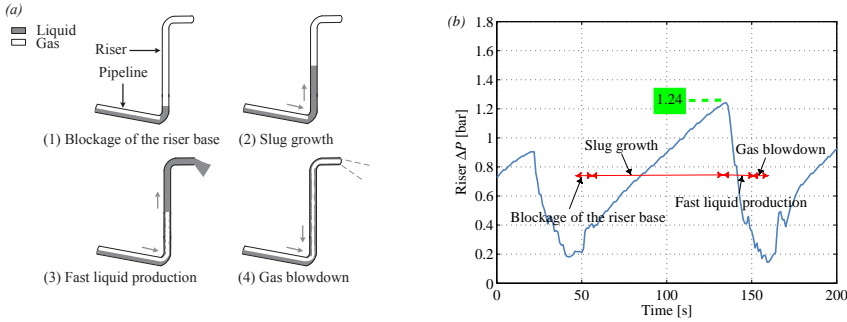
Figure 7.4: *Stages for severe slugging of type 2 (a) a graphical illustration (b) marked on a cycle of an experimental riser ΔP trace (U_{SL}=0.10 $m\,s^{-1}$ & U_{SG0}=2.00 $m\,s^{-1}$).*

7.3.5   Severe slugging of type 3

We describe a cycle of SS3 in four stages: (1) transient slugs; (2) aerated slug growth; (3) fast aerated liquid production; (4) gas blowdown. In Fig. 7.5a these four stages are illustrated. They are also marked on the experimental cycle for the riser ΔP of SS3 corresponding to U_{SL}=0.39 $m\,s^{-1}$ and U_{SG0}=2.33 $m\,s^{-1}$, as shown in Fig. 7.5b. The process of SS3 can be described as follows.
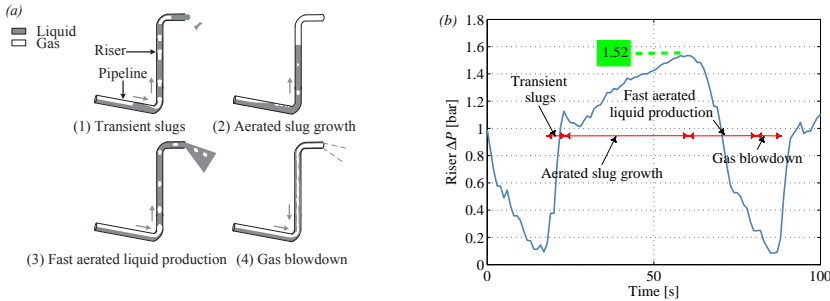
Figure 7.5: *Stages for severe slugging of type 3 (a) a graphical illustration (b) marked on a cycle of an experimental riser ΔP trace (U_{SL}=0.39 $m\,s^{-1}$ & U_{SG0}=2.33 $m\,s^{-1}$).*

Transient slugs are generated in the pipeline upstream of the riser base and they flow up the riser. This stage is called transient slugs. Part of the liquid in the transient slugs falls back through the riser and creates local flow reversal of liquid and gas (as small bubbles) at the riser base, generating a long aerated liquid slug. As a result, the flow regime in the pipeline close to the riser base changes

from hydrodynamic slug flow to elongated bubble flow. This long aerated liquid slug contains small bubbles of different size and shape. The aerated liquid slug gradually flows in the riser and the liquid content of the riser (the riser ΔP) gradually increases. This is the aerated slug growth stage. Contrary to the severe slugging of type 1, SS3 does not give full riser base blockage and production starvation as small bubbles continuously flow from the riser base and penetrate into the riser. When the compressed gas upstream of the riser base penetrates into the riser, the hydrostatic head of the riser decreases, the gas will expand and accelerate the aerated slug into the separator. This stage is called fast aerated liquid production. Finally, when the aerated liquid has been produced, the gas will flow out at a high velocity, causing a quick depressurization of the system. When the gas is expelled, the pressure reaches its minimum leading to the fallback of the remaining liquid. This is the gas blowdown stage. During the gas blowdown, the gas velocity in the pipeline increases. This leads to the generation of transient slugs in the pipeline and the cycle is repeated.

As can be seen from Fig. 7.5b, the pure liquid production stage, which implies a period of constant riser ΔP of 1.53 bar, does not exist. Instead, only the maximum riser ΔP (of 1.52 bar) is reached and then the riser ΔP starts dropping immediately. It should be noted that, part of the liquid in the transient slugs flows into the separator. Then after a while the aerated liquid slug flows in the riser. This is visible from the dip in the riser ΔP trace (at time=23 s) and it is also confirmed by visual observation and by the measured liquid outflow.
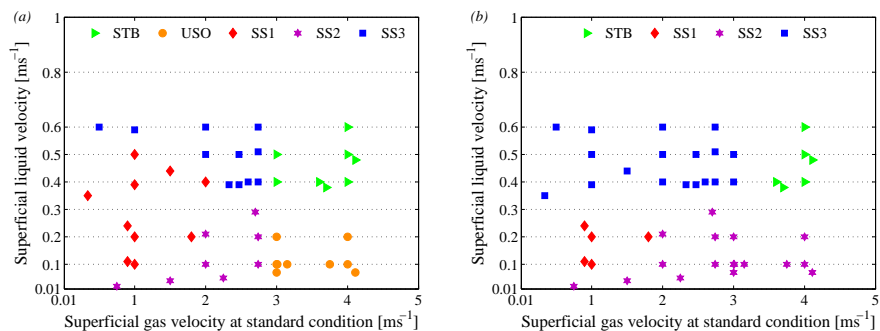
Figure 7.6: *Flow pattern map of the system, indicating stable flow (STB), unstable oscillations (USO), severe slugging of type 1 (SS1), severe slugging of type 2 (SS2), and severe slugging of type 3 (SS3) (a) experimental flow pattern map (b) numerical flow pattern map.*

Fig. 7.6a shows the flow map of the downward inclined pipeline-riser system generated based on our experimental data, indicating whether each point is in STB, USO, SS1, SS2 or SS3 flow regime. Flow patterns have an important in-

fluence on the prediction of the multiphase flow parameters, e.g. liquid holdup and pressure gradient (Shoham, 2006). Therefore, such a flow pattern map can be used in design and operation phase in an offshore oil-production system.

Table 7.1 summarizes the considered experimental cases with their associated superficial liquid and gas velocities for SS1, SS2, SS3, USO, and STB. The measured time period as well as the average maximum, minimum and amplitude of the riser ΔP are also given in Table 7.1.

Table 7.1: *Experimental and simulation results of the period, the average maximum, minimum and amplitude of the riser ΔP for all cases. Colours distinguish different experimentally-observed flow regimes.*

Case	U_{SL} (ms^{-1})	U_{SG0} (ms^{-1})	Type Exp.	Type Sim.	Period (s) Exp.	Period (s) Sim.	Max ΔP (bar) Exp.	Max ΔP (bar) Sim.	Min ΔP (bar) Exp.	Min ΔP (bar) Sim.	Amplitude of ΔP (bar) Exp.	Amplitude of ΔP (bar) Sim.
1	0.10	1.00	SS1	SS1	179	211	1.53	1.53	0.09	0.14	1.44	1.39
2	0.20	1.00	SS1	SS1	135	154	1.53	1.53	0.11	0.16	1.42	1.37
3	0.39	1.00	SS1	SS3	109	105	1.53	1.19	0.10	0.21	1.43	0.98
4	0.40	2.00	SS1	SS3	78	77	1.53	1.23	0.07	0.22	1.46	1.01
5	0.50	1.00	SS1	SS3	95	95	1.53	1.25	0.09	0.19	1.44	1.06
6	0.11	0.90	SS1	SS1	185	211	1.53	1.53	0.08	0.14	1.45	1.39
7	0.20	1.80	SS1	SS1	101	108	1.53	1.53	0.10	0.17	1.43	1.36
8	0.24	0.90	SS1	SS1	148	138	1.53	1.53	0.11	0.18	1.42	1.35
9	0.35	0.34	SS1	SS3	173	143	1.53	1.16	0.55	0.39	0.98	0.77
10	0.44	1.50	SS1	SS3	90	85	1.53	1.23	0.10	0.18	1.43	1.05
11	0.10	2.00	SS2	SS2	92&138	76&191	1.35	1.49	0.14	0.11	1.21	1.38
12	0.10	2.74	SS2	SS2	72	108&160	1.02	1.50	0.20	0.14	0.82	1.36
13	0.21	2.00	SS2	SS2	96	98	1.52	1.50	0.08	0.16	1.44	1.34
14	0.20	2.74	SS2	SS2	68	63	1.50	1.50	0.13	0.18	1.37	1.32
15	0.02	0.75	SS2	SS2	227&159	138&286	1.45	0.71	0.12	0.12	1.33	0.59
16	0.04	1.50	SS2	SS2	119	211	0.75	1.11	0.19	0.09	0.56	1.02
17	0.05	2.25	SS2	SS2	93	143	0.89	0.99	0.18	0.11	0.71	0.88
18	0.29	2.70	SS2	SS2	82	72	1.52	1.20	0.09	0.20	1.43	1.00
19	0.39	2.33	SS3	SS3	72	72	1.53	1.23	0.08	0.21	1.45	1.02
20	0.39	2.47	SS3	SS3	69	70	1.52	1.23	0.10	0.19	1.42	1.04
21	0.40	2.60	SS3	SS3	63	67	1.50	1.23	0.10	0.19	1.40	1.04
22	0.40	2.74	SS3	SS3	60	66	1.40	1.22	0.15	0.19	1.25	1.03
23	0.50	2.00	SS3	SS3	72	73	1.53	1.28	0.08	0.20	1.45	1.08
24	0.50	2.47	SS3	SS3	64	66	1.44	1.29	0.11	0.20	1.33	1.09
25	0.51	2.74	SS3	SS3	57	63	1.35	1.30	0.20	0.20	1.15	1.10
26	0.60	0.50	SS3	SS3	113	98	1.53	1.28	0.73	0.49	0.80	0.79
27	0.59	1.00	SS3	SS3	86	89	1.53	1.29	0.09	0.23	1.44	1.06
28	0.60	2.00	SS3	SS3	64	68	1.51	1.33	0.13	0.23	1.38	1.10
29	0.60	2.74	SS3	SS3	57	59	1.21	1.34	0.33	0.24	0.88	1.10
30	0.10	3.00	USO	SS2	64	98	0.56	1.11	0.27	0.17	0.29	0.94
31	0.10	3.01	USO	SS2	64	98	0.58	1.11	0.27	0.17	0.31	0.94
32	0.10	3.15	USO	SS2	65	95&191	0.49	1.09	0.27	0.17	0.22	0.92
33	0.10	4.00	USO	SS2	53	86&155	0.46	0.98	0.26	0.18	0.20	0.80
34	0.20	3.00	USO	SS2	60	60&236	0.60	1.49	0.35	0.20	0.25	1.29
35	0.20	4.00	USO	SS2	43	60	0.57	0.56	0.37	0.19	0.20	0.37
36	0.07	3.00	USO	SS2	72	56&111	0.57	1.06	0.23	0.14	0.34	0.92
37	0.07	4.11	USO	SS2	73	95	0.49	0.80	0.23	0.15	0.26	0.65
38	0.10	3.75	USO	SS2	67	87&174	0.53	1.02	0.25	0.19	0.28	0.83
39	0.40	3.00	STB	SS3	51&25	63	0.82	1.21	0.50	0.19	0.32	1.02
40	0.40	4.00	STB	STB	11	54	0.77	0.83	0.48	0.24	0.29	0.59
41	0.50	3.00	STB	SS3	53&26	60	0.91	1.30	0.50	0.20	0.41	1.10
42	0.50	4.00	STB	STB	11	53	0.85	0.99	0.52	0.30	0.33	0.69
43	0.60	4.00	STB	STB	12	52	0.97	1.08	0.62	0.39	0.35	0.69
44	0.38	3.70	STB	STB	14	56	0.74	0.83	0.51	0.20	0.23	0.63
45	0.40	3.60	STB	STB	16	56	0.79	0.88	0.48	0.20	0.31	0.68
46	0.48	4.11	STB	STB	23	53	0.84	0.94	0.53	0.27	0.31	0.67

The uncertainty in the measured amplitude of the riser ΔP is less than 1%. U_{SG0} and U_{SL} are calculated from the inflow measurements obtained by the

thermal mass flow meter and by the electromagnetic flow meter, respectively. The uncertainties in the measured air and water flow rates are less than 1%.

It can be seen from Table 7.1 that the time period of all types of severe slugging decreases by increasing U_{SG0} at constant U_{SL} or by increasing U_{SL} at constant U_{SG0}.

7.4   Stability criteria

The analytical stability model predicts the boundary between stable (steady state) and unstable (severe slugging) flow in the flow regime map. As mentioned in Section 7.2, the experimental facility included a choke which is placed at the riser top, upstream of the separator. During all experiments this choke was left fully open. However, a non-zero pressure drop even across this fully open choke was observed during the experiments. Fig. 7.7a shows the pressure drop across the choke for an experimental case of SS1 corresponding to $U_{SL}=$ 0.10 m s^{-1} and $U_{SG0}=$ 1.00 m s^{-1}. In order to do a stability analysis of the system the back pressure imposed by the choke should be considered. Therefore, the stability criteria presented by Jansen et al. (1996) were used in this study. As shown in Appendix C, this stability model is derived from an overall force balance of the system including the effect of the choke.
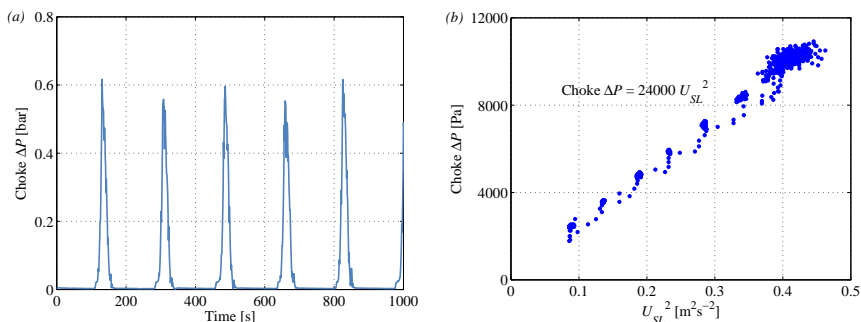

Figure 7.7: *(a) Experimental pressure drop across the choke corresponding to case 1 mentioned in Table 7.1 (b) the choke coefficient determined by measuring the pressure drop across the fully open choke for single-phase water flow.*

In Eqs. (C.1)-(C.3), C is the choke coefficient and can be determined experimentally by measuring the pressure drop across the choke for single-phase liquid flow and for a given choke opening. The choke coefficient C in the experiments (fully open choke) is 24,000 Pa s^2 m^{-2}, see Fig. 7.7b. The stability map is given in Fig. 7.8a. In this figure, the transition from stratified flow in the downward

inclined pipeline (Eq. (A.1)), the Bøe (1981) criterion (Eq. (B.1)), the modified Taitel (1986) stability of severe slugging (Eq. (C.2)), the Jansen et al. (1996) stability of steady operation (Eq. (C.3)), together with the experimental data are shown.
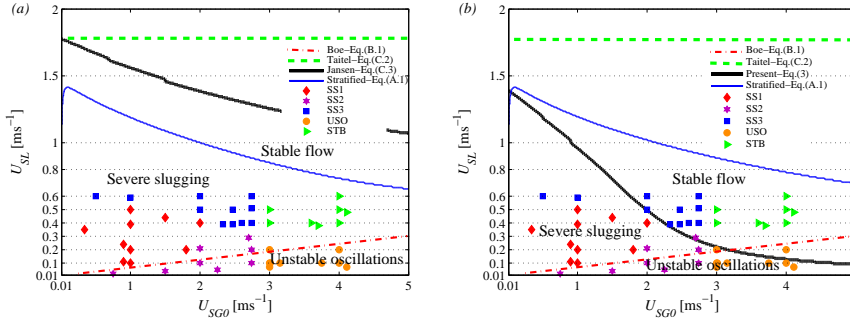

Figure 7.8: *Stability map for the present long pipeline-riser experiments. The map is based on (a) the single-phase choking relationship (the model proposed by Jansen et al. (1996)) (b) the two-phase choking relationship (the present model), for the steady operation stability criterion.*

The cyclic flow in the area below the line given by the Bøe (1981) criterion and below the line given by the Jansen et al. (1996) stability of steady operation criterion has been called unstable oscillations. The unstable area within the region given by the Bøe (1981) criterion and also the transition from stratified flow (above the line given by Eq. (B.1) and below the line given by Eq. (A.1)), and below the line given by the Jansen et al. (1996) stability of steady operation criterion has been called severe slugging region. In the remaining area in the flow pattern map stable flow occurs (Jansen et al., 1996). As can be seen from Fig. 7.8*a*, the above mentioned stability criteria did not accurately reproduce the experimentally obtained severe slugging and unstable oscillations regions. The severe slugging region was highly over predicted by the Jansen et al. (1996) stability of steady operation (Eq. (C.3)). It was assumed by Jansen et al. (1996) that the two-phase time averaged pressure drop across the choke is mainly a function of the superficial liquid velocity. Based on our experimental results, the two-phase time averaged pressure drop across the choke can be approximated by:

$$\Delta P_{\text{choke}} = C' U_{\text{mix}}^2, \tag{7.1}$$

where $U_{\text{mix}} = U_{SL} + U_{SG}$ denotes the mixture velocity of the fluids flowing through the choke, which can be obtained through multiplying the mixture velocity at the inlet of the pipeline ($U_{SL} + U_{SG0}$) by $(D_p/D_r)^2$. Here, D_p and D_r

denote the diameters of the pipeline and the riser, respectively. In Eq. 7.1, C' is the adjusted choke coefficient, which is given by:

$$C' = C\rho_s, \tag{7.2}$$

where C is the single-phase choke coefficient and $\rho_s = \left(\alpha\rho_G + (1 - \alpha)\rho_L\right)/\rho_L$ is the specific density of the fluid flowing through the choke. In this equation, ρ_G and ρ_L denote the gas and the liquid densities, and α represents the void fraction of the fluid flowing through the choke, which can be estimated by the volume fraction of the gas phase U_{SG}/U_{mix}. Note that here U_{SG} is approximated by $U_{SG0}(D_p/D_r)^2$. Fig. 7.9a shows the comparison between the predicted two-phase time averaged pressure drop across the choke by the model proposed by Jansen et al. (1996) (Eq. (C.1)) and the experimental results corresponding to the stable flow (cases 39 - 46 in Table 7.1). Fig. 7.9a shows that the model proposed by Jansen et al. (1996) under predicts the two-phase time averaged pressure drop across the choke. Fig. 7.9b shows the comparison between the predicted two-phase time averaged pressure drop across the choke by the present model (Eq. (7.1)) and the same experimental results (cases 39 - 46 in Table 7.1). As can be seen, the present model correctly predicts the two-phase time averaged pressure drop across the choke. Thus, the two-phase time averaged pressure drop across the choke cannot be approximated by the single-phase liquid flow and it depends on the mixture velocity and on the specific density of the fluids flowing through the choke.
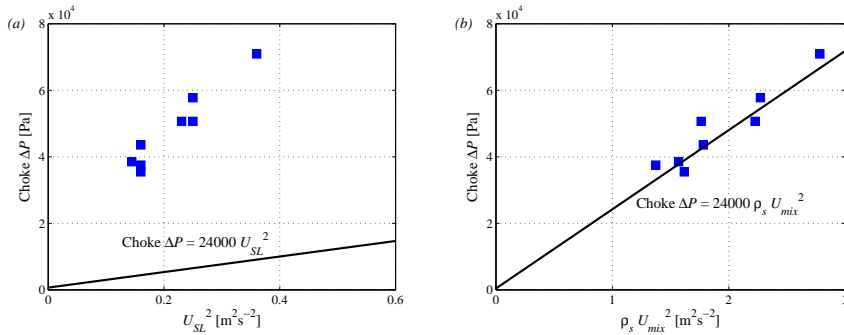

Figure 7.9: *Experimental two-phase time averaged pressure drop across the choke corresponding to the stable flow cases mentioned in Table 7.1 against (a) the performance of the model proposed by Jansen et al. (1996) (b) the performance of the present model.*

Therefore, the single-phase choking relationship in the stability model presented by Jansen et al. (1996) is replaced with the two-phase choking relationship. After using the same stability analysis, as given by Jansen et al. (1996), the

modified stability criterion for steady operation is then:

$$\frac{P_s + C'U_{\text{mix}}^2}{P_0} > \frac{\frac{\alpha L}{\alpha'}\left(\phi - \frac{2C'U_{\text{mix}}^2}{\rho_L g H}\right) - \phi H}{\frac{P_0}{\rho_L g}}, \tag{7.3}$$

where P_s denotes the separator pressure, P_0 is the atmospheric pressure, α is the average void fraction in the pipeline, L is the pipeline length, α' is the void fraction of the gas front entering the liquid column in the riser, ϕ denotes the average liquid holdup in the riser, ρ_L is the liquid density, g is the gravitational acceleration and H is the riser height. In Eq. 7.3, the variables α and ϕ are flow-regime dependent and can be calculated by using mechanistic models (see Petalas and Aziz, 2000). The value of α' was found to be in the order of 0.5.

The stability map based on the modified criterion for the stability of the steady operation (Eq. (7.3)) is given in Fig. 7.8b. In comparison with the Jansen et al. (1996) stability of steady operation, a reasonable agreement between the analytical line given by the modified criterion and the experimental data is observed. However, the present model could not accurately include all the experimental SS3 cases inside the predicted severe slugging region.

As mentioned, only α and ϕ are calculated by using mechanistic models and the remaining parameters are independent of the flow dynamics in the system. A sensitivity analysis was carried out to evaluate the influence of these variables on the performance of the proposed stability criterion. It was found that a relatively small variation in the value of α (e.g. 5%) does not change the position of the stability line predicted by the present model. However, this variation in the value of ϕ slightly moves this predicted stability line up or down, depending on whether the variation is positive or negative, respectively. For instance, 5% increase in the value of ϕ shifted the position of the stability line from $U_{SL}=0.50$ m s^{-1} to $U_{SL}=0.53$ m s^{-1} at constant $U_{SG0}=2.00$ m s^{-1}. It was also found that 10% increase in the value of α' does not appreciably change the position of the stability line. However, 10% increase in the value of C shifted the position of the stability line down from $U_{SL}=0.50$ m s^{-1} to $U_{SL}=0.44$ m s^{-1} at constant $U_{SG0}=2.00$ m s^{-1}.

The parameters α, ϕ, and C' depend non-linearly on the values of superficial liquid and gas velocities. A sensitivity analysis was carried out to evaluate the effects of the uncertainties in the values of U_{SL} and U_{SG0} in the values of α, ϕ, and C'. It was found that 5% increase in the value of superficial liquid velocity from $U_{SL}=0.50$ m s^{-1} to $U_{SL}=0.52$ m s^{-1} at constant $U_{SG0}=2.00$ m s^{-1} decreased the value of α by 0.6%, increased the value of ϕ by 2%, and increased the value of C' by 4%. Also, 5% increase in the value of superficial gas velocity from $U_{SG0}=2.00$ m s^{-1} to $U_{SG0}=2.10$ m s^{-1} at constant $U_{SL}=0.50$ m s^{-1} increased the value of α by 0.4%, decreased the value of ϕ by 2%, and decreased the value of C' by 3%.

It should be noted that the diameters for the pipeline (50.8 mm) and the riser (45 mm) used in the test loop imply an approximately 20% reduction of the

cross-sectional area of the riser compared to that of the pipeline. This reduction will increase the superficial liquid and gas velocities at the riser base. The flow pattern in the riser and consequently ϕ in the stability criterion (Eq. 7.3) depend non-linearly on the local values of superficial liquid and gas velocities. The superficial liquid velocity in the riser is calculated by $U_{SL}(D_p/D_r)^2$ and the superficial gas velocity in the riser is obtained from $U_{SG0}(D_p/D_r)^2(\rho_{G0}/\rho_G)$. Here, ρ_{G0} denotes the gas density at standard conditions and ρ_G is the average gas density in the riser which can be calculated by using a mechanistic model. These local superficial velocities are then used to compute the stability criterion, especially ϕ. The reduction of the pipe diameter shifted the position of the stability line down from U_{SL}=0.84 m s^{-1} to U_{SL}=0.50 m s^{-1} at constant U_{SG0}=2.00 m s^{-1}. Furthermore, this reduction of the cross-sectional area of the riser may act as a partially closed choke and may impose an additional back pressure (on the order of 100 Pa) that may attenuate severe slugging. However, this is negligible compared to the back pressure imposed by the choke placed at the riser top (about 0.6 bar). The reduction of the pipe diameter thus does change the position of the stability line but does not affect the basic mechanisms for the onset of slugging. This was also confirmed by the comparison with the model simulations.

7.4.1   Comparison with Jansen et al. (1996) experimental data

We compare the performance of the present model and the Jansen et al. (1996) stability of steady operation with the experimental data published by Jansen et al. (1996). The test loop consisted of a 9.1 m long, -1° inclined pipeline connected to a 3 m high vertical riser. The pipeline and riser internal diameters were 0.0254 m. Air and water were used as the experimental fluids. One equivalent pipe-length of 10 m, filled with air was used to obtain extra pipeline compressibility. No back pressure was imposed by a separator and only choking was applied.

The experimental data, together with the results from the stability analysis are given in Fig. 7.10. Fig. 7.10a shows the stability map obtained by using the Jansen et al. (1996) stability of steady operation. The stability map based on the present model is given in Fig. 7.10b. As can be seen, a reasonable agreement between the analytical lines given by both models and the experimental data is observed. For this relatively short pipeline-riser system (a 10 m long pipeline represented by a gas buffer vessel connected to a 9.1 m long pipeline followed by a 3 m high riser), steady state operation occurs at a low gas flow rate ($U_{SG0} > 0.3$ m s^{-1}). The two-phase time averaged pressure drop across the choke at low gas flow rate is mainly due to the liquid flow (Jansen et al. (1996)). Therefore, for this short pipeline-riser system, the single-phase choking relationship can also be used as an approximation in the stability criterion for the steady operation. However, generally in real production systems (long pipeline-riser systems), a steady state operation occurs at higher gas flow rate and the single-phase choking relationship is no longer a valid approximation in the equation for the stability of steady operation. In the present model the two-phase choking relationship is

implemented to enable the prediction of the flow behaviour in long pipeline-riser systems, e.g. our experimental set-up which is a 123 m long pipeline represented by a gas buffer vessel connected to a 100 m long pipeline followed by a 15.5 m high riser.
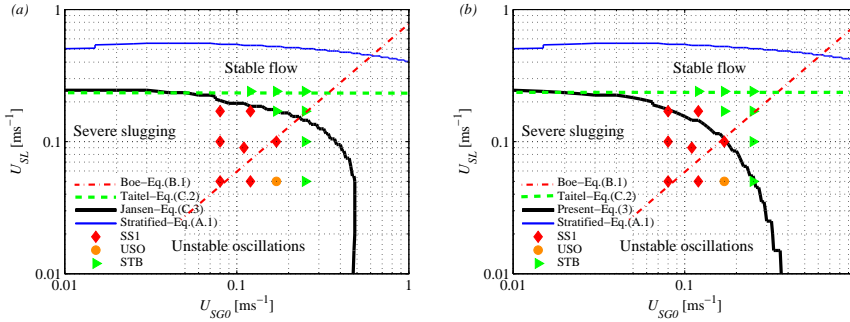

Figure 7.10: *Stability map corresponding to the Jansen et al. (1996) experiments with choke coefficient $C = 120000 \ Pa \, s^2 \, m^{-2}$ (a) the performance of the model proposed by Jansen et al. (1996) (b) the performance of the present model.*

Here, a sensitivity analysis was also carried out to evaluate the influence of α and ϕ on the performance of the present model for this relatively small pipeline. It was found that a relatively small variation (e.g. 5%), in the value of α or ϕ slightly moves the predicted stability line up or down depending on whether this variation is positive or negative, respectively. As an example, 5% increase in the value of α or ϕ shifted the position of the stability line predicted by the present model from U_{SL}=0.15 m s^{-1} to U_{SL}=0.16 m s^{-1} at constant U_{SG0}=0.10 m s^{-1}.

7.5   Numerical simulations

A one-dimensional numerical model of air-water two-phase flow in the downward inclined pipeline-riser system was developed using the multiphase flow simulator OLGA (version 6.3.0, released in 2010). This is a transient one-dimensional, commercial computer code based on a two-fluid flow model. The three-dimensional velocity profile in the pipeline and riser is averaged over the cross section, which simplifies the flow equations from three-dimensional to one-dimensional. This simplification requires using empirical closure relations in the model for the wall friction and for the interfacial stress between the liquid and the gas. The one-dimensional model contains three separate mass balance equations for the gas, liquid droplets and liquid film, which are coupled through interfacial mass transfer terms. Two momentum balance equations are applied: one combined equation

for the gas flow with liquid droplets, and one equation for the liquid film flow (see Bendiksen et al., 1991).

It was confirmed by the temperature transmitters located in the test loop that the temperature change throughout the test loop is negligible. Thus, the fluid temperature in the numerical model is set to a constant value of 15.56 °C. In the numerical model constant mass flow rates and pressure were specified as the inlet and outlet boundaries, respectively. As mentioned in Section 7.4, a non-zero pressure drop across the choke was observed during the experiments. Therefore, a valve with K_v value of 10 m^3 h^{-1} bar$^{-1/2}$ was included in the numerical model. The numerical model, with a grid resolution of 25 cm giving a total of 533 grid cells in the pipeline and riser, is used to simulate all cases mentioned in Table 7.1. The maximum and minimum simulation time steps were 0.1 s and 0.0001 s, respectively. We have performed a grid independence study to verify that the number of grid cells is such that the results are grid independent. This was accomplished by meshing the computation domain with five different cell sizes of 150 cm, 100 cm, 50 cm, 25 cm, and 15 cm. Fig. 7.11 shows the predicted time period and amplitude of the riser ΔP for a severe slugging cycle corresponding to case 1 in Table 7.1, by all five mentioned cell sizes. As can be seen, the predicted time period and amplitude of the riser ΔP for the severe slugging converges to 211 s and 1.39 bar as the grid is refined. The numerical simulations were performed to mainly support our experimental observations about the effective contribution of the transient slugs generated in the pipeline to the initial blockage of the riser base.
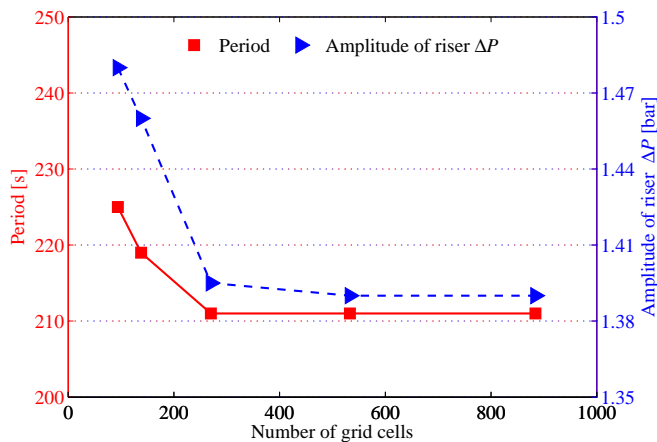

Figure 7.11: *The predicted period and amplitude of the riser ΔP for a severe slugging cycle corresponding to case 1 in Table 7.1, by meshing the computation domain with five different cell sizes of 150 cm, 100 cm, 50 cm, 25 cm, and 15 cm giving a total of 94, 138, 270, 533, and 884 grid cells in the pipeline and riser, respectively.*

Fig. 7.6b shows the flow pattern map of the downward inclined pipeline-riser system which has been developed based on numerical simulation results. The numerical simulations were performed using U_{SL} and U_{SG0} values of all experimental cases given in Table 7.1. A good agreement is observed in the prediction of the different types of severe slugging. However, the numerical model fails to predict the USO cases. As mentioned in Section 7.3.2, during the process of USO, the gas and liquid phases flow continuously through the riser base into the riser. Therefore, a full liquid blockage at the riser base does not exist. However, the numerical model incorrectly predicts a full blockage at the riser base (due to the inaccurate prediction of the flow regime in the pipeline and in the riser) which consequently leads to the prediction of severe slugging of type 2 for these experimental USO cases. Note that the change in the pipeline-riser diameter (from 50.8 mm to 45 mm) is incorporated in the numerical model.

The predicted periods as well as the average maximum, minimum and amplitude of the riser ΔP are also given in Table 7.1. Although most of the predicted riser ΔP traces showed a dominant period, there are some in which two dominant periods appeared.
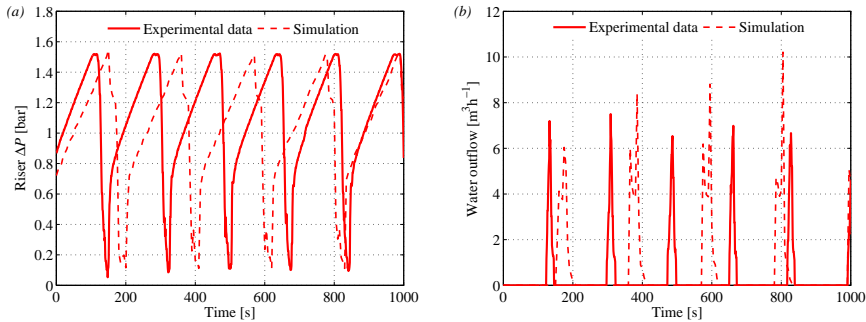

Figure 7.12: *Comparisons of measured and predicted traces of SS1 corresponding to case 1 in Table 7.1 (a) riser ΔP traces (b) liquid outflow traces.*

Figs. 7.12a, 7.13a and 7.14a compare the experimental and numerical riser ΔP traces of three different slug types of SS1, SS2 and SS3 corresponding to case 1, 11 and 28 in Table 7.1, respectively. There is good agreement for the SS1 cycle with $U_{SL}= 0.10$ m s^{-1} and $U_{SG0}= 1.00$ m s^{-1}, case 1 in Table 7.1. The measured time period of a cycle is 179 s, whereas the numerical model predicts a slightly higher value of 211 s. The initial riser base blockage with 6% liquid in the riser is formed from fallback of liquid during the end of the gas blowdown stage. The gas blowdown stage has caused transient slugs to form in the pipeline which contribute to the initial riser base blockage and rapidly increase the riser ΔP, filling the riser with liquid to about 44%. The SS2 cycle for $U_{SL}= 0.10$ m s^{-1}

and $U_{SG0}= 2.00$ m s^{-1}, case 11 in Table 7.1, is predicted fairly well. It is clear from the riser ΔP trace that the riser never gets fully filled with liquid and the amount of the liquid in the riser changes after each cycle. The measured time periods of this case of SS2 are 92 s and 138 s, and the predicted values are 76 s and 191 s. Also the SS3 cycle for $U_{SL}= 0.60$ m s^{-1} and $U_{SG0}= 2.00$ m s^{-1}, case 28 in Table 7.1, is predicted well. The initial liquid fallback is about 8% liquid in the riser. Transient slugs rapidly increase the total liquid content of the riser to about 80%. The measured time period of a cycle is 64 s, and the predicted value is 68 s.
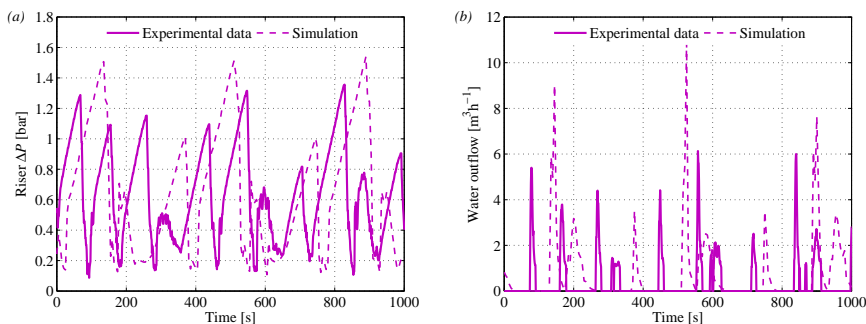

Figure 7.13: *Comparisons of measured and predicted traces of SS2 corresponding to case 11 in Table 7.1 (a) riser ΔP traces (b) liquid outflow traces.*
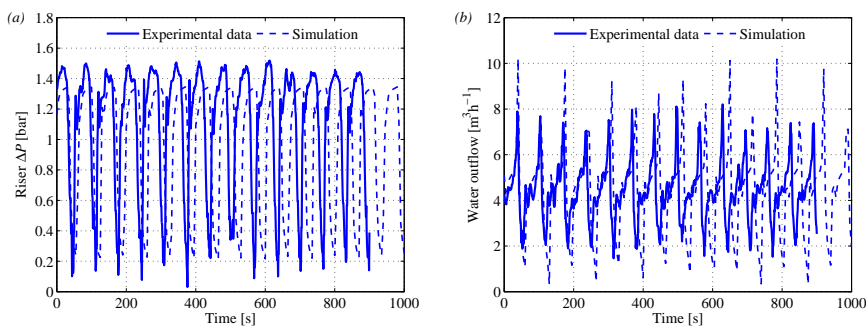

Figure 7.14: *Comparisons of measured and predicted traces of SS3 corresponding to case 28 in Table 7.1 (a) riser ΔP traces (b) liquid outflow traces.*

Figs. 7.12b, 7.13b and 7.14b compare the experimental and numerical water

outflow of these three mentioned different slug types, respectively. The SS1 case exhibits periods of no water production (production starvation) followed by large peaks of water outflow of about 7 $m^3 h^{-1}$. This feature is also reproduced by the numerical model. As it is expected, the time period of oscillations in the water outflow is the same as the one observed in the riser ΔP trace. The SS2 case also shows the production starvation cycles. However, the maximum water outflow ranges from 1 to 6 $m^3 h^{-1}$. The numerical simulation also shows production starvation and the unequal peaks of water outflow. The SS3 case does not give production starvation as water is continuously produced at the riser top. In each cycle, the water outflow changes from a minimum of 2 $m^3 h^{-1}$ to a maximum peak of 8 $m^3 h^{-1}$. As can be seen, the numerical model can also reproduce the experimental data for this case fairly well. As mentioned earlier, during the gas blowdown stage, transient slugs are generated in the pipeline upstream of the riser base and will play an important role in the process of severe slugging. The transient slugs can be recognized from the jump in the riser ΔP trace. This is captured in the numerical simulations of all these severe slugging cases.

7.6   Conclusions

The relatively long pipeline used in the laboratory experiments allowed to study new details of severe slugging and it allowed for a comparison with numerical predictions. This model validation on a laboratory scale gives some more confidence in the model when applying it to the full pipeline-riser scales used by the oil and gas industry. The need for full scale experiments on unstable flow with slugging for model validation, however, remains.

From the results and discussions presented above the following conclusions can be drawn:

(1) Five types of flow regime were found in our new laboratory experiments in the downward inclined pipeline-riser systems: stable flow (characterized by hydrodynamic slugs initiated in the pipeline and flowing into the riser), unstable oscillations (exhibiting cyclic, low amplitude pressure fluctuations), severe slugging of type 1 (having a pure liquid slug length larger than the riser height), severe slugging of type 2 (having a pure liquid slug length smaller than the riser height), and severe slugging of type 3 characterized by a growing long aerated liquid slug in the riser followed by the gas blow down stage.

(2) A cycle of severe slugging of type 3 was considered to consist of four stages: transient slugs, aerated slug growth, fast aerated liquid production, and gas blow down. These stages were illustrated and marked on a cycle of an experimental riser ΔP trace of severe slugging of type 3.

(3) The two-phase time averaged pressure drop across the choke is found to be a function of both the specific density and the mixture velocity of the

fluid flowing through the choke. Consequently, the single-phase choking relationship in the steady operation stability criterion is replaced with the two-phase choking relationship. The modified criterion for the stability of the steady operation gives a reasonable agreement with the experimental results in comparison with the Jansen et al. (1996) criterion.

(4) It was found experimentally, as also reproduced numerically, that transient slugs were generated in the pipeline upstream of the riser base. These transient slugs effectively contributed to the initial blockage of the riser base.

(5) The dynamic simulation tool OLGA was used to reproduce the characteristics of all considered experimental cases. The flow pattern map constructed based on the simulation results is in good agreement with the experimental one. Also the numerical model gives a fairly good prediction of the time period and of the amplitude of the riser pressure drop for all experimental cases.

Acknowledgements

References

Baliño, J.L., Burr, K.P., Nemoto, R.H., 2010. Modeling and simulation of severe slugging in air-water pipeline-riser systems. Int. J. Multiphase Flow 36, 643-660.

Bendiksen, K., Malnes, D., Moe, R., Nuland, S., 1991. The dynamic two-fluid model OLGA: Theory and application. SPE Production Eng. J. 6, 171-180.

Bøe, A., 1981. Severe slugging characteristics; part 1: Flow regime for severe slugging; part 2: Point model simulation study. Presented at Selected Topics in Two-Phase Flow, Trondheim, Norway.

Fabre, J., Peresson, L., Corteville, J., Odello, R., Bourgeols, T., 1990. Severe slugging in pipeline/riser systems. SPE Production Eng. J. 5, 299-305.

Jansen, F.E., Shoham, O., Taitel, Y., 1996. The elimination of severe slugging: Experiments and modeling. Int. J. Multiphase Flow 22, 1055-1072.

Malekzadeh, R., Mudde, R.F., Henkes, R.A.W.M., 2012. Experimental and numerical investigation of severe slugging in horizontal pipeline-riser systems. Int. J. Multiphase Flow, submitted.

Petalas, N., Aziz, K., 2000. A mechanistic model for multiphase flow in pipes. Journal of Canadian Petroleum Technology 39, 43-55.

Pots, B., Bromilow, I., Konijn, M., 1987. Severe slug flow in offshore flowline/riser systems. SPE Production Eng. J. 2, 319-324.

Sarica, C., Shoham, O., 1991. A simplied transient model for pipeline-riser systems. Chemical Engineering Science 46, 2167-2179.

Schmidt, Z., Brill, J., Beggs, H., 1980. Experimental study of severe slugging in a two-phase-flow pipeline-riser pipe system. SPE J. 20, 407-414.

Schmidt, Z., Doty, D., Dutta-Roy, K., 1985. Severe slugging in offshore pipeline riser-pipe systems. SPE J. 25, 27-38.

Seim, J., van Beusekom, V., Henkes, R., Nydal, O., 2011. Experiments and modelling for the control of riser instabilities with gas lift. Presented at 15th International Conference on Multiphase Production Technology, Cannes.

Shoham, O., 2006. Mechanistic Modeling of Gas-Liquid Two-Phase Flow in Pipes. Society of Petroleum Engineers, Richardson, Texas.

Taitel, Y., 1986. Stability of severe slugging. Int. J. Multiphase Flow 12, 203-217.

Taitel, Y., Dukler, A., 1976. A model for predicting flow regime transitions in horizontal and near horizontal gas-liquid flow. AIChE Journal 22, 47-55.

Taitel, Y., Vierkandt, S., Shoham, O., Brill, J., 1990. Severe slugging in a pipeline-riser system: Experiments and modeling. Int. J. Multiphase Flow 16, 57-68.

Appendix A. Stability of stratified flow

Schmidt et al. (1985) found that severe slugging occurs if there is stratified flow in the pipeline upstream of the riser base. They used the Taitel and Dukler (1976) model to check the stability of stratified flow. Taitel and Dukler (1976) proposed

the following equation for the transition from stratified flow to either intermittent or annular flow.

$$U_G > \left(1 - \frac{h_L}{D}\right) \left[\frac{(\rho_L - \rho_G)\, g\, \cos\theta\, A_G}{\rho_G\ dA_L/dh_L}\right]^{1/2},$$

(A.1)

where U_G denotes the gas velocity, h_L is the height of the liquid layer, A_G and A_L denote the areas occupied by the gas and the liquid, ρ_G and ρ_L are the gas and the liquid densities, θ is the inclination angle of the pipe from the horizontal and D denotes the diameter of the pipe.

Appendix B. The Bøe (1981) criterion

The Bøe (1981) criterion is a simple and a conservative mathematical expression which states that severe slugging can occur if the hydrostatic pressure build-up in the riser exceeds the gas pressure build-up in the pipeline. This criterion is given by the following equation:

$$U_{SL} \geq \frac{\rho_{G0}RT}{\rho_L g \alpha L} U_{SG0},$$

(B.1)

where ρ_{G0} denotes the gas density at standard conditions, R is the universal gas constant, T denotes temperature and α is the average void fraction in the pipeline which depends on the flow regime.

Appendix C. The Jansen et al. (1996) criteria

Jansen et al. (1996) assumed that both the single-phase and the two-phase time averaged pressure drop across the choke can be approximated by:

$$\Delta P_{\text{choke}} = C U_{SL}^2.$$

(C.1)

They modified the Taitel (1986) stability criterion for severe slugging to include the effect of the back pressure imposed by choke at the riser top. This criterion is referred to as stability of severe slugging and is given by the following equations:

$$\frac{P_s + C U_{SL}^2}{P_0} > \frac{\frac{\alpha L}{\alpha'}\left(1 - \frac{2C U_{SL}^2}{\rho_L g H}\right) - H}{\frac{P_0}{\rho_L g}}.$$

(C.2)

Jansen et al. (1996) also extended Eq. (C.2) for the case where a steady state operation occurs (contrary to stability of severe slugging, total blockage of the pipeline does not occur). This criterion is referred to as stability of steady operation and is given by:

$$\frac{P_s + C U_{SL}^2}{P_0} > \frac{\frac{\alpha L}{\alpha'}\left(\phi - \frac{2C U_{SL}^2}{\rho_L g H}\right) - \phi H}{\frac{P_0}{\rho_L g}}.$$

(C.3)

Experimental and Numerical Investigation of Severe Slugging in Horizontal Pipeline-Riser Systems§

Abstract

It is well known that for certain constant inflow conditions, large-amplitude flow oscillations that will resemble severe slugging can occur in two-phase flow of gas and liquid in a *downward* inclined pipeline-riser system. The present experimental and numerical study investigates whether severe slugging and other flow instabilities can also occur in a *horizontal* pipeline-riser system. The experiments were carried out in a 100 m long, 50.8 mm diameter horizontal pipeline followed by a 15 m high, 50.8 mm diameter vertical riser operating at atmospheric end pressure. The experimental facility also included a 400 litre gas buffer vessel, placed upstream of the pipeline, to obtain extra pipeline compressibility. Air and water were used as the experimental fluids. Four types of flow regime were found and characterized based on visual observation and measured pressure drop over the riser. Severe slugging of type 3, unstable oscillations, and hydrodynamic slug flow, which are commonly found in a downward inclined pipeline-riser system, were also observed in the horizontal configuration. Also, a new type of flow instability, which will be referred to as "dual-frequency severe slugging", was found. This instability exhibits a dual-frequency behaviour. The high-frequency fluctuations are about 0.01 Hz, and the low-frequency fluctuations are about 0.001 Hz. Numerical

simulations were performed using a one-dimensional two-fluid flow model. Comparison of simulations and experimental data showed that the numerical model enables the prediction of the dual-frequency severe slugging, unstable oscillations, and stable flow regimes in the horizontal pipeline-riser system.

8.1   Introduction

According to the latest estimate by the International Energy Agency, "currently about a third of the world's oil production comes from offshore and it will increase to about half in 2015". Pipeline-riser systems in an offshore oil and gas production facility are required to transport multiphase hydrocarbons from a subsurface oil and gas reservoir to a central production platform. The diameter of the pipeline and the riser ranges from typically 0.1 to 0.8 m. The length of the pipeline can vary from a few kilometres (for liquid dominated systems) to more than hundred kilometres (for gas dominated systems). The height of the riser depends on the water depth, which can range from a few tens of metres (in lakes) to more than two kilometres (in deepwater areas). Severe slugging is an oscillatory flow regime that may occur in such multiphase pipeline-riser systems, and is characterized by large-amplitude, relatively long-period pressure and flow rates fluctuations.

The process of severe slugging formation can be described as follows. At relatively low flow rates, liquid accumulates at the bottom of the riser, creating a blockage for the gas, until sufficient upstream pressure has been built up to flush the liquid slug out of the riser. After this liquid surge, and subsequent gas surge, part of the liquid in the riser falls back to the riser base to create a new blockage and the cycle repeats. Severe slugging can significantly reduce the production from the reservoir (due to an increased back pressure) and also can damage or can even trigger the shut down of the platform facilities downstream of the riser, like separators, pumps, and compressors. Therefore, the accurate prediction of severe slugging characteristics is essential for the proper design and operation of multiphase flow in these systems.

Severe slugging in a downward inclined pipeline-riser system was first reported by Yocum (1973). Schmidt et al. (1980) proposed the first model to predict the severe slugging characteristics and tested its performance against their experimental data for downward inclined pipeline-riser configurations. Bøe (1981) and Taitel (1986) investigated the conditions in which severe slugging occurs. Their proposed mathematical criteria generate a severe slugging region in the flow pattern map of a downward inclined pipeline-riser system. Severe slugging in downward pipeline-riser systems has been the subject of many studies (see e.g. Pots et al., 1987; Taitel et al., 1990; Baliño et al., 2010). Fabre et al. (1990) observed severe slugging not only with a downward inclined pipeline, but also with a horizontal pipeline followed by a riser albeit with a smaller amplitude only. Sarica and Shoham (1991) proposed a simplified transient model to simulate severe slugging. They tested their model against a broad range of data, including the

data obtained by Fabre et al. (1990) for the horizontal pipeline-riser system. The simulations for downward inclined pipeline-riser systems showed better accuracy than previously published models. However, their model did not correctly predict the severe slugging cycle reported by Fabre et al. (1990) for the horizontal pipeline-riser system. Sarica and Shoham (1991) concluded that the horizontal pipeline in the experiments by Fabre et al. (1990) might have actually been slightly downward inclined.

Most of the existing laboratory experiments for severe slugging were conducted for downward inclined pipeline-riser systems. Because of the importance of flow oscillations in practical applications, the flow behaviour needs to be known for each orientation angle of the pipeline upstream of the riser base, and this should not be limited to a downward configuration only. Therefore, we have carried out experiments for the two-phase flow of air and water in a horizontal pipeline-riser system. This was specifically aimed at finding any possible flow oscillations.

The main objective of this study is to investigate experimentally the characteristics of two-phase flow in a horizontal pipeline-riser system. Specific objectives are to identify both experimentally and numerically the possible severe slugging region within a flow pattern map and improve the understanding of the severe slugging initiation mechanism in horizontal pipeline-riser systems.

This paper is organized as follows: in Section 8.2 the experimental facility is described; in Section 8.3 the experimentally observed flow regimes, the flow pattern map and also the analysis of the experimental data are presented; in Section 8.4 numerical simulations are performed and a comparison is made with the experimental data; in the last section the conclusions of the study are presented.

8.2   Experimental facility

The existing two-phase, air and water flow facility of the Shell Technology Centre in Amsterdam (STCA), see Fig. 8.1, was used to conduct experiments. The test facility comprises four main parts: the fluid supply, test loop (pipeline and riser), separation area and measurement and control devices. This facility is powered and controlled by the Fieldpoint 2000 system of National Instruments and by Labview, which are the control hardware and software, respectively. They help to ensure that the complete instrumentation of the system is operated, controlled and monitored separately, the desired operating conditions are achieved and the required data are recorded. The full experimental procedures, including startup, control, shutdown and data logging are done remotely through dedicated control and data acquisition systems.

Dry air at a pressure of 6 barg is delivered via a connection with the main air supply at the STCA. The air is supplied to a thermal mass flow meter and controller of model 5853i by Brooks, which automatically provides an almost constant mass flow rate into the test loop. The gas mass inflow rate varies by less than 0.2%. A maximum air flow rate of 30 $\mathrm{Sm^3\,h^{-1}}$ can be supplied (the
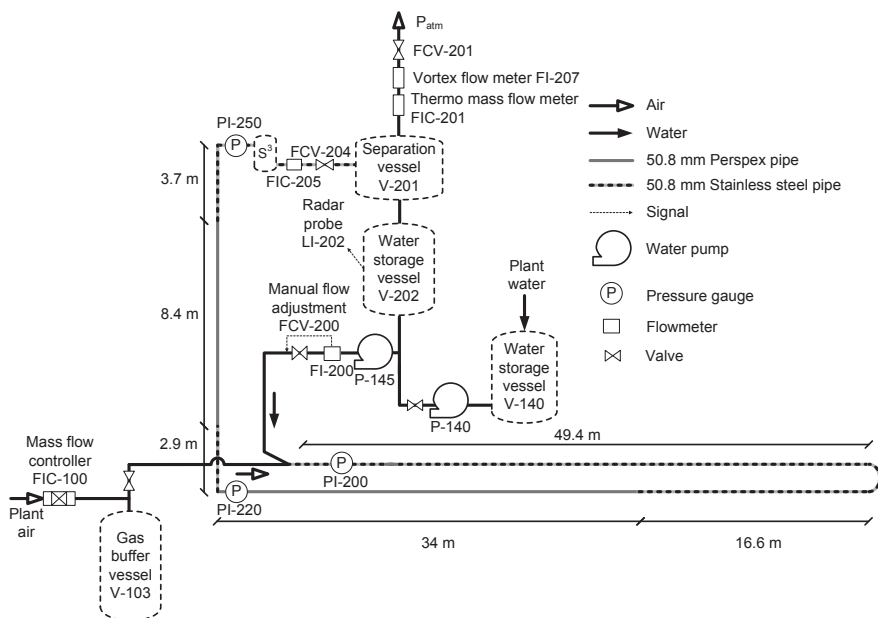
Figure 8.1: *Schematic of the experimental facility.*

S refers to standard conditions at 1.00 bara and 15.56 °C). The water supply is city tap water connected to the first water storage tank (V-140), see Fig. 8.1. A worm pump connected to V-140 brings water to the second water storage tank situated right below the separator. Then water is supplied to the pipeline by a variable speed centrifugal pump. A relatively constant water volumetric flow rate can be achieved by manually adjusting the pump speed and by adjusting the opening of a control valve, which is located directly downstream of the pump. The liquid inflow rate varies by less than 2%. A maximum water flow rate of 5 $m^3\,h^{-1}$ can be supplied. The water flow rate into the test loop is measured with an electromagnetic flow meter of type Promag 50W by Endress & Hauser.

The test loop consists of a 66 m long, 50.8 mm diameter horizontal steel pipeline connected to a 34 m long, 50.8 mm diameter horizontal Perspex pipeline followed by a 15 m high, 50.8 mm diameter vertical Perspex riser. The elevation of the horizontal pipeline was measured by a laser-level measurement sensor of type PR 25 IF by Hilti. The level-change of the horizontal pipeline was 1 mm over 15 m. The Perspex pipes are transparent which enables visual observation of the flow behaviour. The riser discharges the fluid into the two-phase separator, operating at atmospheric pressure. The separator pressure varies by less than 3%. Air and water are separated by gravity. The upper section of the separator has a mist mat and dry air is vented to the open air, monitored by one vortex and

one thermo mass flow indicators. The lower section of the separator drains the water, which flows down and returns to the second water storage tank. The water level in this tank is measured with a continuous level transmitter of type Levelflex M-FMP40 by Endress & Hauser. A variable-volume gas buffer vessel is located between the gas mass flow controller and the gas inlet, upstream of the pipeline. The air volume of the buffer vessel can be changed by partly filling it with water. The function of the gas buffer vessel is to create a virtually longer pipeline. In the current study, the maximum applied air volume of the buffer vessel is 400 litre, which corresponds to an additional (gas-filled) pipeline length of 197 m. It should be noted that the facility also included a slug suppression system (S^3) at the riser top. The active parts of the S^3 are: a small vessel with a total volume of 9.4 litres, an electromagnetic flow meter, and a liquid control valve, which has a K_v value (flow factor) of 12 $m^3\,h^{-1}\,bar^{-1/2}$. During all experiments, however, this liquid control valve was left fully open. Pressure transducers are located at the inlet of the pipeline, at the riser base and at the top of the riser. They are manufactured by Endress & Hauser and are of type Cerebar M-PMC41. Additional pressure devices are also used to measure and monitor the pressure in the gas buffer vessel, the inlet of the gas line, the outlet of the liquid pump and in the two-phase separator. The temperatures of the fluids are measured with temperature transmitters that are located at various locations in the test loop. Table 8.1 provides a summary of the instrumentation used in the experimental facility.

Although the dimensions of this experimental set-up are relatively large, the flow behaviour under full scale field conditions (i.e. longer pipeline and riser, larger pipe diameter, higher pressure, different fluids) might differ from the laboratory results. The laboratory experiments are meant, however, to gain physical understanding of slug types, which with the help of numerical models, can lead to predictions under the actual field conditions.

Table 8.1: *Specifications of the equipment in the flow loop. E+H and D/M are acronyms for Endress+Hauser and Dresser/Masoneilan, respectively.*

Label (Fig. 8.1)	Instrument	Manufacture	Type	Range	Units	Accuracy
PI-200	Pressure transmitter	E+H	Cerebar M-PMC41	0 - 10	bara	0.2%
PI-220	Pressure transmitter	E+H	Cerebar M-PMC41	0 - 10	bara	0.2%
PI-250	Pressure transmitter	E+H	Cerebar M-PMC41	0 - 10	bara	0.2%
FI-200	Electromagnetic flow meter	E+H	Promag 50W	0 - 7.5	$m^3\,h^{-1}$	0.5%
FIC-205	Electromagnetic flow meter	E+H	Promag 50W	0 - 18	$m^3\,h^{-1}$	0.5%
FIC-100	Thermal Mass flow meter & controller	Brooks	5853i	0 - 30	$Sm^3\,h^{-1}$	1%
FIC-201	Thermal mass flow meter	E+H	t-mass 65F	0 - 110	$Sm^3\,h^{-1}$	1.5%
LI-202	Continuous level transmitter	E+H	Levelflex M-FMP40	0 - 100	%	+/-3 mm
FCV-200	Control valve	D/M	35-35112	0 - 12	$m^3\,h^{-1}\,bar^{-1/2}$	-
FCV-204	Control valve	D/M	35-35202	0 - 12	$m^3\,h^{-1}\,bar^{-1/2}$	-

8.3   Riser-induced instabilities

Based on preliminary numerical simulations an experimental matrix is defined to cover all possible flow regimes occurring in the test loop. Later, by obtaining further experimental results this matrix was refined to establish both the characteristics of each flow regime and the transition boundaries between the flow regimes. The water flow rate ranges from 0.34 $m^3 h^{-1}$ to 4.45 $m^3 h^{-1}$ and the air flow rate from 3.70 $Sm^3 h^{-1}$ to 29.38 $Sm^3 h^{-1}$. The corresponding superficial water velocity ranges from U_{SL}= 0.05 - 0.61 $m s^{-1}$ and superficial air velocity at standard conditions (1.00 bara, 15.56 °C) ranges from U_{SG0}= 0.51 - 4.03 $m s^{-1}$. Different flow regimes have been obtained by fixing the water flow rate and by changing the air flow rate. The observed flow regimes are classified into four categories: stable flow (STB), severe slugging of type 3 (SS3), unstable oscillations (USO), and dual-frequency severe slugging (DFSS). A classification of severe slugging in a downward inclined pipeline-riser configuration is given by Baliño et al. (2010), who distinguished the types 1, 2, and 3. In this paper, the same abbreviations were used for the classification of the flow regimes. The flow regimes were delineated based on visual observations and analysis of the pressure drop over the riser (riser ΔP). The riser ΔP is also used for defining different stages of a severe slugging cycle. Typical riser ΔP traces of these four flow regimes are shown in Fig. 8.2. The above mentioned, experimentally observed, flow regimes are described below.
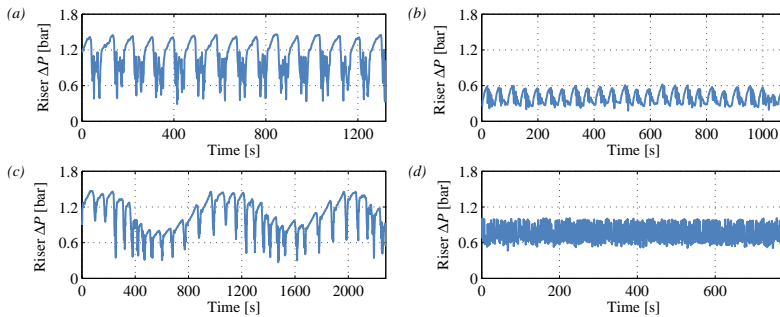
Figure 8.2: *Experimental riser ΔP traces of the four mentioned flow patterns corresponding to (a) SS3 (U_{SL}=0.40 $m s^{-1}$ & U_{SG0}=1.01 $m s^{-1}$), (b) USO (U_{SL}=0.10 $m s^{-1}$ & U_{SG0}=3.02 $m s^{-1}$), (c) DFSS (U_{SL}=0.20 $m s^{-1}$ & U_{SG0}=0.51 $m s^{-1}$) and (d) STB (U_{SL}=0.61 $m s^{-1}$ & U_{SG0}=2.01 $m s^{-1}$).*

8.3.1   Stable flow

Hydrodynamic slugs are generated in the pipeline and they are moving up into the riser. Therefore, the flow patterns in the pipeline and in the riser are mainly

hydrodynamic slug flow. Such flow is characterized by a series of gas pockets separated by liquid slugs. The riser ΔP exhibits fluctuations with a small amplitude (approximately less than 0.4 bar in our experiments) and high frequency. Thus, hydrodynamic slug flow is considered to be stable flow as compared to other types of flow regime mentioned in this study.

8.3.2   Severe slugging of type 3

A cycle of severe slugging of type 3 was found to consist of four stages: (1) transient slugs; (2) aerated slug growth; (3) fast aerated liquid production; (4) gas blowdown. In Fig. 8.3(a) these four stages are illustrated. Also they are marked on a cycle of an experimental riser ΔP trace of SS3 corresponding to U_{SL}=0.40 m s^{-1} and U_{SG0}=1.01 m s^{-1}, as shown in Fig. 8.3(b). The process of SS3 can be described as follows.
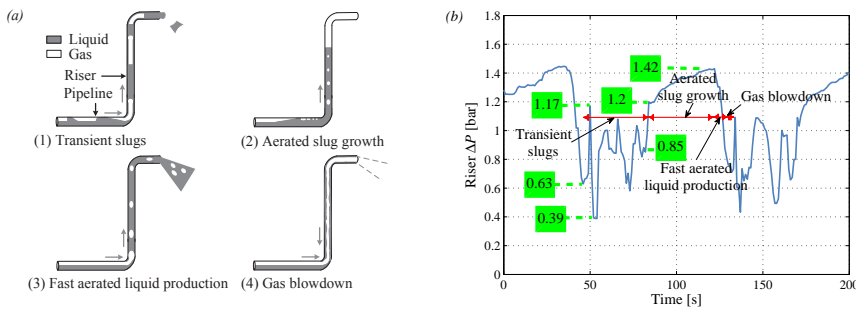

Figure 8.3: *Stages for severe slugging of type 3 in the horizontal pipeline-riser experiment (a) a graphical illustration (b) marked on a cycle of an experimental riser ΔP trace (U_{SL}=0.40 m s^{-1} & U_{SG0}=1.01 m s^{-1}).*

Transient slugs of different sizes are generated in the pipeline upstream of the riser base and flowing up along the riser. Part of the liquid in the transient slugs falls back through the riser and accumulates again in the riser and in the pipeline. The interaction between the horizontal pipeline and the vertical riser creates flow reversal of liquid and gas (as small bubbles) at the riser base, generating a long aerated liquid slug. The flow behaviour at the riser base is illustrated in Fig. 8.3(a). The generated long aerated liquid slug contains small bubbles of different size and shape. The aerated liquid slug gradually flows into the riser and the riser ΔP gradually increases. This is the growth stage of the aerated slug. Small gas bubbles at the riser base continuously penetrate into the riser. The hydrostatic head of the riser decreases when the compressed gas, initially present upstream of the riser base, enters the riser. This will cause the gas to expand, which

will accelerate the aerated liquid slug into the separator. This stage is called fast aerated liquid production. Finally, when the aerated liquid slug has been produced, gas will flow out at a high velocity. This is the gas blowdown stage. During the gas blowdown, the gas velocity in the pipeline increases. This generates transient slugs in the pipeline upstream of the riser base and the cycle is repeated.

It should be noted that SS3 can also occur in a downward inclined pipeline-riser system and shows the same stages which are mentioned above. However, a cycle of SS3 occurring in the horizontal pipeline-riser system consists of a stage with transient slugs over a relatively long period of time. Fig. 8.4(a) shows the different stages marked on a cycle of an experimental riser ΔP trace of SS3 corresponding to an experiment in a downward inclined pipeline-riser system. We have also carried out experiments in a downward inclined pipeline-riser system.
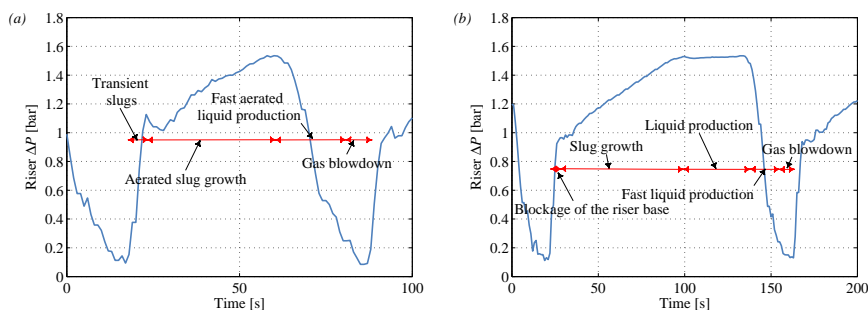

Figure 8.4: *Stages marked on a cycle of an experimental riser ΔP trace in a downward inclined pipeline-riser experiment (a) severe slugging of type 3 (b) severe slugging of type 1.*

Contrary to the classical severe slugging of type 1 (SS1), which can occur in a downward inclined pipeline-riser system and which shows periods of full production starvation, SS3 does not give full riser base blockage and production starvation. Fig. 8.4(b) shows different stages marked on a cycle of an experimental riser ΔP trace of SS1 corresponding to an experiment in a downward inclined pipeline-riser system.

The following features can be observed in Fig. 8.3(b).

- The initial liquid fallback (after the gas blowdown stage) gives a pressure drop of about 0.63 bar. This is equivalent to a 6.3 m water column in the riser. The minimum liquid content of the riser is about 3.9 m, occurring after the first transient slug left the riser.

- As a direct consequence of the quick depressurization of the pipeline in each cycle, the gas velocity in the pipeline increases and then transient slugs will

be generated. During transient slugging the total liquid column in the riser increases to about 12 m during 38 s (which is the duration of the transient slugs stage).

- The length of a transient slug can be estimated from the variation in the riser ΔP when this slug enters the riser. The length of the first transient slug is calculated to be about 5.4 m and the length of the last transient slug is about 3.5 m. Therefore, transient slugs of different size are generated in the pipeline. This is also confirmed by the visual observations.

- The maximum riser ΔP is 1.42 bar. This corresponds to 95% of liquid volume fraction in the riser. Therefore, the pure liquid production step, which implies 100% of liquid volume fraction in the riser (the maximum riser ΔP of 1.5 bar), does not exist here. This is in contrast to the SS1 in Fig. 8.4(b), which gives a 100% liquid production surge.

It should be noted that the above mentioned observations are based on two assumptions. First, the air density is negligible compared to the water density, and second, frictional and accelerational pressure drops in the riser are negligible compared to the gravitational pressure drop. Therefore, the riser ΔP is considered to be equal to the hydrostatic head of the liquid in the riser.

It is worth pointing out that also severe slugging of type 2 (SS2) can occur in a downward inclined pipeline-riser system. SS2 is qualitatively similar to SS1, but the slug length is shorter than the height of the riser.

8.3.3   Unstable oscillations

USO flow is characterized by an oscillatory gas void fraction in the riser and also in the pipeline. The gas phase flows continuously through the riser base into the riser. Two-phase flow of liquid and gas in the riser is highly aerated and the pressure oscillations have a much smaller amplitude compared to SS3. The flow pattern changes from hydrodynamic slug flow to churn flow in the riser and from hydrodynamic slug flow to stratified flow in the pipeline. This process exhibits a cyclic behaviour.

8.3.4   Dual-frequency severe slugging

This flow regime exhibits a slow slugging cycle that connects severe slugging of type 3 and unstable oscillations. DFSS has two different frequencies. The high-frequency fluctuations are related to the occurrence of SS3 and USO (each having their own value for the high frequency). The low-frequency oscillations are associated with the cyclic transition of the system between SS3 and USO. When the liquid content of the system is relatively high the system exhibits SS3 with the high-frequency oscillations and the associated flow pattern in the riser is changing between bubbly flow and intermittent flow. The liquid content of the system

gradually reduces and the system moves toward the USO flow pattern. Again at the lower liquid content, the system exhibits the high-frequency oscillations. This is not a stable operating condition and the system moves back to the state with the higher liquid content (SS3). These oscillations between the higher and the lower liquid content in the system exhibit a cyclic behaviour with a lower frequency, thus creating another level of instability to the whole system.

The uncertainty in the measured amplitude of the riser ΔP is less than 1%. U_{SG0} and U_{SL} are calculated from the measurements obtained by the thermal mass flow meter and electromagnetic flow meter, respectively. The uncertainties in the measured air and water inflow rates are less than 1%.
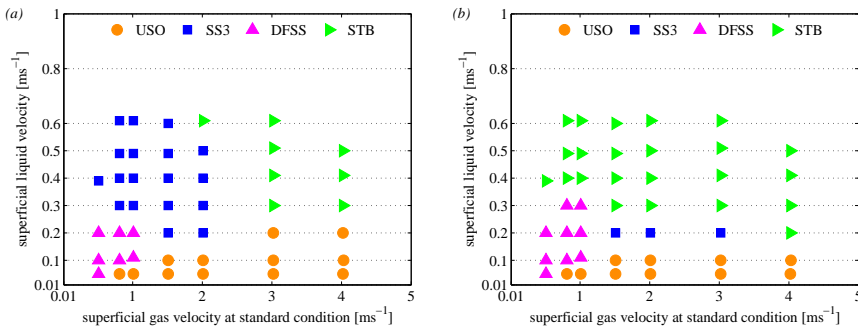

Figure 8.5: *Flow pattern map of the system, indicating unstable oscillations (USO), severe slugging of type 3 (SS3), dual-frequency severe slugging (DFSS), and stable flow (STB) (a) experimental flow pattern map (b) numerical flow pattern map.*

Fig. 8.5(a) shows the flow map of the horizontal pipeline-riser system generated based on our experimental data, indicating whether each point is in STB, SS3, USO or DFSS regime. Such a flow pattern map can be of help in design and operation phase in an offshore oil-production system.

Table 8.2 summarizes the considered DFSS cases in the experiments with their associated superficial liquid and gas velocities. The measured periods and the average amplitude of the riser ΔP for both high- and low-frequency oscillations are also given in Table 8.2. The measured periods for high-frequency oscillations are associated with SS3 and USO flow regimes, respectively. The considered experimental cases for SS3, USO, and STB with their associated superficial liquid and gas velocities are summarized in Table 8.3. The measured period as well as the average maximum, minimum and amplitude of the riser ΔP for these cases are also given in Table 8.3.

A Fast Fourier Transformation (FFT) was applied to derive the frequency components in the riser ΔP traces of the considered experimental cases. We applied a MATLAB built-in function which uses several algorithms in combination,

Table 8.2: *Experimental and simulation results of the periods and the average amplitude of the riser ΔP for all DFSS cases.*

Case	U_{SL} (ms^{-1})	U_{SG0} (ms^{-1})	Type		High-frequency oscillations				Low-frequency oscillations			
					Period (s)		Amplitude of ΔP (bar)		Period (s)		Amplitude of ΔP (bar)	
			Exp.	Sim.	Exp.	Sim.	Exp.	Sim.	Exp.	Sim.	Exp.	Sim.
1	0.05	0.51	DFSS	DFSS	120 & 84	225&117	0.3	0.4	1040	1052	0.7	0.6
2	0.10	0.51	DFSS	DFSS	109 & 63	229&186	0.5	0.4	1200	980	1.1	0.9
3	0.10	0.81	DFSS	DFSS	75 & 62	152&75	0.4	0.5	901	1063	0.6	0.6
4	0.11	1.01	DFSS	DFSS	59 & 43	133&66	0.4	0.5	675	995	0.5	0.6
5	0.20	0.51	DFSS	DFSS	99 & 52	408&272	0.7	0.3	1141	817	1.1	1.1
6	0.20	0.81	DFSS	DFSS	71 & 45	118&68	0.6	0.7	781	465	0.9	1.1
7	0.20	1.01	DFSS	DFSS	49 & 39	138&61	0.6	0.7	680	539	0.9	1.1

Table 8.3: *Experimental and simulation results of the period, the average maximum, minimum and amplitude of the riser ΔP for all SS3, USO and STB cases. Colours distinguish different experimentally-observed flow regimes.*

Case	U_{SL} (ms^{-1})	U_{SG0} (ms^{-1})	Type		Period (s)		Max ΔP (bar)		Min ΔP (bar)		Amplitude of ΔP (bar)	
			Exp.	Sim.	Exp.	Sim.	Exp.	Sim.	Exp.	Sim.	Exp.	Sim.
8	0.20	1.51	SS3	SS3	38	95	0.91	1.17	0.33	0.24	0.58	0.93
9	0.20	2.01	SS3	SS3	28	82	0.79	1.06	0.33	0.23	0.46	0.83
10	0.30	0.81	SS3	DFSS	53	143, 72&668	1.35	1.50	0.42	0.40	0.93	1.10
11	0.30	1.01	SS3	DFSS	95	167, 83&668	1.41	1.50	0.40	0.39	1.01	1.11
12	0.30	1.51	SS3	STB	74	0	1.30	0.49	0.33	0.49	0.97	0.00
13	0.30	2.01	SS3	STB	60	0	1.08	0.42	0.30	0.42	0.78	0.00
14	0.39	0.51	SS3	STB	57	0	1.45	0.68	0.58	0.68	0.87	0.00
15	0.40	0.81	SS3	STB	104	0	1.47	0.72	0.45	0.72	1.02	0.00
16	0.40	1.01	SS3	STB	88	0	1.45	0.66	0.42	0.66	1.03	0.00
17	0.40	1.51	SS3	STB	71	0	1.38	0.57	0.36	0.57	1.02	0.00
18	0.40	2.01	SS3	STB	57	0	1.17	0.51	0.34	0.51	0.83	0.00
19	0.49	0.81	SS3	STB	92	0	1.46	0.79	0.56	0.79	0.90	0.00
20	0.49	1.01	SS3	STB	83	0	1.47	0.74	0.40	0.74	1.07	0.00
21	0.49	1.51	SS3	STB	67	0	1.46	0.65	0.48	0.65	0.98	0.00
22	0.50	2.01	SS3	STB	57	0	1.33	0.60	0.37	0.60	0.96	0.00
23	0.61	0.81	SS3	STB	79	0	1.48	0.88	0.52	0.88	0.96	0.00
24	0.61	1.01	SS3	STB	77	0	1.48	0.83	0.51	0.83	0.97	0.00
25	0.60	1.51	SS3	STB	64	0	1.41	0.74	0.42	0.74	0.99	0.00
26	0.05	0.81	USO	USO	75	211	0.54	0.63	0.28	0.20	0.26	0.43
27	0.05	1.01	USO	USO	79	108	0.50	0.54	0.26	0.20	0.24	0.34
28	0.05	1.51	USO	USO	75&52	200&87	0.47	0.47	0.24	0.14	0.23	0.33
29	0.05	2.01	USO	USO	71	174&85	0.48	0.47	0.24	0.13	0.24	0.34
30	0.05	3.02	USO	USO	48	121&68	0.48	0.47	0.26	0.14	0.22	0.33
31	0.05	4.02	USO	USO	41&55	100&44	0.48	0.47	0.27	0.13	0.21	0.34
32	0.10	1.51	USO	USO	90&47	121	0.60	0.67	0.27	0.21	0.33	0.46
33	0.10	2.01	USO	USO	64	105	0.60	0.63	0.27	0.16	0.33	0.47
34	0.10	3.02	USO	USO	45	77	0.58	0.57	0.27	0.11	0.31	0.46
35	0.10	4.03	USO	USO	33	60&35	0.54	0.41	0.26	0.10	0.28	0.31
36	0.20	3.02	USO	SS3	42&21	66	0.73	0.97	0.28	0.15	0.45	0.82
37	0.20	4.02	USO	STB	31	15&13	0.63	0.46	0.25	0.09	0.38	0.37
38	0.30	3.02	STB	STB	41&20	29&14	0.76	0.46	0.30	0.32	0.46	0.14
39	0.30	4.02	STB	STB	5	0	0.62	0.32	0.28	0.32	0.34	0.00
40	0.41	3.02	STB	STB	4	0	0.73	0.44	0.36	0.44	0.37	0.00
41	0.41	4.02	STB	STB	5	0	0.71	0.41	0.35	0.41	0.36	0.00
42	0.51	3.02	STB	STB	3	0	0.79	0.53	0.46	0.53	0.33	0.00
43	0.50	4.02	STB	STB	5&2	0	0.78	0.48	0.38	0.48	0.40	0.00
44	0.61	2.01	STB	STB	4	0	0.98	0.69	0.59	0.69	0.39	0.00
45	0.61	3.02	STB	STB	3	0	0.90	0.62	0.52	0.62	0.38	0.00

including a variation of Cooley-Tukey, a prime factor algorithm, and a split-radix algorithm. The experimental periods mentioned in Tables 8.2 and 8.3 were calculated from the corresponding FFT of the riser ΔP traces. Although most of the experimental riser ΔP traces mentioned in Table 8.3 showed FFT with a dom-

inant peak (one dominant period), there are some in which two dominant peaks are found. For these cases two dominant periods are given.

It can be observed from Table 8.3 that for the considered experimental SS3 cases a dominant frequency (1/period) appeared. As an example of the SS3 behaviour, Fig. 8.6(*a*) shows the FFT corresponding to the riser ΔP trace of case 17 (U_{SL}=0.40 m s^{-1} & U_{SG0}=1.51 m s^{-1}), which gives a dominant frequency and the subsequent dominant time period can be determined. However, as can be seen from Table 8.3, for some of the considered experimental USO and STB cases two dominant frequencies appeared. As an example of this, Fig. 8.6(*b*) shows the FFT corresponding to the riser ΔP trace of case 32 (U_{SL}=0.10 m s^{-1} & U_{SG0}=1.51 m s^{-1}), which gives two dominant frequencies for this USO case.
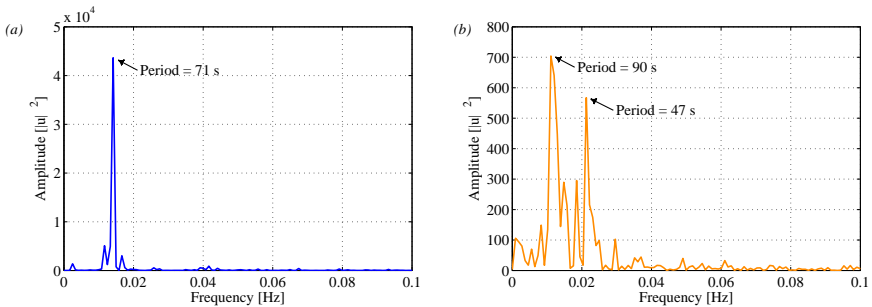
Figure 8.6: *FFT for different riser ΔP traces (a) SS3 (case 17, Table 8.3) (b) USO (case 32, Table 8.3).*

It can be observed from the experimental flow pattern map that at relatively higher liquid flow rates, the flow regime changes from SS3 to STB with the increase of U_{SG0} at constant U_{SL}. Fig. 8.7 depicts the variation of the average fluctuation amplitude of the riser ΔP with the increase of U_{SG0} at $U_{SL} \simeq 0.40$ m s^{-1}. It can be seen that the average fluctuation amplitude of the riser ΔP decreases significantly as U_{SG0} exceeds a critical value at $U_{SL} \simeq 0.40$ m s^{-1}. Also, the relation between the measured frequency and U_{SG0} at $U_{SL} \simeq 0.40$ m s^{-1} is illustrated in Fig. 8.7. It can be observed that the measured frequency increases significantly as U_{SG0} exceeds a critical value at $U_{SL} \simeq 0.40$ m s^{-1}. Therefore, the flow regime transition can also be recognized from the measured frequency and the fluctuation amplitude of the riser ΔP. In Fig. 8.8(*a*) and (*b*) the experimental riser ΔP traces of two cases corresponding to SS3 (relatively low gas flow rate, U_{SG0} =0.81 m s^{-1}) and STB (relatively high gas flow rate, U_{SG0} =3.02 m s^{-1}) at $U_{SL} \simeq 0.40$ m s^{-1} are shown.

It can also be observed from the experimental flow pattern map that at relatively low liquid flow rates, the flow regime changes from DFSS to USO with the increase of U_{SG0} at constant U_{SL}. In Fig. 8.9(*a*) and (*b*) the experimental
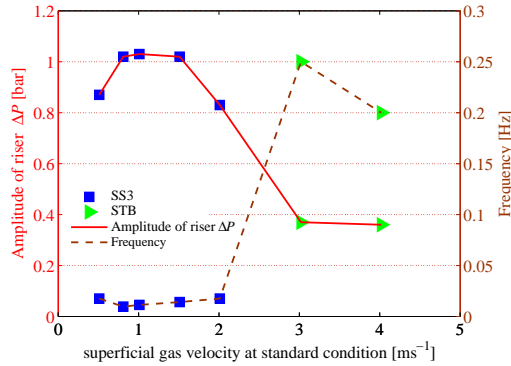
Figure 8.7: *Dependency of the experimental average amplitude of the riser ΔP and frequency on U_{SG0} at $U_{SL} \simeq 0.40$ ms^{-1}.*
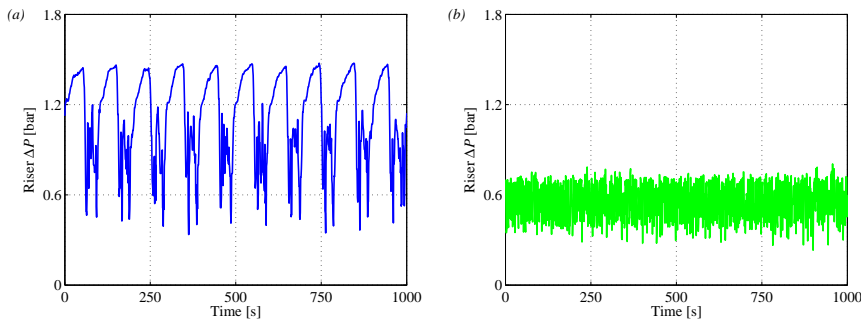

Figure 8.8: *Experimental riser ΔP traces (a) SS3 (case 15, Table 8.3) (b) STB (case 40, Table 8.3).*

riser ΔP traces of two cases corresponding to DFSS (relatively low gas flow rate, U_{SG0} =0.81 ms^{-1}) and USO (relatively high gas flow rate, U_{SG0} =1.51 ms^{-1}) at $U_{SL} = 0.10$ ms^{-1} are shown. The dual-frequency fluctuations can easily be observed in Fig. 8.9(a). The measured periods of high- and low-frequency oscillations for this case are 75, 62 and 901 s, respectively. Fig. 8.9(b) shows two dominant high-frequency fluctuations which were also captured by the FFT, see Fig. 8.6(b). The measured periods of the oscillations for this case are 90 s and 47 s. The amplitude of the fluctuation of the riser ΔP is small and also does not exhibit a gradual cyclic transition between two meta-stable states, as a DFSS case does. Therefore, this case is classified as an unstable oscillations flow regime.
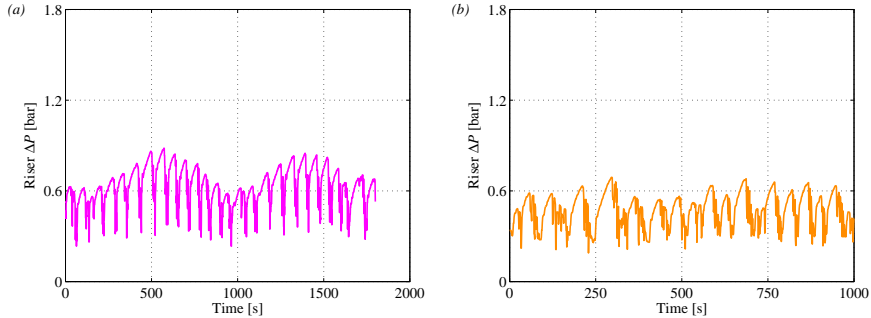
Figure 8.9: *Experimental riser ΔP traces (a) DFSS (case 3, Table 8.2) (b) USO (case 32, Table 8.3).*

8.4   Numerical simulations

A one-dimensional numerical model of air-water two-phase flow in the horizontal pipeline-riser system was developed using the multiphase flow simulator OLGA (version 6.3.0, released in 2010). This is a transient one-dimensional, commercial computer code based on a two-fluid flow model. The three-dimensional velocity profile in the pipeline and riser is averaged over the cross section, which simplifies the flow equations from three-dimensional to one-dimensional. This simplification requires using empirical closure relations in the model for the wall friction and for the interfacial stress between the liquid and the gas layers. The one-dimensional model contains three separate mass balance equations for the gas, liquid droplets and liquid film, which are coupled through interfacial mass transfer terms. Two momentum balance equations are applied: one combined equation for the gas flow with liquid droplets, and one equation for the liquid film flow (see Bendiksen et al., 1991).

The applied model is the state-of-the-art engineering approach used for the multiphase flow design of oil and gas pipelines. Through the years the model was compared with various laboratory and field data sets (see Nossen et al., 2000). Most of the laboratory data were for air and water flows. Most of the field data concerned pipe flows of gas-condensate (i.e. light oil). The model was not a-priori tuned or optimized for severe slugging conditions. The model can optionally include so called slugtracking, which applies a dedicated numerical scheme to follow the propagation of hydrodynamic slugs with a relatively coarse grid. In the present study slugtracking was not used. Instead a sufficiently fine numerical grid was used to see if we can reproduce the details of the various slug types found in the experiments. The numerical simulations are mainly meant to support that the dual frequency found in the experiments is not an artefact of the experimental

set-up. Furthermore the simulations can help to explain the physical background of the occurrence of the dual-frequency instability.

It was confirmed by the temperature transmitters located in the test loop that the temperature change throughout the test loop is negligible. Thus, the fluid temperature in the numerical model is set to be constant, 15.56 °C in our model. In the numerical model constant mass flow rates and pressure were specified as the inlet and outlet boundaries, respectively. A non-zero pressure drop across the S^3 was observed during the experiments. Therefore, a valve with K_v value of 12 $m^3\,h^{-1}\,bar^{-1/2}$ was included in the numerical model. The numerical model, with a grid resolution of 25 cm giving a total of 570 grid cells in the pipeline and riser, is used to simulate all cases mentioned in Tables 8.2 and 8.3. The maximum and minimum simulation time steps were 0.1 s and 0.0001 s, respectively. We carried out a sensitivity analysis to verify that the number of grid cells is such that the results are numerically accurate. This was accomplished by repeating the simulation with three different cell sizes of 5.08 cm, 25 cm and 100 cm. The optimum grid size (25 cm) was selected based on the comparison between simulation results with experimental data of one typical severe slugging case. However, the severe slugging flow pattern was predicted by all three mentioned cell sizes.

Fig. 8.5(b) shows the flow pattern map of the horizontal pipeline-riser system which has been developed based on numerical simulation results. The numerical simulations were performed using U_{SL} and U_{SG0} values of all experimental cases given in Tables 8.2 and 8.3. In Table 8.2 for all considered DFSS cases, the predicted periods and the average amplitude of the riser ΔP for both high- and low-frequency oscillations are given. The predicted period as well as the average maximum, minimum and amplitude of the riser ΔP for all considered SS3, USO and STB cases are given in Table 8.3. A good agreement is observed in the predictions of DFSS, USO and STB flow regimes. However, the numerical model fails to predict most of the SS3 cases.

During the process of severe slugging of type 3, the flow pattern in the pipeline close to the riser base changes from hydrodynamic slug flow to elongated bubble flow. However, for most of the cases, during the whole process of SS3, just hydrodynamic slug flow was predicted by the numerical model. Consequently, the closure relations for hydrodynamic slug flow were used in the flow calculations.

It is worth mentioning that all the predicted periods were obtained using the MATLAB FFT algorithm, see Section 8.3. The numerical model predicted the DFSS flow regime for two experimental SS3 cases, 10 and 11. For these cases, three predicted periods are given, two periods related to the high-frequency oscillations and one period associated with the low-frequency oscillations. Also, some of the predicted riser ΔP traces showed an FFT with two dominant peaks. For these cases two predicted periods are given in Table 8.3.

Fig. 8.10(a) shows the comparison of the riser ΔP between the numerical prediction and experimental data for case 2, Table 8.2. As can be seen, the numerical model correctly predicts the dual-frequency characteristics of this case. Although the period and amplitude of the low-frequency oscillations are predicted
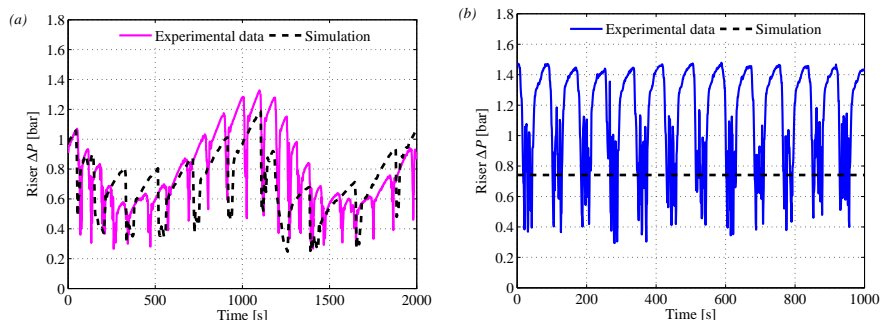
Figure 8.10: *Experimental and predicted riser ΔP (a) DFSS (case 2, Table 8.2) (b) SS3 (case 20, Table 8.3).*

well, the predicted periods of the high-frequency oscillations are not very accurate. The measured periods of the high- and low-frequency oscillations are 109, 63 (high-frequency oscillations) and 1200 s, respectively. The predicted values are 229, 186 and 980 s, respectively. Fig. 8.11(*a*) shows the comparison of the water outflow rate between the simulation and experiment for this DFSS case. The water outflow rate can be estimated through measuring the water level in the second water storage tank (V-202), see Fig. 8.1. There are periods of almost no water production followed by large peaks of water outflow. However, the water production peaks are not of equal size and show the low-frequency oscillations with a period of approximately 1200 s and an amplitude of 6 $\mathrm{m^3\,h^{-1}}$. It should be noted that other types of severe slugging; e.g. SS3, exhibit water production peaks of equal size. These oscillations are the characteristics of the DFSS flow regime and are captured by the simulation as well. As expected, the observed period of the low-frequency oscillations in the water outflow is the same as the one observed in the riser ΔP trace. Also, the comparison of the air outflow between the simulation and experiment for this case is shown in Fig. 8.11(*b*). The air outflow rate shows the same pattern as observed and explained for the water outflow rate. It is not surprising that the observed period of the low-frequency oscillations is equal to the one observed in Fig. 8.11(*a*). The amplitude of the low-frequency oscillations in the measured air outflow rate is approximately 10 $\mathrm{Sm^3\,h^{-1}}$. It can also be seen that the numerical model could not correctly predict the air outflow rate. As mentioned in the description of SS3, many air bubbles with different shapes and sizes are distributed in the horizontal pipeline as the elongated bubble, and penetrate the liquid slug in the riser. These widely distributed air bubbles are not modeled appropriately.

Fig. 8.10(*b*) shows the comparison of the riser ΔP between the numerical prediction and experimental data for case 20, Table 8.3. The measured period
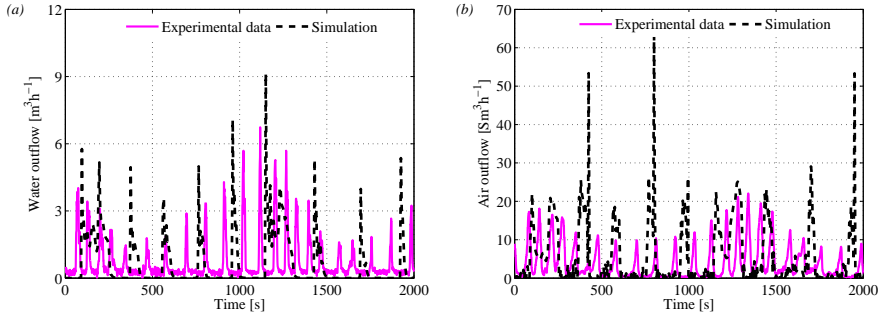
Figure 8.11: *Experimental and predicted outflows for case 2, Table 8.2 (a) water out-flow (b) air outflow.*

of this SS3 case is 83 s, whereas the numerical model predicts a steady state condition.

Figs. 8.12(a) and 8.12(b) compare the riser ΔP traces between the numerical simulations and experiments for case 29 and 41 in Table 8.3, respectively. The numerical model is capable of predicting these two USO and STB flow regimes. However, the measured period of the USO case is 71 s, and the numerical model predicts 174 s and 85 s. For the STB case, the measured period is 5 s, and the model gives a steady state solution.
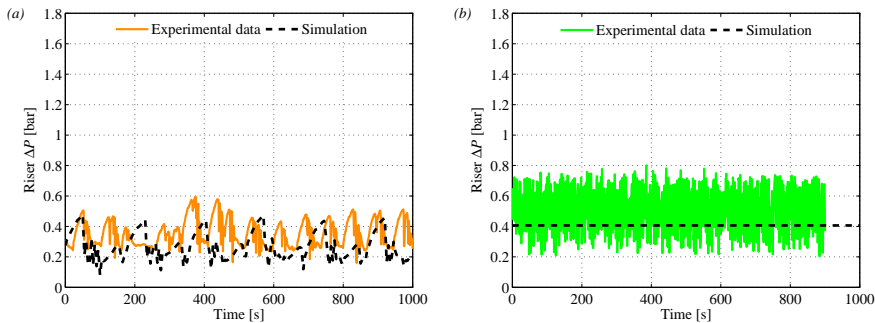

Figure 8.12: *Experimental and predicted riser ΔP (a) USO (case 29, Table 8.3) (b) STB (case 41, Table 8.3).*

To assess the impact of the pipeline length on the characteristics of the DFSS, four simulations with a 100 m, 200 m, 300 m and 400 m long horizontal pipeline fol-

lowed by the riser at equal operating conditions (U_{SL}=0.20 m s^{-1} and U_{SG0}=0.51 m s^{-1}) and 0.0 m^3 air buffer volume, were performed. The simulated case corresponding to a 300 m long horizontal pipeline is equivalent to case 5 in Table 8.2 corresponding to 0.4 m^3 air buffer volume (albeit that in the simulated extra 200 m pipeline some liquid holdup will be present which is absent in the buffer volume used in the experiment). Fig. 8.13 shows that the DFSS flow regime evolves when the pipeline length exceeds a certain threshold between 100 m and 200 m. The predicted flow regimes are SS3, DFSS, DFSS and DFSS, respectively. Also the period of the low-frequency oscillations increases by increasing the pipeline length. The liquid balance in the model shows that the period of the low-frequency oscillations is equal to the time required to fill the pipeline with an amount of liquid that is equal to the difference in holdup for the two states (SS3 and USO) between which the low-frequency oscillations occur. Note that the predicted period of low-frequency oscillations associated to the numerical model with 300 m long horizontal pipeline (1220 s) is higher than the one associated to case 5 in Table 8.2 with the air buffer volume of 0.4 m^3 (817 s) as it takes longer to fill the additional length of the pipeline with extra liquid holdup and reduce it again in each cycle of the low-frequency oscillations.
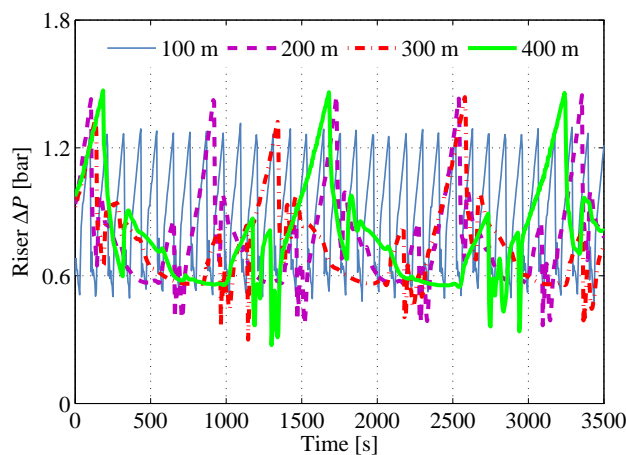

Figure 8.13: *Predicted riser ΔP for 100 m, 200 m, 300 m and 400 m long horizontal pipeline followed by the riser corresponding to 0.0 m^3 air buffer volume (U_{SL}=0.20 m s^{-1} and U_{SG0}=0.51 m s^{-1}).*

8.5   Conclusions

(1) It has been shown that even in the horizontal pipeline-riser system, severe slugging can develop.

(2) Four types of flow regime were found in our new laboratory experiments in the horizontal pipeline-riser system: unstable oscillations (exhibiting cyclic, low amplitude pressure fluctuations), severe slugging of type 3 (consisting of four stages; transient slugs, aerated slug growth, fast aerated liquid production, and gas blowdown), dual-frequency severe slugging (characterized by dual-frequency instabilities; high-frequency fluctuations related to the severe slugging of type 3 and unstable oscillations, and low-frequency fluctuations related to the transition between severe slugging of type 3 and unstable oscillations), and hydrodynamic slugs initiated in the pipeline and flowing into the riser.

(3) A cycle of severe slugging of type 3 in the horizontal pipeline-riser system exhibits a relatively long-period transient slugs stage compared to the one occurring in a downward inclined configuration.

(4) The dynamic simulation tool OLGA was used to reproduce the characteristics of all experimentally observed flow regimes. The numerical model correctly predicts the occurrence of dual-frequency severe slugging, unstable oscillations, and stable flow regimes. However, the numerical model predicted stable flow for almost all experimental cases of severe slugging of type 3.

Acknowledgements

References

Baliño, J.L., Burr, K.P., Nemoto, R.H., 2010. Modeling and simulation of severe slugging in air-water pipeline-riser systems. Int. J. Multiphase Flow 36, 643-660.

Bendiksen, K., Malnes, D., Moe, R., Nuland, S., 1991. The dynamic two-fluid model OLGA: Theory and application. SPE Production Eng. J. 6, 171-180.

Bøe, A., 1981. Severe slugging characteristics; part 1: Flow regime for severe slugging; part 2: Point model simulation study. Presented at Selected Topics in Two-Phase Flow, Trondheim, Norway.

Fabre, J., Peresson, L., Corteville, J., Odello, R., Bourgeols, T., 1990. Severe slugging in pipeline/riser systems. SPE Production Eng. J. 5, 299-305.

Nossen, J., Shea, R., Rasmussen, J., 2000. New developments in flow modeling and field data verification. 2nd North American Conference on Multiphase Technology, Banff, Canada, 21-23 June.

Pots, B., Bromilow, I., Konijn, M., 1987. Severe slug flow in offshore flowline/riser systems. SPE Production Eng. J. 2, 319-324.

Sarica, C., Shoham, O., 1991. A simplied transient model for pipeline-riser systems. Chemical Engineering Science 46, 2167-2179.

Schmidt, Z., Brill, J., Beggs, H., 1980. Experimental study of severe slugging in a two-phase-flow pipeline-riser pipe system. SPE J. 20, 407-414.

Taitel, Y., 1986. Stability of severe slugging. Int. J. Multiphase Flow 12, 203-217.

Taitel, Y., Vierkandt, S., Shoham, O., Brill, J., 1990. Severe slugging in a pipeline-riser system: Experiments and modeling. Int. J. Multiphase Flow 16, 57-68.

Yocum, B., 1973. Offshore riser slug flow avoidance, mathematical model for design and optimization. paper SPE 4312 presented at SPE Annual European Meeting, London.

Chapter 9

Dual-Frequency Severe Slugging in Horizontal Pipeline-Riser Systems§

Abstract

A new type of severe slugging is found that can occur in two-phase flow of gas and liquid in pipeline-riser systems. This instability, which will be referred to as "dual-frequency severe slugging (DFSS)", generates a different class of flow oscillations compared to the classical severe slugging cycle, having a dominant single frequency, that is commonly found in a pipe downward inclined by a few degrees from the horizontal connected to a vertical riser. The DFSS flow pattern was found in laboratory experiments carried out in a 100 m long, 50.8 mm diameter horizontal pipeline followed by a 15 m high, 50.8 mm diameter vertical riser operating at atmospheric end pressure. The experimental facility also included a 400 litre gas buffer vessel, placed upstream of the pipeline, to obtain extra pipeline compressibility. Air and water were used as the experimental fluids. At constant inflow conditions, we observed a type of severe slugging exhibiting a dual-frequency behaviour. The relatively high-frequency fluctuations, which are in the order of 0.01 Hz, are related to the classical severe slugging cycle or to an unstable oscillatory process. The relatively low-frequency fluctuations, which are in the order of 0.001 Hz, are associated with the gradual cyclic transition of the system between two meta-stable states, i.e. severe slugging and unstable oscillations. Numerical simulations were performed using OLGA, a one-dimensional two-fluid flow model. The numerical model predicts the relatively low-frequency fluctuations associated with the DFSS flow regime. The laboratory experiments

111

and the numerical simulations showed that the evolution of the DFSS is proportional to the length of the pipeline.

9.1   Introduction

Gas-liquid two-phase flows are encountered in various industrial fields, such as the petroleum [1], chemical processing [2], nuclear [3], and space industries [4]. Gas-liquid two-phase flows occur in the petroleum industry during the production and transportation of oil and gas [5, 6]. Pipeline-riser systems are often found in offshore oil and gas production facilities. They transport hydrocarbons (plus often also some water) from subsurface oil and gas wells to a central production platform [7, 8]. The diameter of the pipeline and the riser ranges from typically 0.1 to 0.8 m. The length of the pipeline can vary from a few kilometers (for liquid dominated systems) to more than one hundred kilometers (for gas dominated systems). The height of the riser depends on the water depth, which can range from a few tens of meters (in lakes) to more than two kilometers (in deepwater areas). In these pipeline-riser systems both liquid and gas flow simultaneously, creating a two-phase flow.

Even at constant boundary conditions represented by liquid and gas mass inflow rates and separator back pressure, transient flow conditions may occur in a pipeline-riser system. Here, at relatively low flow rates, liquid accumulates at the bottom of the riser, creating a blockage for the gas, until sufficient upstream pressure has been built up to flush the liquid slug out of the riser. After this liquid surge, and subsequent gas surge, part of the liquid in the riser falls back to the riser base to create a new blockage and the cycle repeats. This transient cyclic phenomenon causes periods of no liquid and gas production at the riser top followed by very high liquid and gas surges, and is called severe slugging [9]. This poses serious problems to the designers and operators of such pipeline-riser systems. Large-amplitude fluctuations in the liquid and gas flow rates can significantly reduce the production from the reservoir (due to an increased back pressure) and it can also lead to shut down or even damage of the platform facilities, downstream of the riser, like separators and compressors. Therefore, the accurate prediction of severe slugging characteristics is essential for the proper design and operation of two-phase flow in these systems [10, 11].

Severe slugging in a downward inclined pipeline-riser system (a pipe downward inclined by a few degrees from the horizontal connected to a vertical riser) had been studied both experimentally and numerically by various researchers (see Schmidt et al. [12], Taitel [13], Pots et al. [14], Taitel et al. [15]). Montgomery and Yeung [16] conducted an experimental study of severe slugging for an s-shaped pipeline-riser system. Fabre et al. [17] observed severe slugging not only with a downward inclined pipeline, but also with a horizontal pipeline followed by a vertical riser albeit with a smaller amplitude of pressure fluctuations compared to that of the downward inclined pipeline-riser configuration. Sarica and Shoham

[18] proposed a simplified transient model to simulate severe slugging. They tested their model against a broad range of data, including the data obtained by Fabre et al. [17] for the horizontal pipeline-riser system. The simulations for downward inclined pipeline-riser systems showed better accuracy than the previously published model by Taitel [13]. However, their model did not correctly predict the severe slugging cycle reported by Fabre et al. [17] for the horizontal pipeline-riser system. Sarica and Shoham [18] concluded that the horizontal pipeline in the experiments by Fabre et al. [17] might have actually been slightly downward inclined.

Most of the existing laboratory experiments for severe slugging were conducted in a pipe that is downward inclined from the horizontal by a few degrees, followed by a vertical pipe [9, 12, 15, 19]. Because of the importance of flow oscillations in practical applications, the flow behaviour needs to be known for downward inclined, horizontal, as well as upward inclined orientation of the first pipe. In this paper, we have carried out experiments for the two-phase flow of air and water in a horizontal pipeline followed by a vertical riser (a horizontal pipeline-riser system). The aim is to confirm the observation made by Fabre et al. [17] that severe slugging exists in a horizontal pipeline-riser system.

The objective of this study is twofold. The first objective is to identify experimentally at what flow rates severe slugging occurs in a flow pattern map of a horizontal pipeline-riser system. The second objective is to investigate both experimentally and numerically the characteristics of dual-frequency severe slugging, that has not been reported before.

9.2   Experimental Facility

The existing two-phase, air and water flow facility of the Shell Technology Centre in Amsterdam (STCA), see Fig. 9.1, was used to conduct experiments. The test facility comprises four main parts: the fluid supply, test loop (pipeline and riser), separation area and measurement and control devices. The full experimental procedures, including startup, control, shutdown and data logging are done remotely through dedicated control and data acquisition systems.

Air at a pressure of 6 barg is delivered via a connection with the main air supply at the STCA. The air is supplied to a thermal mass flow meter and controller of model 5853i by Brooks, which automatically provides an almost constant mass flow rate into the test loop. The provided gas mass inflow rate varies by less than 0.2% of the reading range. A maximum air flow rate of 30 $\mathrm{Sm^3\,h^{-1}}$ can be supplied (the S refers to standard conditions at 1.01 bara and 15.56 °C). The water supply is city tap water connected to the first water storage tank, see Fig. 9.1. A worm pump connected to this tank brings water to the second water storage tank situated right below the separator. Then water is supplied to the pipeline by a variable speed centrifugal pump. A relatively constant water volumetric flow rate can be achieved by manually adjusting the pump speed and by adjusting the
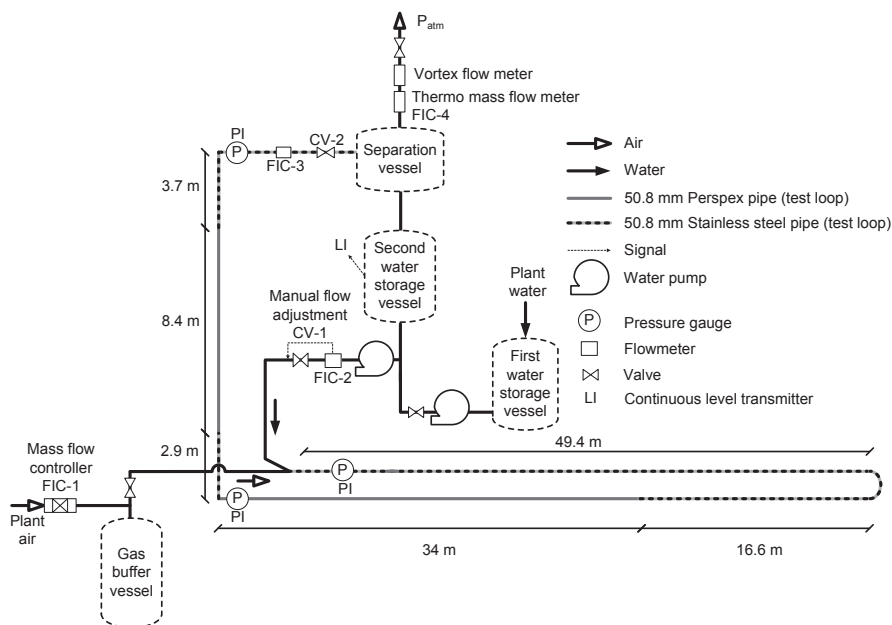
Figure 9.1: *Schematic of the experimental facility. The test loop comprises both the horizontal pipeline and the vertical riser.*

opening of a control valve, which is located directly downstream of the pump. The liquid inflow rate varies by less than 2% of the reading range. A maximum water flow rate of 5 $\text{m}^3\,\text{h}^{-1}$ can be supplied. The water flow rate into the test loop is measured with an electromagnetic flow meter of type Promag 50W by Endress & Hauser.

The test loop consists of a 66 m long, 50.8 mm inside diameter horizontal steel pipeline connected to a 34 m long, 50.8 mm inside diameter horizontal Perspex pipeline followed by a 15 m high, 50.8 mm inside diameter vertical Perspex riser. The elevation of the horizontal pipeline was measured by a laser-level measurement sensor of type PR 25 IF by Hilti. The level-change of the horizontal pipeline was 1 mm over 15 m showing that the first part of the test loop was virtually horizontal. The Perspex pipes are transparent which enables visual observation of the flow behaviour.

The riser discharges the fluid into the two-phase separator, operating at atmospheric pressure. The separator pressure varies by less than 3% of the reading range, providing an almost constant boundary condition. Air and water are separated by gravity. The upper section of the separator has a mist mat and air flows out of the experimental facility, monitored by one vortex and one thermo mass flow indicators. The lower section of the separator drains the water, which

flows down and returns to the second water storage tank. The water level in the second water storage tank is measured with a continuous level transmitter of type Levelflex M-FMP40 by Endress & Hauser, see Fig. 9.1.

A variable-volume gas buffer vessel is located between the gas mass flow controller and the gas inlet, upstream of the pipeline. The air volume of the buffer vessel can be changed by partly filling it with water. The function of the gas buffer vessel is to create a virtually longer pipeline. In the current study, the maximum applied air volume of the buffer vessel is 400 litre, which corresponds to an additional pipeline length of 197 m. The facility also includes a liquid control valve, which has a K_v value (flow factor) of 12 m^3 h^{-1} bar$^{-1/2}$, at the riser top. During all experiments this liquid control valve was left fully open. It was verified (through comparison with numerical simulations) that the presence of the fully-open liquid control valve (with its relatively large K_v value) has a negligible effect on the slugging behaviour.

Pressure transducers are located at the inlet of the pipeline, at the riser base and at the top of the riser. They are manufactured by Endress & Hauser and are of type Cerebar M-PMC41. Additional pressure devices are also used to measure and monitor the pressure in the gas buffer vessel, the inlet of the gas line, the outlet of the liquid pump and in the two-phase separator. The temperature was monitored using thermocouples that are located at various locations in the test loop, and fluctuated by less than 1 °C during an experimental run. Table 9.1 provides a summary of the instrumentation used in the experimental facility.

In this paper we report the inaccuracies of the pressure measurements and flow rates based on the actual readout of the instruments (which may fluctuate during an experiment) and the full range inaccuracy given in Table 9.1.

Table 9.1: *Specifications of the equipment in the flow loop. E+H and D/M are acronyms for Endress+Hauser and Dresser/Masoneilan, respectively.*

Label (Fig. 9.1)	Instrument	Manufacture	Type	Range	Units	Accuracy (full scale)
PI	Pressure transmitter	E+H	Cerebar M-PMC41	0 - 10	bara	0.2%
FIC-1	Thermal Mass flow meter & controller	Brooks	5853i	0 - 30	Sm^3 h^{-1}	1%
FIC-2	Electromagnetic flow meter	E+H	Promag 50W	0 - 7.5	m^3 h^{-1}	0.5%
FIC-3	Electromagnetic flow meter	E+H	Promag 50W	0 - 18	m^3 h^{-1}	0.5%
FIC-4	Thermal mass flow meter	E+H	t-mass 65F	0 - 110	Sm^3 h^{-1}	1.5%
LI	Continuous level transmitter	E+H	Levelflex M-FMP40	0 - 100	%	+/-3 mm
CV-1	Control valve	D/M	35-35112	0 - 12	m^3 h^{-1} bar$^{-1/2}$	-
CV-2	Control valve	D/M	35-35202	0 - 12	m^3 h^{-1} bar$^{-1/2}$	-

9.3   Riser-Induced Instabilities

Based on preliminary numerical simulations an experimental matrix was defined to cover all possible flow regimes occurring in the test loop. Later, by obtaining further experimental results this experimental matrix was refined to establish both

the characteristics of each flow regime and the transition boundaries between the flow regimes. The water flow rate ranged from 0.34 $m^3 h^{-1}$ to 4.45 $m^3 h^{-1}$ and the air flow rate from 3.70 $Sm^3 h^{-1}$ to 29.38 $Sm^3 h^{-1}$. The corresponding superficial water velocity ranged from U_{SL}= 0.05 - 0.61 $m s^{-1}$ and superficial air velocity at standard conditions (1.01 bara, 15.56 °C) ranged from U_{SG0}= 0.51 - 4.03 $m s^{-1}$.

Different flow regimes have been obtained by changing the water and air flow rates. The observed flow regimes are classified into four categories: stable flow (STB), severe slugging of type 3 (SS3), unstable oscillations (USO), and "dual-frequency severe slugging (DFSS)". Severe slugging in a downward inclined pipeline-riser system was classified by several researchers including Baliño et al. [19] and Malekzadeh et al. [20] into three types; severe slugging of type 1 (having a pure liquid slug length larger than the riser height), severe slugging of type 2 (having a pure liquid slug length smaller than the riser height), and severe slugging of type 3 (characterized by a growing long aerated liquid slug in the riser followed by a gas blow down stage). Here, the same abbreviations were used for the classification of the flow regimes. The flow regimes were delineated based on visual observations and analysis of the pressure drop over the riser (riser ΔP). Typical riser ΔP traces of these four flow regimes are shown in Fig. 9.2. The above mentioned, experimentally observed, flow regimes are described below.
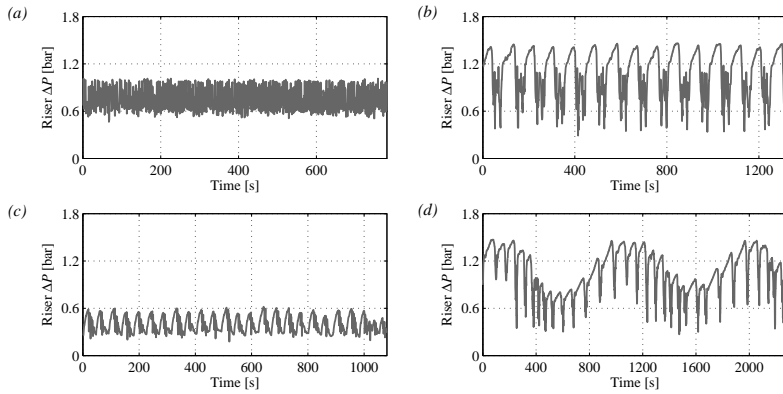

Figure 9.2: *Experimental riser ΔP traces of the four mentioned flow patterns corresponding to (a) STB (U_{SL}=0.61 $m s^{-1}$ & U_{SG0}=2.01 $m s^{-1}$), (b) SS3 (U_{SL}=0.40 $m s^{-1}$ & U_{SG0}=1.01 $m s^{-1}$), (c) USO (U_{SL}=0.10 $m s^{-1}$ & U_{SG0}=3.02 $m s^{-1}$) and (d) DFSS (U_{SL}=0.20 $m s^{-1}$ & U_{SG0}=0.51 $m s^{-1}$).*

9.3.1   Stable Flow

Hydrodynamic slugs are generated in the pipeline and move up into the riser. Therefore, the flow patterns in the pipeline and in the riser are mainly slug flow. Hydrodynamic slug flow is characterized by a series of gas pockets separated by liquid slugs. The riser ΔP exhibits fluctuations with a small amplitude (approximately less than 0.4 bar in our experiments) and high frequency. Thus, hydrodynamic slug flow is considered stable flow as compared to other types of flow regime mentioned in this study. The riser ΔP trace of this flow regime is shown in Fig. 9.2(a).

9.3.2   Severe Slugging of Type 3

Severe slugging of type 3 is characterized by pulsating long liquid slugs separated by small gas pockets in the riser followed by gas blow down. Fig. 9.2(b) shows the riser ΔP trace of this flow regime. SS3 visually might resemble normal hydrodynamic slug flow but it generates a different level of instabilities to the system. The process of the SS3 consists of 4 stages: transient slugs, aerated slug growth, fast aerated liquid production and gas blowdown. In Fig. 9.3(a) these four stages are illustrated. They are also marked on a measured cycle of the riser ΔP for SS3 corresponding to U_{SL}=0.40 m s^{-1} and U_{SG0}=1.01 m s^{-1}, as shown in Fig. 9.4(a).

   The interaction between the horizontal pipeline and the vertical riser creates flow reversal of liquid and gas (as small bubbles) at the riser base, generating a long aerated liquid slug. The aerated liquid slug gradually flows into the riser and the riser ΔP gradually increases. This is the growth stage of the aerated slug. During this stage the flow pattern in the pipeline far upstream of the riser base is stratified flow. In the pipeline close to the riser base elongated bubbles are present. In the riser bubbly flow is exhibited; here small elongated bubbles from the riser base penetrate the liquid slug in the riser. During the gas blowdown stage, the flow pattern in the riser changes to intermittent flow (churn flow) and shortly after that transient slugs are generated in the pipeline as a result of increased gas velocity.

   Contrary to the classical severe slugging of type 1 (SS1), which can occur in the downward inclined pipeline-riser system and shows periods of full production starvation, SS3 does not give full riser base blockage and production starvation. In Fig. 9.3(b) different stages of SS1 are illustrated. They are also marked on a cycle of an experimental riser ΔP trace of SS1 corresponding to an experiment in a downward inclined pipeline-riser system, as shown in Fig. 9.4(b). We have also carried out experiments in a downward inclined pipeline-riser system. As can be seen for the SS3 in Fig. 9.4(a), the maximum riser ΔP is 1.42 bar. This corresponds to 95% of liquid volume fraction in the riser. Therefore, the pure liquid production step, which implies 100% of liquid volume fraction in the riser (the maximum riser ΔP of 1.5 bar), does not exist here. This is in contrast to

the SS1 in Fig. 9.4(*b*), which gives a 100% liquid production surge.

It is worth pointing out that also severe slugging of type 2 (SS2) can occur in the downward inclined pipeline-riser system. SS2 is qualitatively similar to SS1, but the slug length is shorter than the height of the riser.
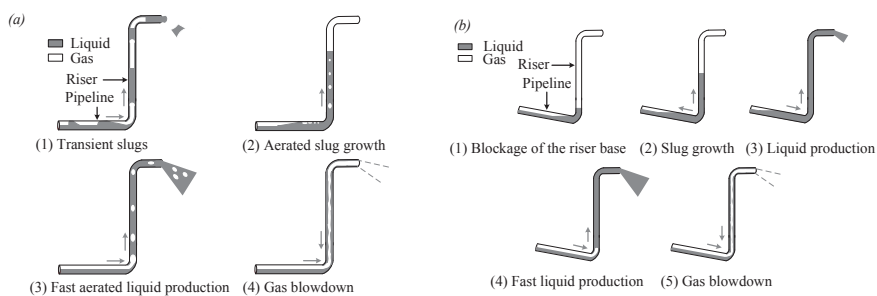

Figure 9.3: *A graphical illustration of (a) severe slugging of type 3 in the horizontal pipeline-riser experiment and (b) severe slugging of type 1 in a downward inclined pipeline-riser experiment.*
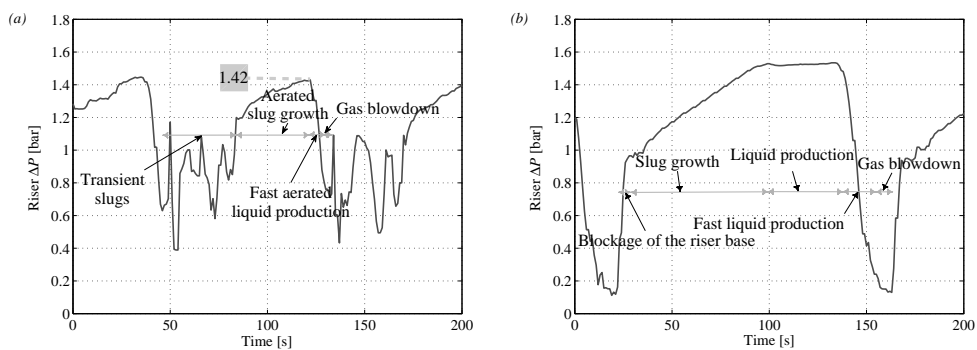

Figure 9.4: *Stages marked on a cycle of an experimental riser ΔP trace of (a) severe slugging of type 3 in the horizontal pipeline-riser experiment ($U_{SL}= 0.40\ m\,s^{-1}$ & $U_{SG0}= 1.01\ m\,s^{-1}$) and (b) severe slugging of type 1 in a downward inclined pipeline-riser experiment.*

9.3.3   Unstable Oscillations

This flow regime is characterized by oscillatory gas void fraction in the riser and also in the pipeline. The gas phase flows continuously through the riser base into the riser. Two-phase flow of liquid and gas in the riser is highly aerated and the pressure oscillations have a much smaller amplitude compared to SS3. Fig. 9.2(c) shows the riser ΔP trace of this flow regime. The flow pattern in the riser changes from hydrodynamic slug flow to churn flow and in the pipeline from hydrodynamic slug flow to stratified flow.

9.3.4   Dual-Frequency Severe Slugging

Through analyzing the experimental data a new type of severe slugging with different characteristics has been found. We observed this physical instability, which we will refer to as "dual-frequency severe slugging", at low liquid flow rate within the severe slugging region of the flow pattern map. This flow regime can be classified as a slow slugging cycle that connects two other types of instability, i.e. severe slugging of type 3 and unstable oscillations. DFSS exhibits a second frequency which is a relatively slow oscillation between these two types of instability on top of the high-frequency oscillations related to them. Thus, DFSS has two distinctly different frequencies. The riser ΔP trace of this flow regime is shown in Fig. 9.2(d).

It was visually observed that when the liquid content of the system was relatively high, the system exhibited the characteristics of SS3 and the flow pattern in the riser changed between bubbly flow and intermittent flow. Also, it was visually observed that at the lower liquid content, the system exhibited unstable oscillations and the flow pattern in the riser changed between hydrodynamic slug flow and churn flow. Churn flow is characterized by a chaotic flow of gas and liquid in which the shape of both the gas pockets and the liquid slugs are distorted.

The occurrence of the low-frequency oscillations can be described as follows. Imagine that the system starts to operate under the USO flow regime. The gas flow rate is not sufficient to maintain the USO flow regime. Thus, the liquid phase gradually accumulates in the system (pipeline and riser) and consequently the system gradually moves toward the SS3 flow regime. The pressure upstream of the riser base follows the same trend and gradually increases. Now the system operates under the SS3 flow regime. However, the liquid flow rate is not high enough to maintain the SS3 flow regime. The pressure of the gas in the pipeline upstream of the riser base is also not sufficient to blow out all the accumulated liquid from the system into the separator. However, this compressed upstream gas gradually expands and shifts the system back to the USO flow regime.

DFSS is not a stable operating condition within the flow pattern map and the system exhibits oscillations between two mentioned meta-stable states, i.e. USO and SS3. These oscillations between the higher and the lower liquid content in the system exhibit a cyclic behaviour with a lower frequency, thus creating another

level of instability to the whole system.

9.4   Results and Discussion

Figure 9.5(a) shows the flow map of the horizontal pipeline-riser system generated based on our experimental data, indicating whether each point is in STB, SS3, USO or DFSS regime. Flow patterns have an important influence on the prediction of the pressure gradient, liquid holdup, heat- and mass-transfer coefficients, residence-time distribution, and rate of chemical reaction (Shoham [5]). Thus, such a flow pattern map is of particular importance to design and operation of an offshore oil-production system.
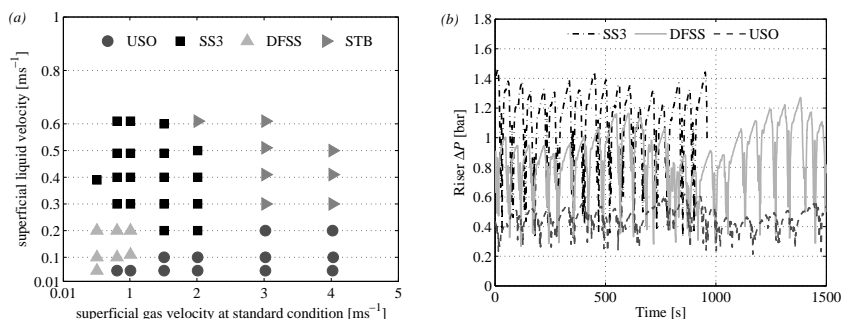

Figure 9.5: *(a) Experimental flow map of the system, indicating unstable oscillations (USO), severe slugging of type 3 (SS3), dual-frequency severe slugging (DFSS), stable flow (STB) and (b) experimental riser ΔP traces of DFSS, SS3 and USO (U_{SG0}=0.81 $m\,s^{-1}$ & U_{SL}=0.2 $m\,s^{-1}$, 0.3 $m\,s^{-1}$ and 0.05 $m\,s^{-1}$ respectively) showing DFSS fluctuates between SS3 and USO.*

In our experiments we observed an oscillating flow pattern, i.e. dual-frequency severe slugging, with two distinct frequencies that has not been reported in the open literature so far. The other flow patterns, i.e. severe slugging of type 3, unstable oscillations, and stable flow, have already been reported for downward inclined pipeline-riser systems by several researchers (see e.g. Malekzadeh et al. [20]). Table 9.2 summarizes the considered DFSS cases in the experiments with their associated superficial liquid and gas velocities. The measured periods and the amplitude of the riser ΔP for both high- and low-frequency oscillations are also given in Table 9.2.

The uncertainty in the measured amplitude of the riser ΔP is less than 1%. U_{SG0} and U_{SL} are calculated from the inflow measurements obtained by the thermal mass flow meter and electromagnetic flow meter, respectively. The uncertainties in the measured air and water inflow rates are less than 1%.

Table 9.2: *Experimental results of periods and amplitude of riser ΔP for all DFSS cases. The measured periods for high-frequency oscillations are associated with SS3 and USO flow regimes, respectively. The air buffer volume is 0.4 m^3.*

Case	U_{SL} (ms^{-1})	U_{SG0} (ms^{-1})	High-frequency oscillations		Low-frequency oscillations	
			Period (s) SS3&USO	Amplitude of ΔP (bar)	Period (s)	Amplitude of ΔP (bar)
1	0.05	0.51	120 & 84	0.3	1040	0.7
2	0.10	0.51	109 & 63	0.5	1200	1.1
3	0.10	0.81	75 & 62	0.4	901	0.6
4	0.11	1.01	59 & 43	0.4	675	0.5
5	0.20	0.51	99 & 52	0.7	1141	1.1
6	0.20	0.81	71 & 45	0.6	781	0.9
7	0.20	1.01	49 & 39	0.6	680	0.9

It is worth noting that the measured periods for high-frequency oscillations associated with DFSS cases mentioned in Table 9.2 are related to the process of severe slugging of type 3 and unstable oscillations, respectively. The periods of both the high-frequency and the low-frequency oscillations associated with dual-frequency severe slugging reduce by increasing U_{SGO} at constant U_{SL}. Although the period of the associated high-frequency oscillations reduces by increasing U_{SL} at constant U_{SG0}, we could not find any simple dependency between the period of the associated low-frequency oscillations and U_{SL} at constant U_{SGO}. However, at low superficial gas velocity, as can be seen from the flow pattern map (Fig. 9.5(a)), by increasing U_{SL} at constant U_{SG0}, the low-frequency oscillations disappears and the flow regime changes from DFSS to SS3.

Figure 9.5(b) shows the comparison of the measured riser ΔP between three operating scenarios selected from the flow pattern map, Fig. 9.5(a). U_{SGO} for all three operating scenarios is equal to 0.81 m s^{-1}. The associated superficial water velocities are 0.05 m s^{-1}, 0.2 m s^{-1} and 0.3 m s^{-1}. The observed flow patterns are USO, DFSS and SS3 respectively. These three operating scenarios are chosen in such a way that the DFSS case is closely surrounded by the USO and SS3 cases in the flow pattern map. As can be seen from Fig. 9.5(b), the USO and the SS3 flow patterns exhibit a single-frequency oscillations and the DFSS flow pattern exhibits a dual-frequency oscillations. The DFSS flow regime slowly fluctuates between two limits which are USO and SS3. In Fig. 9.5(b), the SS3 case still exhibits the low-frequency oscillations but with much smaller amplitude as this operating scenario is very close to the boundary between DFSS and SS3 in the flow pattern map.

9.5   Influence of the Effective Pipeline Length

To assess the impact of the effective length of the pipeline, as represented by the air buffer volume, on the characteristics of the DFSS, three separate experiments

with 0.4 m^3, 0.2 m^3 and 0.0 m^3 air buffer volume have been conducted at equal operating conditions. They represent an extra effective length of the 50.8 mm diameter pipeline by 197 m, 99 m, and 0 m, respectively; this extra length, however, does not contain any liquid holdup. As an example, the corresponding water and air superficial velocities are kept constant at 0.20 m s^{-1} and 0.51 m s^{-1}, respectively. Figures 9.6(a), 9.6(b) and 9.6(c) show the riser ΔP traces for the three mentioned different air buffer volumes, respectively. By comparing the above mentioned figures, it can be concluded that the evolution of the DFSS strongly depends on the effective length of the pipeline. At constant boundary conditions, the dual-frequency severe slugging appears as the effective length of the pipeline exceeds a certain threshold (here about 197 m). The amplitude of the slow oscillations reduced significantly and the flow regime changed from DFSS (Fig. 9.6(a)) to SS3 (Figs. 9.6(b) and 9.6(c)) when the air buffer volume is decreased. These two SS3 cases are very close to the boundary between SS3 and DFSS.
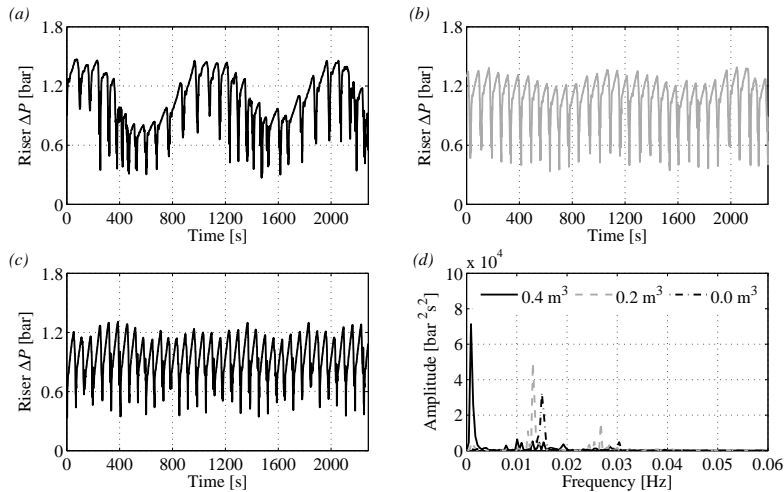

Figure 9.6: *Experimental riser ΔP traces corresponding to (a) 0.4 m^3 air buffer volume (U_{SL}=0.20 m s^{-1} & U_{SG0}=0.51 m s^{-1}), (b) 0.2 m^3 air buffer volume (U_{SL}=0.21 m s^{-1} & U_{SG0}=0.51 m s^{-1}), (c) 0.0 m^3 air buffer volume (U_{SL}=0.20 m s^{-1} & U_{SG0}=0.51 m s^{-1}) and (d) FFT of the experimental riser ΔP traces of the three mentioned gas buffer volumes.*

Note that in a real pipeline-riser system the length of the near horizontal part will be much longer. Moreover, it contains both the liquid and gas phases. In our experiments we mimicked the effect of gas compressibility in a long pipe by introducing a gas buffer vessel.

A Fast Fourier Transformation (FFT) was applied to derive the frequency

components in the riser ΔP traces of the three experiments mentioned above. Figure 9.6(d) shows the FFT of these riser ΔP traces. The x-axis is limited to the range [0, 0.06] in this plot to show more details. The frequency response contains three main spikes. The first spike is at approximately 0.001 Hz, which is the frequency of the slow oscillations. The other two spikes are at approximately 0.015 Hz and 0.025 Hz, which are the high frequencies of the SS3 and USO, respectively.

Figures 9.7(a), 9.7(b) and 9.7(c) show the water outflow rates of the three experiments mentioned above. There are periods of almost no water production (production starvation) followed by large peaks of water outflow of about 6 m^{3}h^{-1}(more than 4 times higher than the water inflow rate). The DFSS flow regime can be recognized from Fig. 9.7(a). Here, the water production peaks are not of equal size and show the low-frequency oscillations with a period of 1141 s (the same as the one observed in the corresponding riser ΔP trace) and an amplitude of about 3 m^{3}h^{-1}. Furthermore, the produced slug length ranges from 7 m to 16 m. Note that Figs. 9.7(b) and 9.7(c) exhibit water production peaks of almost equal size (severe slugging of type 3).
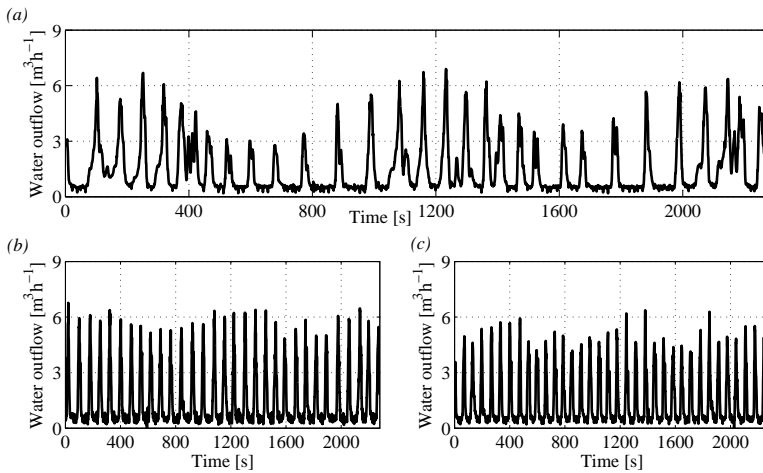

Figure 9.7: *Experimental water outflow rates corresponding to (a) 0.4 m^3 air buffer volume (U_{SL}=0.20 m s^{-1} & U_{SG0}=0.51 m s^{-1}), (b) 0.2 m^3 air buffer volume (U_{SL}=0.21 m s^{-1} & U_{SG0}=0.51 m s^{-1}) and (c) 0.0 m^3 air buffer volume (U_{SL}=0.20 m s^{-1} & U_{SG0}=0.51 m s^{-1}).*

9.6 Numerical Simulations

A one-dimensional numerical model of air-water two-phase flow in the horizontal pipeline-riser system was developed using the multiphase flow simulator OLGA (version 6.3.0, released in 2010). This is a transient one-dimensional, commercial computer code based on a two-fluid flow model. The three-dimensional velocity profile in the pipeline and riser is averaged over the cross section, which simplifies the flow equations from three-dimensional to one-dimensional. This simplification requires using empirical closure relations in the model for the wall friction and for the interfacial stress between the liquid and the gas. The one-dimensional model contains three separate mass balance equations for the gas, liquid droplets and liquid film, which are coupled through interfacial mass transfer terms. Two momentum balance equations are applied: one combined equation for the gas flow with liquid droplets, and one equation for the liquid film flow (see Bendiksen et al. [21]).

A sufficiently fine numerical grid (without slug tracking module) was used focused on capturing sufficient details of the dual-frequency severe slugging found in the experiments. The numerical simulations can help to further explain the physical background of the occurrence of the dual-frequency instability.
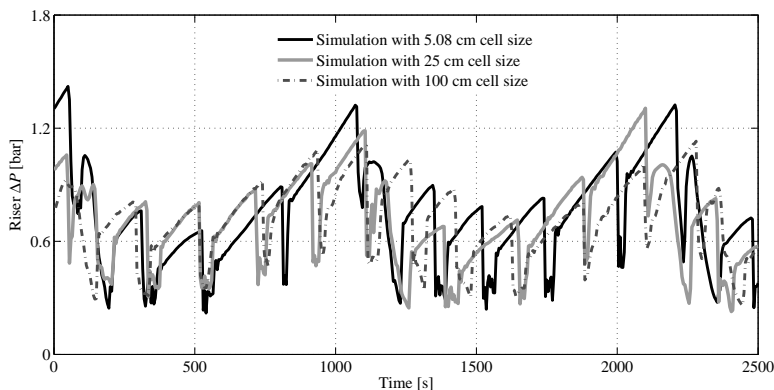

Figure 9.8: *Predicted riser ΔP with three different cell sizes of 100 cm, 25 cm, and 5.08 cm for case 2 in Table 9.2 (U_{SL}=0.10 $m\,s^{-1}$ & U_{SG0}=0.51 $m\,s^{-1}$).*

In the numerical model constant mass flow rates and pressure were specified as the inlet and outlet boundaries, respectively. A non-zero pressure drop across the fully-open liquid control valve located at the riser top, was observed during the experiments. Therefore, a valve with K_v value of 12 $m^3\,h^{-1}\,bar^{-1/2}$ was included in the numerical model. The numerical model, with a grid resolution of 25 cm giving a total of 570 grid cells in the pipeline and riser, was used to simulate all cases mentioned in Table 9.2. The simulation time step varies from 0.0001 - 0.1 s.

We carried out a sensitivity analysis to verify that the number of grid cells is such that the results are numerically accurate. This was accomplished by meshing the computation domain with three different cell sizes of 100 cm, 25 cm, and 5.08 cm. Figure 9.8 shows the predicted riser ΔP traces for a dual-frequency severe slugging cycle corresponding to case 2 in Table 9.2, by all three mentioned cell sizes. The DFSS flow pattern was predicted by all three mentioned cell sizes and the predicted time periods of high- and low-frequency oscillations are 229, 186 (SS3 and USO) and 980 s.
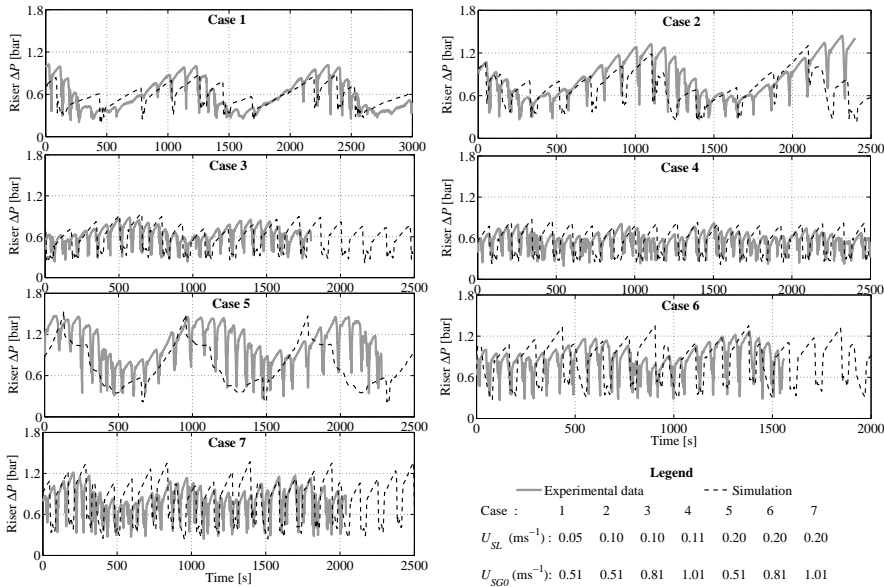

Figure 9.9: *Experimental and predicted riser ΔP for all experimental cases of DFSS mentioned in Table 9.2. The air buffer volume is 0.4 m^3.*

Figure 9.9 shows the comparison of riser ΔP between numerical predictions and experimental data. As can be seen in this figure, the numerical model correctly predicts the dual-frequency characteristic of the DFSS. Also the period and amplitude of the low-frequency oscillations are predicted fairly well. The values of the high-frequency oscillations, however, are not very accurate in the model. For example in case 2, the measured periods of high- and low-frequency oscillations are 109, 63 (SS3 and USO) and 1200 s, respectively. The predicted values are 229, 186 and 980 s, respectively. In case 5, the measured periods of high- and low-frequency oscillations are 99, 52 and 1141 s, respectively. The predicted period of low-frequency oscillations is 817 s and the high-frequency oscillations are almost not predicted. As mentioned in the description of DFSS, many air bubbles with different shapes and sizes are distributed in the pipeline as the elongated bubble,

and penetrate the liquid slug in the riser. These widely distributed air bubbles are not modeled appropriately.

The impact of the pipeline length on the characteristics of the DFSS is evaluated by performing four separate simulations with 100 m, 200 m, 300 m and 400 m long horizontal pipeline followed by the riser at equal operating conditions and 0.0 m^3 air buffer volume. The corresponding U_{SL} and U_{SGO} are 0.2 m s^{-1} and 0.51 m s^{-1} respectively. As can be seen from Fig. 9.10, the DFSS evolves when the pipeline length exceeds a certain threshold (between 100 m and 200 m). This is in line with what we observed in the experiments with the effective pipeline length, see section 9.5. Also the period of the low-frequency oscillations increases by increasing the pipeline length. The simulated cases corresponding to the 100, 200 and 300 m long horizontal pipeline are equivalent to the experimental cases corresponding to 0.0, 0.2 and 0.4 m^3 buffer volume (Figs. 9.6(c), 9.6(b) and 9.6(a)). The predicted flow regimes are severe slugging of type 3 for the 100 m long horizontal pipeline, and dual-frequency severe slugging for the 200 m and 300 m long horizontal pipeline. Whereas, the observed flow regimes are severe slugging of type 3 for the 0.0 m^3 and 0.2 m^3 gas buffer volume, and dual-frequency severe slugging for the 0.4 m^3 gas buffer volume. However, the impact of the pipeline length is different from that of the buffer volume as it takes longer to fill the additional length of the pipeline with extra liquid holdup (or reduce the liquid holdup) when switching between severe slugging of type 3 and unstable oscillations.
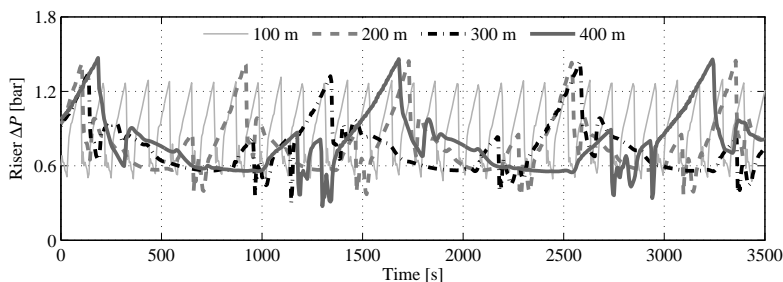

Figure 9.10: *predicted riser ΔP for 100 m, 200 m, 300 m and 400 m long horizontal pipeline followed by the riser (U_{SL}=0.20 m s^{-1} & U_{SG0}=0.51 m s^{-1}). The air buffer volume is 0.0 m^3. The simulated 100, 200 and 300 m long horizontal pipeline are equivalent to Figs. 9.6(c), 9.6(b) and 9.6(a), respectively.*

Table 9.3 gives the predicted time for the low-frequency oscillations between severe slugging of type 3 and unstable oscillations for the above mentioned numerical cases of 200 m, 300 m and 400 m long horizontal pipeline followed by the riser (U_{SL}=0.20 m s^{-1} & U_{SG0}=0.51 m s^{-1}). The average holdup in the pipeline-riser system during the process of severe slugging of type 3 and unstable oscillations as well as the amount of the produced liquid during the oscillations

between SS3 and USO are also given in Table 9.3. The time required to fill the pipeline-riser system with an amount of liquid that is equal to the difference in holdup for severe slugging of type 3 and unstable oscillations is calculated and given in Table 9.3. It can be seen that this required filling time is equivalent to the predicted time for the low-frequency oscillations between severe slugging of type 3 and unstable oscillations.

Table 9.3: *Predicted and calculated (based on the predicted holdup difference and U_{SL}) time for the low-frequency oscillations between severe slugging of type 3 and unstable oscillations for 200 m, 300 m and 400 m long horizontal pipeline followed by the riser (U_{SL}=0.20 $m\,s^{-1}$ & U_{SG0}=0.51 $m\,s^{-1}$). The corresponding predicted riser ΔP traces are given in Fig. 9.10.*

Pipeline length (m)	Time between SS3/USO (s)	Holdup (m^3) SS3	USO	Holdup difference (m^3)	Produced liquid (m^3)	Filling time (s)
200	408	0.38	0.26	0.12	0.046	410
300	598	0.54	0.38	0.16	0.079	590
400	752	0.76	0.51	0.25	0.055	753

9.7   Conclusions

Flow instabilities in gas-liquid horizontal pipeline-riser system were investigated experimentally and numerically. It was observed that severe slugging can develop even in the horizontal pipeline-riser configuration. Moreover, through analyzing the experimental data a new class of severe slugging was found and referred to as dual-frequency severe slugging, which corresponds to large-amplitude, dual-frequency pressure and flow rate fluctuations. It has been shown that dual-frequency severe slugging evolves when the effective pipeline length or the pipeline length exceeds a certain threshold.

The observed flow regimes were classified into four categories: unstable oscillations (exhibiting cyclic, low amplitude pressure fluctuations), severe slugging of type 3 (characterized by pulsating long liquid slugs separated by small gas pockets in the riser followed by a gas blow down stage), dual-frequency severe slugging (characterized by dual-frequency instabilities; high-frequency fluctuations related to the severe slugging of type 3 and unstable oscillations, and low-frequency fluctuations related to the transition between severe slugging of type 3 and unstable oscillations), and hydrodynamic slugs initiated in the pipeline and flowing into the riser.

Furthermore, the dynamic simulation tool OLGA was found to reproduce the characteristics of dual-frequency severe slugging. The period and the amplitude of the pressure fluctuations for the low-frequency oscillations are predicted fairly well. However, the period of the high-frequency oscillations is over predicted. The time period of the low-frequency oscillations is equal to the time needed to fill the pipeline with the extra amount of liquid needed to overcome the holdup

differences for the two states (severe slugging of type 3 and unstable oscillations) between which the oscillations take place.

Acknowledgment

Nomenclature

K_v = flow factor $[\, \mathrm{m}^3 \, \mathrm{h}^{-1} \, \mathrm{bar}^{-1/2}]$
P = pressure [bar]
U = velocity $[\, \mathrm{m}\,\mathrm{s}^{-1}]$

Greek Letter

Δ = difference [-]

Subscripts

SG0 = superficial gas at standard conditions
SL = superficial liquid

References

[1] Gomez, L., Mohan, R., and Shoham, O., 2004. "Swirling gas-liquid two-phase flow - experiment and modeling - part i: Swirling flow field". *J Fluids Eng-Trans ASME*, **126**(6), pp. 935-942.

[2] Law, D., Jones, S., Heindel, T., and Battaglia, F., 2011. "A combined numerical and experimental study of hydrodynamics for an air-water external loop airlift reactor". *J Fluids Eng-Trans ASME*, **133**(2).

[3] Paruya, S., and Bhattacharya, P., 2008. "A moving boundary analysis for start-up performance of a nuclear steam generator". *J Fluids Eng-Trans ASME*, **130**(5).

[4] Zhao, L., and Rezkallah, K., 1995. "Pressure-drop in gas-liquid flow at microgravity conditions". *Int. J. Multiphase Flow*, **21**(5), pp. 837-849.

[5] Shoham, O., 2006. *Mechanistic modeling of gas-liquid two-phase flow in pipes.* Society of Petroleum Engineers.

[6] Guzman, J., and Zenit, R., 2011. "Application of the euler-lagrange method to model developed hydrodynamic slugs in conduits". *J Fluids Eng-Trans ASME*, **133**(4).

[7] Tengesdal, J., Sarica, C., and Thompson, L., 2003. "Severe slugging attenuation for deepwater multiphase pipeline and riser systems". *SPE Production & Facilities J.*, **18**(4), pp. 269-279.

[8] Denney, D., 2003. ""Self-lifting" method to eliminate severe slugging in offshore production systems". *J. of Petroleum Tech.*, **55**(12), pp. 36-37.

[9] Jansen, F., Shoham, O., and Taitel, Y., 1996. "The elimination of severe slugging - experiment and modeling". *Int. J. Multiphase Flow*, **22**(6), pp. 1055-1072.

[10] Havre, K., and Dalsmo, M., 2002. "Active feedback control as a solution to severe slugging". *SPE Production & Facilities J.*, **17**(3), pp. 138-148.

[11] Mokhatab, S., Towler, B., and Purewal, S., 2007. "A review of current technologies for severe slugging remediation". *Petroleum Science & Tech. J.*, **25**(10), pp. 1235-1245.

[12] Schmidt, Z., Brill, J., and Beggs, H., 1980. "Experimental study of severe slugging in a two-phase-flow pipeline-riser pipe system". *SPE J.*, **20**(5), pp. 407-414.

[13] Taitel, Y., 1986. "Stability of severe slugging". *Int. J. Multiphase Flow*, **12**(2), pp. 203-217.

[14] Pots, B., Bromilow, I., and Konijn, M., 1987. "Severe slug flow in offshore flowline/riser systems". *SPE Production Eng. J.*, **2**(4), pp. 319-324.

[15] Taitel, Y., Vierkandt, S., Shoham, O., and Brill, J., 1990. "Severe slugging in a riser system: experiments and modeling". *Int. J. Multiphase Flow*, **16**(1), pp. 57-68.

[16] Montgomery, J., and Yeung, H., 2002. "The stability of fluid production from a flexible riser". *ASME J. Energy Resour. Technol.*, **124**(2), pp. 83-89.

[17] Fabre, J., Peresson, L., Corteville, J., Odello, R., and Bourgeols, T., 1990. "Severe slugging in pipeline/riser systems". *SPE Production Eng. J.*, **5**(3), pp. 299-305.

[18] Sarica, C., and Shoham, O., 1991. "A simplified transient model for pipeline-riser systems". *Chemical Engineering Science*, **46**(9), pp. 2167-2179.

[19] Baliño, J. L., Burr, K. P., and Nemoto, R. H., 2010. "Modeling and simulation of severe slugging in air-water pipeline-riser systems". *Int. J. Multiphase Flow*, **36**(8), pp. 643-660.

[20] Malekzadeh, R., Henkes, R.A.W.M., and Mudde, R.F. 2012. "Severe Slugging in a Long Pipeline-Riser System: Experiments and Predictions". *Int. J. Multiphase Flow*, **46**(C), pp. 9-21.

[21] Bendiksen, K., Malnes, D., Moe, R., and Nuland, S., 1991. "The dynamic two-fluid model OLGA: Theory and application". *SPE Production Eng. J.*, **6**(2), pp. 171-180.

Chapter **10**

Experimental Study of Flow Instabilities in a Hilly-Terrain Pipeline-Riser System§

Summary

Even at constant inlet and outlet boundary conditions represented by gas and liquid mass flow rates and separator pressure respectively, unsteady state flow may occur in a pipeline-riser system operating at relatively low gas and liquid flow rates. The cyclic unsteady state flow characterized by large-amplitude pressure and flow rate fluctuations has been referred to as severe slugging. This study is an experimental investigation of flow instabilities, especially severe slugging, in a relatively long hilly-terrain pipeline-riser system. Five types of flow regimes were found and characterized based on visual observation and on the measured pressure drop over the riser.

10.1   Introduction

Increasingly, oil and gas are produced from fields far out of the seashore. In order to collect the oil and gas at a central production platform, they are transported through long pipeline-riser systems. The diameter of the pipeline and the riser ranges from typically 0.1 to 0.8 m. The length of the pipeline can vary from a few kilometres (for liquid dominated systems) to more than hundred kilometres

---

(for gas dominated systems). The height of the riser depends on the water depth, which can be more than two kilometres (in deepwater areas). These pipelines are laid out over the seafloor. The uneven seafloor topography results in hilly-terrain pipeline-riser systems. A hilly-terrain pipeline consists of interconnected horizontal, downhill, and uphill sections (Zhang et al. 2003). Although flow instabilities are relatively well understood for downward and horizontal pipeline-riser configurations [see e.g. Malekzadeh et al. (2012, 2011)], there is still a lack of understanding of how flow characteristics change in a hilly-terrain pipeline-riser system.

A familiar flow instability that can occur in the oil and gas production from an offshore oil field is severe slugging (see e.g. Tengesdal et al. 2003 and Denney 2003). At relatively low flow rates, liquid accumulates at the bottom of the riser, creating a blockage for the gas, until sufficient upstream pressure has been built up to flush the liquid slug out of the riser. After this liquid surge, and subsequent gas surge, part of the liquid in the riser falls back to the riser base to create a new blockage and the cycle is repeated. This transient cyclic phenomenon causes a period of no outflow followed by very high liquid and gas surges, and is called severe slugging [see e.g. Jansen et al. (1996) and Malekzadeh et al. (2012)]. Severe slugging causes large-amplitude pressure and flow rate fluctuations. The flow moves with about the velocity of the gas and has the density of the liquid. The resulting forces, especially when the liquid passing through barriers such as orifices, partially closed valves and bends, provoke a faster mechanical fatigue and can eventually lead to a rupture (Santana et al. 1993). Large-amplitude fluctuations in the liquid and gas flow rates can significantly reduce the production from the reservoir (due to an increased back pressure) and also to shut down or even damage of the platform facilities, downstream of the riser, like separators and compressors (due to the peak flow rates during the liquid and gas surges). Therefore, the accurate prediction of severe slugging characteristics is essential for the proper design and operation of multiphase flow in these systems [see Havre et al. (2002) and Mokhatab et al. (2007)].

Severe slugging in a downward inclined pipeline-riser system was first reported by Yocum (1973). Thereafter, the process of severe slugging was described by Schmidt et al. (1985). Mathematical criteria for prediction of the region where severe slugging might occur were proposed by Bøe (1981), Pots et al. (1987) and Taitel (1986). Experimental and numerical investigations of the process of severe slugging in a downward inclined pipeline-riser configuration have been the focus of research for many years [see Schmidt et al. (1980), Taitel et al. (1990), Sarica and Shoham (1991), Baliño et al. (2010) and Malekzadeh et al. (2012)].

Fabre et al. (1990) observed severe slugging in a horizontal pipeline-riser configuration albeit with a smaller amplitude. Malekzadeh et al. (2011) carried out experiments in a long horizontal pipeline-riser system. They confirmed the occurrence of severe slugging and described its process in a horizontal pipeline-riser system.

Based on field measurements from the Upper Zakuim offshore pipeline-riser

system, Farghaly (1987) presented a field study of severe slugging. At low gas and liquid flow rates, severe slugging was observed in undulated, nearly horizontal pipeline-riser configurations. Because of the importance of flow instabilities in practical applications, e.g. offshore oil-production systems, severe slugging characteristics in a hilly-terrain pipeline-riser configuration should be studied further. Therefore, we have carried out experiments for the two-phase flow of air and water in a relatively long hilly-terrain pipeline-riser system.

The objective of this study is to obtain a better understanding of the characteristics of the flow instabilities occurring in a hilly-terrain pipeline-riser configuration. To accomplish this objective, experiments were conducted to identify and characterize any possible flow instability, including severe slugging, in a flow pattern map of a relatively long hilly-terrain pipeline-riser system. The observed flow patterns were classified into five categories: stable flow (characterized by low amplitude pressure fluctuations with frequency of about 0.2 Hz), unstable oscillations (characterized by low amplitude pressure fluctuations with frequency of about 0.02 Hz), severe slugging of type 1 (characterized by a pure liquid slug length larger that the riser height), severe slugging of type 3 (characterized by a growing long aerated liquid slug in the riser), and dual-frequency severe slugging characterized by two distinctly different frequencies.

10.2   Experimental Facility

The existing two-phase, air and water facility of the Shell Technology Centre in Amsterdam (STCA) has been modified to conduct the experiments. A single hilly-terrain unit of 50.8 mm diameter Perspex pipeline was added to the facility. This hilly-terrain unit was placed just upstream of the riser base. A schematic diagram of the STCA hilly-terrain pipeline-riser test facility is shown in Fig. 10.1.

The test facility comprises four main parts: the fluid supply, test loop (pipeline and riser), separation area and measurement and control devices. This facility is powered and controlled by the Fieldpoint 2000 system of National Instruments and by Labview, which are the control hardware and software, respectively. They help to ensure that the complete instrumentation of the system is operated, controlled and monitored separately, the desired operating conditions are achieved and the required data are recorded. The full experimental procedures, including startup, control, shutdown and data logging are done remotely through dedicated control and data acquisition systems.

Dry air at a pressure of 6 barg is delivered via a connection with the main air supply at the STCA. The air is supplied to a thermal mass flow meter and controller of model 5853i by Brooks, which automatically provides an almost constant mass flow rate into the test loop. The gas mass inflow rate varies by less than 0.5%. A maximum air flow rate of 30 $Sm^3 h^{-1}$ can be supplied (the S refers to standard conditions at 1.00 bara and 15.56 °C). The water supply is
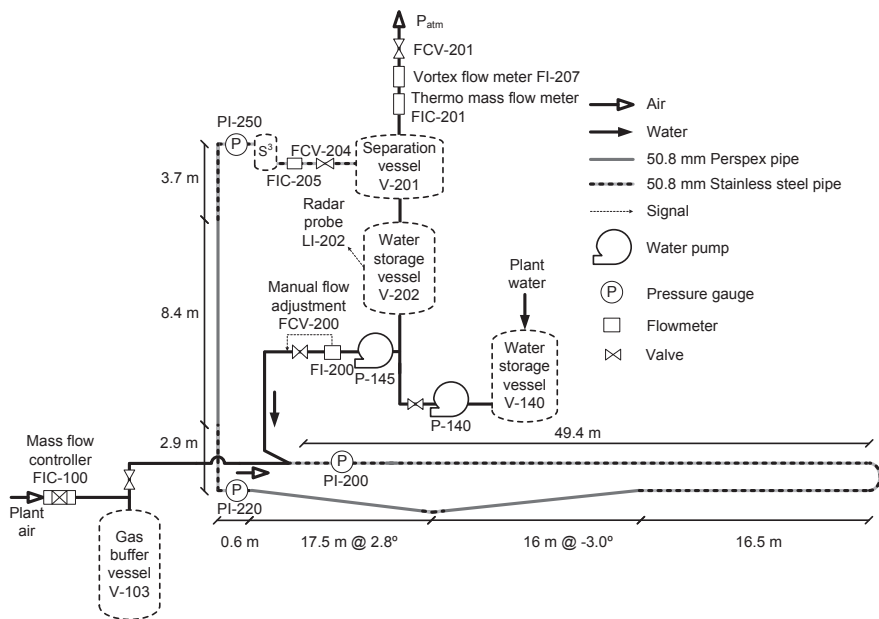
Figure 10.1: *Schematic of the experimental facility.*

city tap water connected to the first water storage tank (V-140), see Fig. 10.1. A worm pump connected to V-140 brings water to the second water storage tank situated right below the separator. Then water is supplied to the pipeline by a variable speed centrifugal pump. A relatively constant water volumetric flow rate can be achieved by manually adjusting the pump speed and by adjusting the opening of a control valve, which is located directly downstream of the pump. The liquid inflow rate varies by less than 3%. A maximum water flow rate of 5 $m^3 \, h^{-1}$ can be supplied. The water flow rate into the test loop is measured with an electromagnetic flow meter of type Promag 50W by Endress & Hauser.

The test loop consists of a 65.9 m long, 50.8 mm diameter horizontal steel pipeline connected to a single hilly-terrain unit of 16 m long, 50.8 mm diameter Perspex pipeline which is inclined to -3.0 ° from the horizontal (downhill section) and 17.5 m long, 50.8 mm diameter Perspex pipeline which is inclined to +2.8 ° from the horizontal (uphill section), followed by a 15 m high, 50.8 mm diameter vertical Perspex riser. The Perspex pipes are transparent which permit visual observation of the flow behaviour. The length-diameter ratios for the horizontal section, the downhill section, the uphill section and the riser are 1297, 315, 344 and 295, respectively.

The riser discharges the fluid into the two-phase separator, operating at atmospheric pressure. The separator pressure varies by less than 3%. Air and water

are separated by gravity. The upper section of the separator has a mist mat and dry air is vented to the open air, monitored by one vortex and one thermo mass flow indicator. The lower section of the separator drains the water, which flows down and returns to the second water storage tank. The water level in this tank is measured with a continuous level transmitter of type Levelflex M-FMP40 by Endress & Hauser, which can provide an estimation of the water outflow.

A variable-volume gas buffer vessel is located between the gas mass flow controller and the gas inlet, upstream of the pipeline. The air volume of the buffer vessel can be changed by partly filling it with water. The function of the gas buffer vessel is to create a virtually longer pipeline. In the current study, the maximum applied air volume of the buffer vessel is 400 litre, which corresponds to an additional pipeline length of 197 m. It should be noted that the facility also included a slug suppression system (S^3) at the riser top. The active parts of the S3 are: a small vessel with a total volume of 9.4 litres, an electromagnetic flow meter, and a liquid control valve, which has a K_v value (flow factor) of 12 $\mathrm{m^3\,h^{-1}\,bar^{-1/2}}$. During all experiments this liquid control valve was left fully open.

Pressure transducers are located at the inlet of the pipeline, at the riser base and at the top of the riser. They are manufactured by Endress & Hauser and are of type Cerebar M-PMC41. Additional pressure devices are also used to measure and monitor the pressure in the gas buffer vessel, the inlet of the gas line, the outlet of the liquid pump and in the two-phase separator. The temperatures of the fluids are measured with temperature transmitters that are located at various locations in the test loop. It should be mentioned that the sampling frequency of the recorded experimental data is 1 Hz. Table 10.1 provides a summary of the instrumentation used in the experimental facility.

Table 10.1: *Specifications of the equipment in the flow loop. E+H and D/M are acronyms for Endress+Hauser and Dresser/Masoneilan, respectively.*

Label (Fig. 10.1)	Instrument	Manufacture	Type	Range	Units	Accuracy
PI-200	Pressure transmitter	E+H	Cerebar M-PMC41	0 - 10	bara	0.2%
PI-220	Pressure transmitter	E+H	Cerebar M-PMC41	0 - 10	bara	0.2%
PI-250	Pressure transmitter	E+H	Cerebar M-PMC41	0 - 10	bara	0.2%
FI-200	Electromagnetic flow meter	E+H	Promag 50W	0 - 7.5	$\mathrm{m^3\,h^{-1}}$	0.5%
FIC-205	Electromagnetic flow meter	E+H	Promag 50W	0 - 18	$\mathrm{m^3\,h^{-1}}$	0.5%
FIC-100	Mass flow meter & controller	Brooks	5853i	0 - 30	$\mathrm{Sm^3\,h^{-1}}$	1%
FIC-201	Thermal mass flow meter	E+H	t-mass 65F	0 - 110	$\mathrm{Sm^3\,h^{-1}}$	1.5%
LI-202	Continuous level transmitter	E+H	Levelflex M-FMP40	0 - 100	%	+/-3 mm
FCV-200	Control valve	D/M	35-35112	0 - 12	$\mathrm{m^3\,h^{-1}\,bar^{-1/2}}$	-
FCV-204	Control valve	D/M	35-35202	0 - 12	$\mathrm{m^3\,h^{-1}\,bar^{-1/2}}$	-

10.3   Hilly Terrain-Riser Induced Instabilities

Based on operating limits of the experimental facility, an experimental matrix was defined such that all possible flow regimes would exist in the test loop. Later, by obtaining further experimental results this experimental matrix was refined to establish both the characteristics of each flow regime and the transition boundaries between the flow regimes. The water flow rate ranges from 0.69 $\mathrm{m^3\,h^{-1}}$ to 4.47 $\mathrm{m^3\,h^{-1}}$ and the air flow rate from 2.23 $\mathrm{Sm^3\,h^{-1}}$ to 29.36 $\mathrm{Sm^3\,h^{-1}}$. The corresponding superficial water velocity ranges from U_{SL}= 0.09 - 0.61 $\mathrm{m\,s^{-1}}$ and the superficial air velocity at standard conditions (1.00 bara, 15.56 °C) ranges from U_{SG0}= 0.31 - 4.02 $\mathrm{m\,s^{-1}}$.

Different flow regimes have been obtained by fixing the water flow rate and by changing the air flow rate. The observed flow regimes are classified into five categories: stable flow (STB), unstable oscillations (USO), severe slugging of type 1 (SS1), severe slugging of type 3 (SS3), and dual-frequency severe slugging (DFSS). A classification of severe slugging in a downward inclined pipeline-riser configuration is given by Baliño et al. (2010), who distinguished the types 1, 2, and 3. In this paper, the same abbreviations were used for the classification of the flow regimes. The flow regimes were delineated based on visual observations and analysis of the pressure drop over the riser (riser ΔP). The riser ΔP was also used for defining different stages of a severe slugging cycle; the riser ΔP is defined as the difference between the pressure at the riser base and the riser top. Typical riser ΔP traces of these five flow regimes are shown in Fig. 10.2. The above mentioned, experimentally observed, flow regimes are described below.

10.3.1   Stable Flow

At relatively high liquid and gas flow rates, hydrodynamic slugs are generated in the horizontal pipeline upstream of the hilly-terrain unit. Hydrodynamic slugs are also generated at the elbow as the liquid phase slowly accumulates at this low spot from the uphill and the downhill sections. It is observed that the frequency of the initiated hydrodynamic slugs at the elbow decreases as the superficial gas velocity increases, owing to the low liquid accumulation rate at the elbow. The riser ΔP exhibits fluctuations with high frequency (about 0.2 Hz) and relatively small amplitude (less than 0.60 bar, associated with several slugs in the order of a meter). Thus, hydrodynamic slug flow is considered to be stable flow as compared to other types of flow regime mentioned in this study.

10.3.2   Unstable Oscillations

This flow regime is observed at low liquid flow rate and characterized by an oscillating gas void fraction in the hilly-terrain pipeline-riser system. The amplitude of the pressure oscillations (less than 0.70 bar) is smaller compared to other types of severe slugging. Also, the frequency of the pressure oscillations (about 0.02
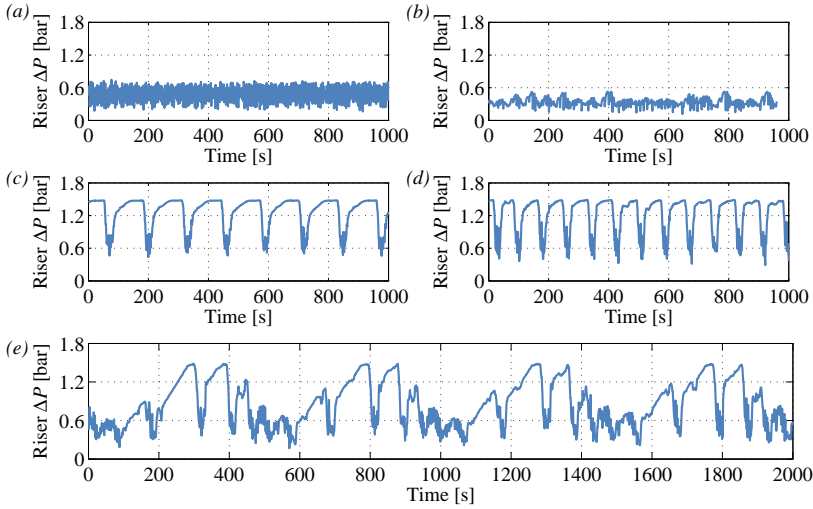
Figure 10.2: *Experimental riser ΔP traces of the five mentioned flow patterns corresponding to (a) STB (U_{SL}=0.40 m s^{-1} & U_{SG0}=4.02 m s^{-1}), (b) USO (U_{SL}=0.10 m s^{-1} & U_{SG0}=3.02 m s^{-1}), (c) SS1 (U_{SL}=0.41 m s^{-1} & U_{SG0}=0.51 m s^{-1}), (d) SS3 (U_{SL}=0.60 m s^{-1} & U_{SG0}=1.01 m s^{-1}) and (e) DFSS (U_{SL}=0.31 m s^{-1} & U_{SG0}=1.51 m s^{-1}).*

Hz) is much lower than the stable flow pattern which mentioned above. The flow pattern in the riser alternates between hydrodynamic slug flow and churn flow and in the hilly-terrain pipeline between hydrodynamic slug flow and stratified flow.

10.3.3 Severe Slugging of Type 1

A cycle of severe slugging of type 1 was found to consist of five stages: (1) blockage of the elbow; (2) slug growth; (3) liquid production; (4) fast liquid production; (5) gas blowdown. In Fig. 10.3(a) these five stages are illustrated. They are also marked on a measured cycle of the riser ΔP for SS1 corresponding to U_{SL}= 0.31 m s^{-1} and U_{SG0}= 0.51 m s^{-1}, as shown in Fig. 10.3(b). The process of SS1 can be described as follows.

Accumulation of a sufficient amount of liquid at the elbow creates a full blockage. Liquid fallback from the uphill section plus from the riser (downstream of the elbow) and also transient slugs generated in the pipeline (upstream of the elbow) will contribute to this initial blockage. This stage is called blockage of the elbow. As both phases continue to flow into the pipeline while the gas passage is blocked, the liquid content in the uphill section and in the riser increases. As a
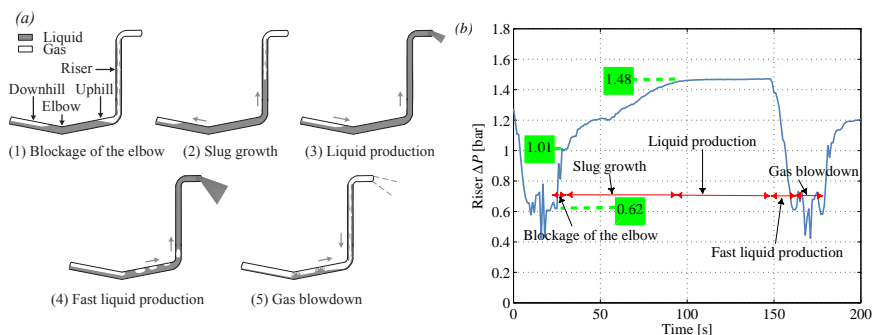
Figure 10.3: *Stages for severe slugging of type 1 (a) a graphical illustration (b) marked on a cycle of an experimental riser ΔP trace (U_{SL}=0.31 $m\,s^{-1}$ & U_{SG0}=0.51 $m\,s^{-1}$).*

consequence, the pressure at the elbow increases, pushing the liquid-gas interface in the downhill section further away from the elbow. This stage is known as slug growth. When the liquid level reaches the riser top, the pressure at the elbow reaches its maximum and the pressure of the compressed gas in the pipeline up-stream of the elbow becomes higher than the hydrostatic head of the liquid-filled uphill section plus riser (downstream of the elbow). Liquid starts to flow out at the riser top and simultaneously the slug tail in the downhill section will be pushed towards the elbow. When the slug tail penetrates into the uphill section through the elbow, elongated bubbles form in the uphill section and the hydrostatic head of the uphill section decreases. However, the total hydrostatic head downstream of the elbow (the uphill section plus the riser) only slightly decreases as the riser is still fully filled with liquid. This is the liquid production stage. When the gas phase penetrates into the riser, the hydrostatic head of the riser decreases. The gas will expand and flush the liquid in the downstream part of the elbow out of the riser. This stage is known as fast liquid production. After that the gas will be produced at a high rate, causing a quick pressure reduction in the system. This is the gas blowdown stage. Once the gas is expelled, the pressure reaches its minimum leading to the fallback of the remaining liquid and accumulation at the elbow, and the cycle is repeated. The following features can also be concluded from Fig. 10.3(*b*):

- As a direct consequence of the quick pressure reduction in the pipeline in each cycle, the gas velocity in the pipeline increases, which in turn gener-ates transient slugs. The transient slugs effectively contribute to the initial blockage of the elbow. Also part of the transient slugs flows into the riser and increases the liquid volume fraction in the riser about 26% (i.e. (1.01 bar - 0.62 bar) / 1.48 bar).

- The slug growth stage can be divided into two sub-stages. These two sub-stages are visible in the riser ΔP trace and they are also confirmed by visual observation. During the first sub-stage (between a time of 29 to 54 s in Fig. 10.3(b)), the slug mainly grows in the uphill section and consequently removes trapped air from this section. When the uphill section is fully filled with liquid, the slug grows faster in the riser. This is the second sub-stage of the slug growth stage (between a time of 54 to 98 s).

- The maximum riser ΔP is 1.48 bar. This corresponds to 100% of liquid volume fraction in the riser. Also the riser ΔP remains at its maximum for a certain period of time (about 50 s).

- During the gas blowdown, the increased gas velocity in the pipeline combined with liquid fallback from the uphill section and also from the riser lead to the generation of short transient slugs at the elbow and they flow the riser up. These short transient slugs form prior to the generation of the long transient slugs in the pipeline which will contribute to the initial blockage of the elbow and are described earlier. The short transient slugs are visible in the riser ΔP trace (between a time of 162 to 177 s) and also confirmed by visual observation and by the measured liquid outflow.

The time period of a severe slugging cycle can be estimated by the following equation derived from a force balance over the elbow [see e.g. Bøe (1981) and Pots et al. (1987)]:

$$T = \frac{H}{U_{SL}} \frac{1}{\Pi_{ss}}, \tag{10.1}$$

where T is the time period of a severe slugging cycle (s), H denotes the length of the riser (m), and Π_{ss} is known as the severe-slugging group and is given by the following equation:

$$\Pi_{ss} = \frac{P_0}{\alpha \rho_l g L} \frac{U_{SG0}}{U_{SL}}, \tag{10.2}$$

where P_0 is the atmospheric pressure (Pa), α is the average void fraction in the pipeline which depends on the flow regime and can be calculated by using mechanistic models (see e.g. Petalas and Aziz 2000), ρ_l denotes the liquid density (kgm^{-3}), g is the gravitational acceleration (ms^{-2}), and L (m) denotes the length of the pipeline. The measured time period of the SS1 cycle for U_{SL}= 0.31 m s^{-1} and U_{SG0}= 0.51 m s^{-1} is 150 s, whereas the theoretical model (Eq. 10.1) predicts a slightly lower value of 122 s.

10.3.4   Severe Slugging of Type 3

A cycle of severe slugging of type 3 consists of four stages: (1) transient slugs; (2) aerated slug growth; (3) fast aerated liquid production; (4) gas blowdown. In Fig. 10.4(a) these four stages are illustrated. They are also marked on the

experimental cycle of the riser ΔP of SS3 corresponding to U_{SL}= 0.40 m s^{-1} and U_{SG0}= 1.01 m s^{-1}, as shown in Fig. 10.4(b). The process of SS3 can be described as follows.

Transient slugs are generated in the pipeline upstream of the elbow and they flow up the riser. This stage is called transient slugs. Part of the liquid of the transient slugs falls back through the riser and the uphill section, creating a local flow reversal of liquid and gas (as small bubbles) at the elbow and generating a long aerated liquid slug. The flow regime in the uphill section and also in the downhill section close to the elbow changes from hydrodynamic slug flow to elongated bubble flow. The corresponding long aerated liquid slug contains small bubbles of different size and shape. The aerated liquid slug gradually flows in the riser and the liquid content of the riser (the riser ΔP) gradually increases. This is the aerated slug growth stage. Contrary to the severe slugging of type 1, SS3 does not give full elbow blockage and production starvation. Here, small bubbles continuously flow from the elbow into the uphill section and finally penetrate into the riser. When the compressed gas upstream of the elbow penetrates into the uphill section, large elongated bubbles form in the uphill section and quickly penetrate into the riser. The hydrostatic head of the riser decreases, the gas will expand and accelerate the aerated slug into the separator. This stage is called fast aerated liquid production. Finally, when the aerated liquid has been produced, the gas will flow out at a high velocity, causing a quick pressure reduction in the system. When the gas is expelled, the pressure reaches its minimum leading to the fallback of the remaining liquid. This is the gas blowdown stage. During the gas blowdown, the gas velocity in the pipeline upstream of the elbow increases. This leads to the generation of transient slugs in the pipeline and the cycle is repeated. The following features can also be concluded from Fig. 10.4(b):

- During the transient slugging, the liquid volume fraction in the riser increases about 54% quickly.

- Two sub-stages of the aerated slug growth stage are visible in the riser ΔP trace. The first sub-stage is between a time of 34 to 42 s, and the second sub-stage is between a time of 42 to 96 s.

- The pure liquid production stage, which implies a period of constant riser ΔP of 1.48 bar, does not exist. Instead, only the maximum riser ΔP of 1.48 bar is reached (a few small bubbles are still present in the riser, however, within the accuracy of the pressure measurements this value of 1.48 bar is obtained) and then the riser ΔP starts dropping immediately.

- The short hydrodynamic slugs generated during the gas blowdown are visible in the riser ΔP trace between a time of 106 to 120 s.
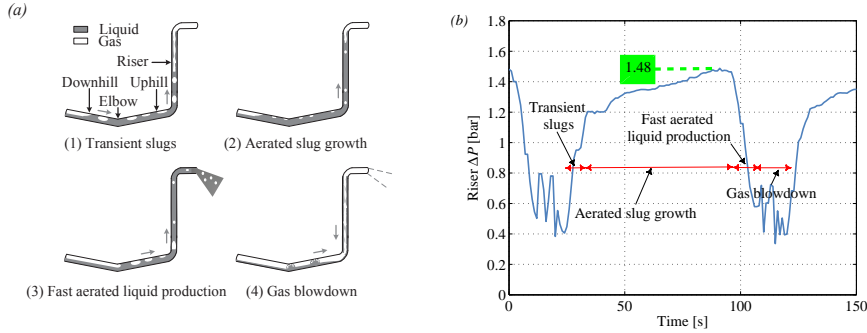
Figure 10.4: *Stages for severe slugging of type 3 (a) a graphical illustration (b) marked on a cycle of an experimental riser ΔP trace (U_{SL}=0.40 $m\,s^{-1}$ & U_{SG0}=1.01 $m\,s^{-1}$).*

10.3.5   Dual-Frequency Severe Slugging

Malekzadeh et al. (2011) observed and characterized this flow regime in a horizontal pipeline-riser system. This flow regime exhibits two distinctly different frequencies: high- and low-frequency fluctuations. It was visually observed that the high-frequency fluctuations are associated with the occurrence of severe slugging and unstable oscillations (each having their own characteristics). Also it was visually observed that the low-frequency oscillations are associated with the cyclic transition of the system between these two mentioned high-frequency states. The physics behind the low-frequency oscillations can be understood as follows. Imagine that the system starts to operate under unstable oscillations flow (the liquid content of the system is relatively low). However, the gas flow rate is not sufficient to maintain this flow regime. Thus, the liquid phase gradually accumulates in the system and consequently the system gradually moves towards the severe slugging state (the liquid content of the system is relatively high). The pressure upstream of the hilly-terrain unit follows the same trend and gradually increases. Neither the liquid flow rate is high enough to maintain severe slugging nor the pressure of the upstream gas is sufficient to blow out all the accumulated liquid from the system into the separator. However, this compressed upstream gas gradually expands and shifts the system back to unstable oscillations flow. These low-frequency fluctuations between the higher and the lower liquid content in the system create another level of instability to the system.

It is worth mentioning that severe slugging of type 2 (SS2) can occur in a downward inclined pipeline-riser system [see Malekzadeh et al. (2012)]. SS2 is qualitatively similar to SS1 and gives a full blockage of liquid at the riser base, but the riser base is generally penetrated by gas prior to the liquid filling the whole riser. Therefore, the slug length is shorter than the height of the riser.

10.4   Results and Discussions

Fig. 10.5(a) shows the flow map of the hilly-terrain pipeline-riser system generated based on our experimental data, indicating whether each point is in STB, USO, SS1, SS3 or DFSS regime. The design variables of a multiphase flow system such as pressure gradient, liquid holdup, heat- and mass-transfer coefficients, are dependent on the existing flow pattern [see Shoham (2006)]. Therefore, such a flow pattern map can be of help in design and operation phase in an offshore oil-production system.
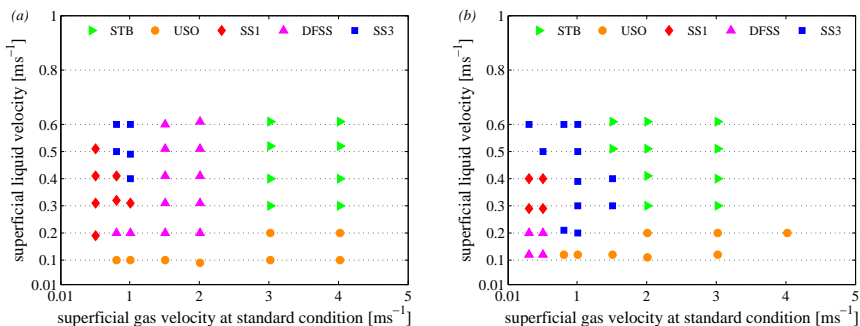

Figure 10.5: *Experimental flow pattern map of the system, indicating stable flow (STB), unstable oscillations (USO), severe slugging of type 1 (SS1), severe slugging of type 3 (SS3), and dual-frequency severe slugging (DFSS) corresponding to (a) 0.4 m^3 air buffer volume (b) 0.0 m^3 air buffer volume.*

Table 10.2 summarizes the considered experimental cases with their associated superficial liquid and gas velocities for DFSS, SS1, SS3, USO, and STB. The measured time period as well as the average maximum, minimum and amplitude of the riser ΔP are also given in Table 10.2. For the considered DFSS cases, two measured dominant periods associated with the low- and the high-frequency oscillations are given, respectively.

The uncertainty in the measured amplitude of the riser ΔP is less than 1%. U_{SG0} and U_{SL} are calculated from the measurements obtained by the thermal mass flow meter and by the electromagnetic flow meter, respectively. The uncertainties in the measured air and water inflow rates are less than 1%.

A Fast Fourier Transformation (FFT) was applied to obtain the frequency components in the riser ΔP traces of the considered experimental cases. The experimental periods mentioned in Table 10.2 were calculated from the corresponding amplitude spectra via the FFT of the riser ΔP traces, using the software MATLAB. The FFT built-in function in MATLAB uses several algorithms in combination, including a variation of Cooley-Tukey, a prime factor algorithm,

Table 10.2: *Experimental results of the period, the average maximum, minimum and amplitude of the riser ΔP for all cases corresponding to 0.4 m^3 air buffer volume. Colours distinguish different experimentally-observed flow regimes.*

Case	U_{SL} (ms^{-1})	U_{SG0} (ms^{-1})	Type	Period (s)	Max ΔP (bar)	Min ΔP (bar)	Amplitude of ΔP (bar)
1	0.20	0.81	DFSS	825&150	1.46	0.28	1.18
2	0.20	1.01	DFSS	650&150	1.46	0.28	1.18
3	0.20	1.51	DFSS	504&90	1.04	0.24	0.80
4	0.20	2.01	DFSS	460&69	0.90	0.20	0.70
5	0.31	1.51	DFSS	540&98	1.47	0.20	1.27
6	0.31	2.01	DFSS	432&77	1.42	0.20	1.22
7	0.41	1.51	DFSS	390&65	1.48	0.25	1.23
8	0.41	2.01	DFSS	408&73	1.41	0.25	1.16
9	0.51	1.51	DFSS	420&73	1.48	0.28	1.20
10	0.51	2.01	DFSS	405&60	1.39	0.24	1.15
11	0.60	1.51	DFSS	390&68	1.46	0.32	1.14
12	0.61	2.01	DFSS	436&57	1.33	0.27	1.06
13	0.19	0.51	SS1	200	1.48	0.37	1.11
14	0.31	0.51	SS1	150	1.48	0.42	1.06
15	0.32	0.81	SS1	120	1.48	0.34	1.14
16	0.31	1.01	SS1	109	1.48	0.30	1.18
17	0.41	0.51	SS1	133	1.48	0.46	1.02
18	0.41	0.81	SS1	109	1.48	0.37	1.11
19	0.51	0.51	SS1	115	1.48	0.58	0.90
20	0.40	1.01	SS3	99	1.48	0.37	1.11
21	0.50	0.81	SS3	100	1.48	0.45	1.03
22	0.49	1.01	SS3	88	1.48	0.38	1.10
23	0.60	0.81	SS3	87	1.48	0.40	1.08
24	0.60	1.01	SS3	83	1.48	0.40	1.08
25	0.10	0.81	USO	154	0.80	0.20	0.60
26	0.10	1.01	USO	145	0.80	0.20	0.60
27	0.10	1.51	USO	100	0.70	0.20	0.50
28	0.09	2.01	USO	80	0.60	0.20	0.40
29	0.10	3.02	USO	53	0.52	0.16	0.36
30	0.10	4.02	USO	120&48	0.52	0.18	0.34
31	0.20	3.02	USO	50	0.60	0.20	0.40
32	0.20	4.02	USO	39&10	0.57	0.20	0.37
33	0.30	3.02	STB	6&39	0.60	0.20	0.40
34	0.30	4.02	STB	4&5	0.60	0.20	0.40
35	0.40	3.02	STB	6&3	0.70	0.26	0.44
36	0.40	4.02	STB	5&4	0.72	0.20	0.52
37	0.52	3.02	STB	6&3	0.86	0.37	0.49
38	0.52	4.02	STB	5&3	0.87	0.27	0.60
39	0.61	3.02	STB	6&3	0.96	0.40	0.56
40	0.61	4.02	STB	5&3	0.97	0.37	0.60

and a split-radix algorithm. Note that the zero padding has not been applied to the data.

The time series of the riser ΔP corresponding to USO and STB cases are divided into smaller series (four time series or records). The resulting amplitude spectra via the FFT are averaged in order to reduce the influence of noise. A similar pattern in the amplitude spectrum was observed by applying different number of records, e.g. one and three records.

It can be observed from the experimental flow pattern map that at low liquid flow rates, unstable oscillations occur. Note that for most of the considered experimental USO cases mentioned in Table 10.2, one dominant frequency appeared.

However, there are two cases in which two dominant frequencies appeared. As an example of this, Fig. 10.6(a) shows the amplitude spectrum via the FFT corresponding to the riser ΔP trace of case 30 in Table 10.2 ($U_{SL} = 0.10$ m s^{-1} & $U_{SG0} = 4.02$ m s^{-1}), which gives two dominant frequencies for this USO case. Here, the number of recorded experimental data is 961. It can also be observed from the experimental flow pattern map that at relatively higher liquid flow rates, the flow regime changes from single-frequency to dual-frequency severe slugging and to hydrodynamic slug flow with the increase of U_{SG0} at constant U_{SL}. As an example, in Figs. 10.2(c), 10.7(a) and 10.7(b) the experimental riser ΔP traces of three cases corresponding to SS1 (relatively low gas flow rate, $U_{SG0} = 0.51$ m s^{-1}), DFSS (moderate gas flow rate, $U_{SG0} = 2.01$ m s^{-1}) and STB (relatively high gas flow rate, $U_{SG0} = 3.02$ m s^{-1}) at $U_{SL} \simeq 0.40$ m s^{-1} are shown.
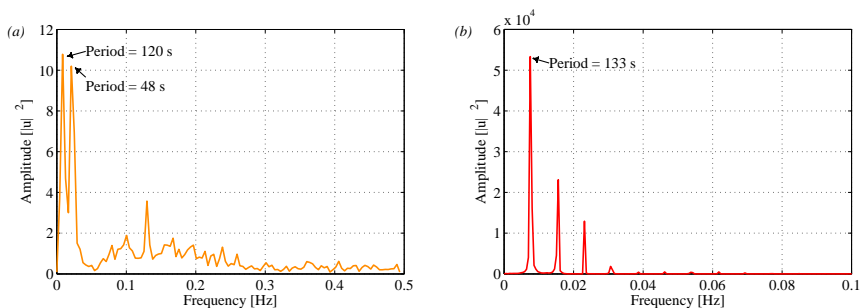
Figure 10.6: *FFT for different riser ΔP traces (a) USO (case 30, Table 10.2) (b) SS1 (case 17, Table 10.2).*
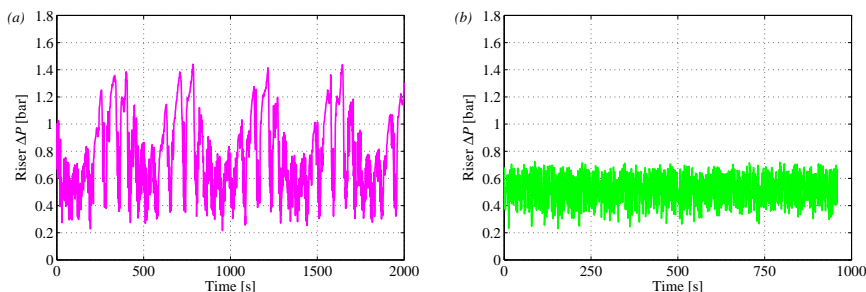

Figure 10.7: *Experimental riser ΔP traces (a) DFSS (case 8, Table 10.2) (b) STB (case 35, Table 10.2).*

It can be observed from Table 10.2 that for the considered experimental SS1 and SS3 cases a dominant frequency appeared. As an example of this behaviour, Fig. 10.6(b) shows the amplitude spectrum via the FFT corresponding to the riser ΔP trace of case 17 in Table 10.2 ($U_{SL} = 0.41$ m s^{-1} & $U_{SG0} = 0.51$ m s^{-1}), which gives a dominant frequency and the subsequent dominant time period can be determined. Here, the number of recorded experimental data is 1861. The experimental riser ΔP trace of this SS1 case was shown in Fig. 10.2(c). The riser ΔP traces of SS1 and SS3 are square-shaped signals. The Fourier transform of a square wave contains an infinite series of odd integer harmonics at diminishing amplitude. This can be observed in the amplitude spectrum of SS1 and SS3, see Fig. 10.6(b). The dual-frequency fluctuations can be clearly observed in the riser ΔP traces. As an example of this, Fig. 10.7(a) shows the riser ΔP trace of case 8 in Table 10.2 ($U_{SL} = 0.41$ m s^{-1} & $U_{SG0} = 2.01$ m s^{-1}). Fig. 10.8(a) depicts the amplitude spectrum via the FFT corresponding to the riser ΔP trace of this DFSS case, which gives two distinctly dominant frequencies. The measured periods of high- and low-frequency oscillations for this case are 73 s and 408 s, respectively. The number of recorded experimental data is 2041. It can also be observed from Table 10.2 that for the considered experimental STB cases two dominant frequencies reported. As an example of this, Fig. 10.8(b) shows the amplitude spectrum via the FFT corresponding to the riser ΔP trace of case 35 in Table 10.2 ($U_{SL} = 0.40$ m s^{-1} & $U_{SG0} = 3.02$ m s^{-1}), which does not show a dominant frequency. For this case two dominant periods are given. The experimental riser ΔP trace of this case is also shown in Fig. 10.7(b). The number of recorded experimental data is 961.
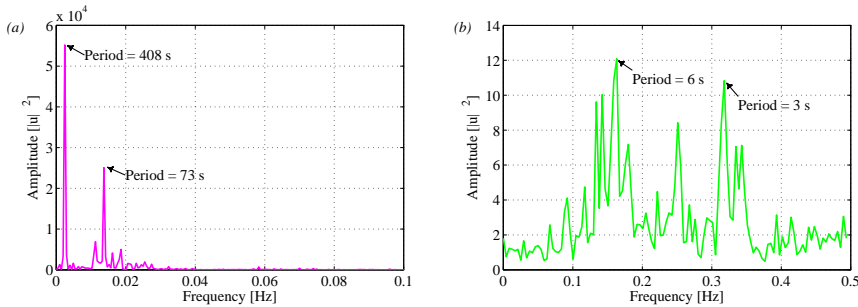

Figure 10.8: *FFT for different riser ΔP traces (a) DFSS (case 8, Table 10.2) (b) STB (case 35, Table 10.2).*

Fig. 10.9(a) shows the water outflow rate of severe slugging of type 1 corresponding to case 17 in Table 10.2 ($U_{SL} = 0.41$ m s^{-1} & $U_{SG0} = 0.51$ m s^{-1}). Here, the water and air inflow rates are constant and equal to 2.98 m^3 h^{-1} and 3.70 Sm^3 h^{-1}, respectively. There are periods of no water outflow (production
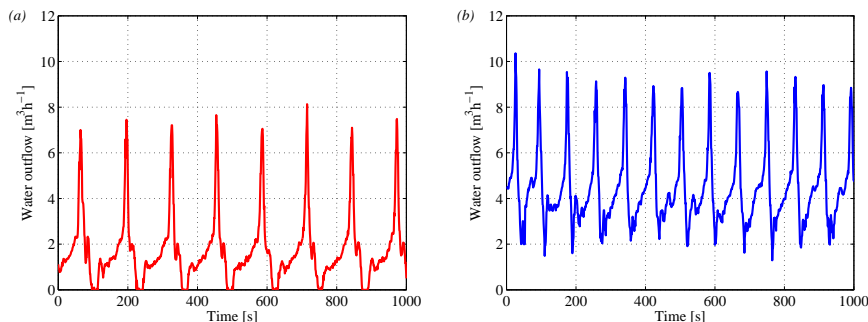
Figure 10.9: *Experimental water outflow traces (a) SS1 (case 17, Table 10.2) (b) SS3 (case 24, Table 10.2).*

starvation) followed by large peaks of water outflow of about 8 $m^3 h^{-1}$. The produced slug length is about 30 m. This large liquid outflow may cause overflow and consequently shutdown of the separator, which may have been designed based on the provided constant inflow rates. As expected, the time period of fluctuations in the water outflow (133 s) is the same as the one observed in the riser ΔP trace, Fig. 10.2(c). The water outflow rate of SS3 corresponding to case 24 in Table 10.2 ($U_{SL} = 0.60$ $m s^{-1}$ & $U_{SG0} = 1.01$ $m s^{-1}$), is shown in Fig. 10.9(b). Here, the water and air inflow rates are constant and equal to 4.36 $m^3 h^{-1}$ and 7.36 $Sm^3 h^{-1}$, respectively. As can be seen, the production starvation does not exist as water is continuously produced at the riser top. In each cycle of oscillations, the water outflow changes from a minimum of about 2 $m^3 h^{-1}$ to a maximum peak of about 10 $m^3 h^{-1}$. The produced slug length in each cycle of oscillations is about 47 m. The measured time period of fluctuations in the water outflow (83 s) is equal to that of the experimental riser ΔP trace of this case which is shown in Fig. 10.2(d).

10.5   Influence of the Effective Pipeline Length

As mentioned above, the gas buffer vessel was included in the experimental facility to achieve an extra compressibility by creating a virtually longer pipeline. All of the experiments mentioned in previous sections were conducted with the empty gas buffer vessel which gives 0.4 m^3 air buffer volume. This air buffer volume represents 197 m extra effective length of the 50.8 mm diameter pipeline; this extra length, however, does not contain any liquid holdup.

To assess the impact of this effective length of the pipeline on the characteristics of the flow instabilities occurring in the hilly-terrain pipeline-riser system,

experiments were also conducted with the gas buffer vessel fully filled with water which gives zero air buffer volume.

An experimental matrix was defined to cover all possible flow regimes occurring in the test loop. The water flow rate ranges from 0.84 $m^3 h^{-1}$ to 4.46 $m^3 h^{-1}$ and the air flow rate from 2.23 $Sm^3 h^{-1}$ to 29.36 $Sm^3 h^{-1}$. The corresponding U_{SL} ranges from 0.11 - 0.61 $m s^{-1}$ and U_{SG0} ranges from 0.31 - 4.02 $m s^{-1}$. All of the flow regimes which have been obtained with 0.4 m^3 air buffer volume were also observed with zero air buffer volume. Fig. 10.5(b) shows the experimental flow map of the hilly-terrain pipeline-riser system with zero air buffer volume, indicating whether each point is in STB, USO, SS1, SS3 or DFSS regime. The considered experimental cases with their associated superficial liquid and gas velocities are summarized in Table 10.3. The measured time period as well as the average maximum, minimum and amplitude of the riser ΔP are also given in Table 10.3.

As can be seen in Figs. 10.5(a) and 10.5(b), similar flow patterns were observed with 0.4 m^3 and with zero air buffer volume. However, the severe slugging region in the flow pattern map strongly depends on air buffer volume (compressibility of the upstream part of the elbow). The unstable area associated with severe slugging of type 1 reduced as air buffer volume decreased from 0.4 m^3 to zero. A similar trend is observed for dual-frequency severe slugging. However, the unstable area associated with severe slugging of type 3 expanded as the air buffer volume decreased. All these three unstable areas can be combined together to form one severe slugging envelope. This severe slugging envelope reduced as the air buffer volume decreased.

10.6   Impact of the Hilly-Terrain Unit

The experimental set-up described in the Experimental Facility section was also used to study flow instabilities in a downward inclined pipeline-riser system (Malekzadeh et al. 2012) and in a horizontal pipeline-riser system (Malekzadeh et al. 2011). In the downward inclined pipeline-riser system severe slugging of type 1, 2 and 3 were observed (Fig. 10.10(a)), whereas in the horizontal pipeline-riser system severe slugging of type 3 and dual-frequency severe slugging were observed (Fig. 10.10(b)). Here, it is confirmed that a low spot in the pipeline, e.g. a hilly-terrain unit, is necessary for the formation of severe slugging of type 1. However, the characteristics of severe slugging of type 1 in the hilly-terrain pipeline-riser system are different from that in the downward inclined pipeline-riser system, e.g. generation of short transient slugs at the elbow during the gas blowdown stage and formation of two sub-stages during the slug growth stage.

As can be seen in Figs. 10.5(a), 10.10(a) and 10.10(b), the size of the severe slugging envelope in the flow pattern map hardly changed as the horizontal pipeline was replaced by the hilly-terrain unit. However, the downward inclined pipeline formed a larger severe slugging envelope even with a small air buffer

Table 10.3: *Experimental results of the period, the average maximum, minimum and amplitude of the riser ΔP for all cases corresponding to 0.0 m^3 air buffer volume. Colours distinguish different experimentally-observed flow regimes.*

Case	U_{SL} (ms^{-1})	U_{SG0} (ms^{-1})	Type	Period (s)	Max ΔP (bar)	Min ΔP (bar)	Amplitude of ΔP (bar)
1	0.12	0.31	DFSS	300&37	1.04	0.49	0.55
2	0.12	0.51	DFSS	120&29	0.88	0.32	0.56
3	0.20	0.31	DFSS	192&36	1.26	0.71	0.55
4	0.20	0.51	DFSS	137&28	1.19	0.42	0.77
5	0.29	0.31	SS1	144	1.48	0.65	0.83
6	0.29	0.51	SS1	120	1.48	0.48	1.00
7	0.40	0.31	SS1	120	1.48	0.79	0.69
8	0.40	0.51	SS1	107	1.48	0.79	0.69
9	0.21	0.81	SS3	120	1.41	0.33	1.08
10	0.20	1.01	SS3	112	1.28	0.27	1.01
11	0.30	1.01	SS3	90	1.44	0.32	1.12
12	0.30	1.51	SS3	72	1.11	0.30	0.81
13	0.39	1.01	SS3	87	1.44	0.39	1.05
14	0.40	1.51	SS3	64	1.25	0.35	0.90
15	0.50	0.51	SS3	103	1.44	0.67	0.77
16	0.50	1.01	SS3	80	1.47	0.42	1.05
17	0.60	0.31	SS3	120	1.44	0.97	0.47
18	0.60	0.81	SS3	80	1.43	0.58	0.85
19	0.60	1.01	SS3	72	1.43	0.54	0.89
20	0.12	0.81	USO	120	0.87	0.29	0.58
21	0.12	1.01	USO	120	0.88	0.24	0.64
22	0.12	1.51	USO	90	0.84	0.15	0.69
23	0.11	2.01	USO	73	0.69	0.17	0.52
24	0.12	3.02	USO	44	0.58	0.19	0.39
25	0.20	2.01	USO	56	0.66	0.25	0.41
26	0.20	3.02	USO	42&7	0.58	0.21	0.37
27	0.20	4.02	USO	40&6	0.57	0.19	0.38
28	0.30	2.01	STB	55&12	0.68	0.30	0.38
29	0.30	3.02	STB	6&3	0.59	0.20	0.39
30	0.41	2.01	STB	4&5	0.73	0.39	0.34
31	0.40	3.02	STB	6&4	0.71	0.25	0.46
32	0.51	1.51	STB	16&60	0.97	0.51	0.46
33	0.51	2.01	STB	4&3	0.85	0.46	0.39
34	0.51	3.02	STB	3&7	0.84	0.36	0.48
35	0.61	1.51	STB	3&66	1.03	0.60	0.43
36	0.61	2.01	STB	4&3	0.97	0.54	0.43
37	0.61	3.02	STB	3&7	0.95	0.40	0.55

volume (0.25 m^3).

As an example, at constant $U_{SL} \simeq 0.31$ m s^{-1} & $U_{SG0} = 1.01$ m s^{-1} and equal air buffer volume of 0.4 m^3, the hilly-terrain pipeline-riser system exhibited severe slugging of type 1 with a measured period of 109 s and a produced slug length of about 30 m, whereas the horizontal pipeline-riser system exhibited severe slugging of type 3 with a slightly shorter period of 95 s and a produced slug length of about 24 m. At higher superficial liquid velocity ($U_{SL} \simeq 0.40$ m s^{-1} & $U_{SG0} \simeq 1.00$ m s^{-1}), the hilly-terrain pipeline-riser system exhibited severe slugging of type 3 with a measured period of 99 s and a produced slug length of about 40 m, whereas the downward inclined pipeline-riser system exhibited severe slugging of type 1 with a measured period of 109 s and a produced slug length of about 42 m even with a smaller air buffer volume (0.25 m^3).
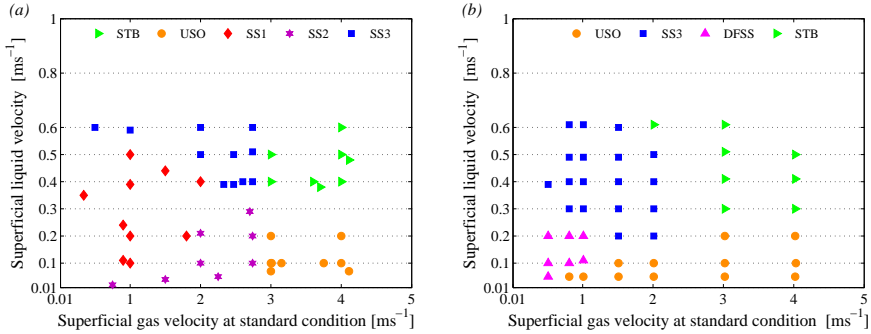
Figure 10.10: *Experimental flow pattern map, indicating stable flow (STB), unstable oscillations (USO), severe slugging of type 1 (SS1), severe slugging of type 2 (SS2), severe slugging of type 3 (SS3), and dual-frequency severe slugging (DFSS) corresponding to (a) downward inclined pipeline-riser system with 0.25 m^3 air buffer volume (b) horizontal pipeline-riser system with 0.4 m^3 air buffer volume.*

10.7   Conclusions

Flow instabilities in a hilly-terrain pipeline-riser system during two-phase gas-liquid flow were investigated experimentally. The observed flow regimes were classified into five categories: stable flow (characterized by hydrodynamic slugs initiated in the horizontal pipeline upstream of the hilly-terrain unit and also in the elbow of the hilly-terrain unit), unstable oscillations (exhibiting cyclic, low amplitude pressure fluctuations), severe slugging of type 1 (characterized by a full production starvation and a pure liquid slug length larger than the riser height), severe slugging of type 3 (characterized by a growing long aerated liquid slug in the riser followed by the gas blowdown stage), and dual-frequency severe slugging characterized by two distinctly different frequencies; the high-frequency fluctuations are related to the process of severe slugging and unstable oscillations, and the low-frequency fluctuations are related to the gradual cyclic transition between these two mentioned meta-stable states.

During the process of severe slugging of type 1, transient slugs generate in the pipeline upstream of the hilly-terrain unit and effectively contribute to the initial blockage of the elbow. In the process of severe slugging of type 3, these transient slugs create a local flow reversal of liquid and gas at the elbow and generate a long aerated liquid slug. It was also observed that the slug growth stage consists of two sub-stages, namely the slug growth in the uphill section and the slug growth in the riser.

Moreover, the existence of a hilly-terrain unit in a pipeline-riser system induces a more severe type of slugging, i.e. severe slugging of type 1, which exhibits longer

slugs than that of a horizontal pipeline-riser system.

Nomenclature

g = gravitational acceleration, Lt^2, ms^{-2}
H = riser length, L, m
K_v= flow factor, $\text{L}^{7/2}\text{m}^{-1/2}$, $\text{m}^3\,\text{h}^{-1}\,\text{bar}^{-1/2}$
L = pipeline length, L, m
P = pressure, m/Lt^2, bar
P_0 = atmospheric pressure, m/Lt^2, bar
T = period, t, s
α = void fraction
Δ = difference
U_{SG0} = superficial air velocity at standard conditions, L/t, $\text{m\,s}^{-1}$
U_{SL} = superficial water velocity, L/t, $\text{m\,s}^{-1}$
Π_{ss} = severe-slugging group
ρ_l = liquid density, m/L^3, kgm^{-3}

Acknowledgements

References

Baliño, J. L., Burr, K. P., and Nemoto, R. H. 2010. Modeling and simulation of severe slugging in air-water pipeline-riser systems. *Int. J. Multiphase Flow* **36**(8): 643-660. doi: 10.1016/j.ijmultiphaseflow.2010.04.003.

Bøe, A. 1981. Severe slugging characteristics; part 1: Flow regime for severe slugging; part 2: Point model simulation study. Presented at Selected Topics in Two-Phase Flow, Trondheim, Norway.

Denney, D. 2003. "Self-lifting" method to eliminate severe slugging in offshore production systems. *J. Pet Tech* **55**(12): 36-37.

Fabre, J., Peresson, L., Corteville, J., Odello, R., and Bourgeols, T. 1990. Severe slugging in pipeline/riser systems. *SPE Prod Eng* **5**(3): 299-305. SPE-16846-PA. doi: 10.2118/16846-PA.

Farghaly, M.A. 1987. Study of Severe Slugging in Real Offshore Pipeline Riser-Pipe System. Paper SPE 15726 presented at the SPE Middle East Oil Show, Bahrain, 7-10 March. doi: 10.2118/15726-MS.

Havre, K., and Dalsmo, M. 2002. Active feedback control as a solution to severe slugging. *SPE Prod & Fac* **17**(3): 138-148. SPE-79252-PA. doi: 10.2118/79252-PA.

Jansen, F., Shoham, O., and Taitel, Y. 1996. The elimination of severe slugging experiment and modeling. *Int. J. Multiphase Flow* **22**(6): 1055-1072. doi: 10.1016/0301-9322(96)00027-4.

Malekzadeh, R., Henkes, R.A.W.M., and Mudde, R.F. 2012. Severe Slugging in a Long Pipeline-Riser System: Experiments and Predictions. *Int. J. Multiphase Flow* **46**(C): 9-21. doi: 10.1016/j.ijmultiphaseflow.2012.06.004.

Malekzadeh, R., Mudde, R.F., and Henkes, R.A.W.M. In press. Experimental and Numerical Investigation of Severe Slugging in Horizontal Pipeline-Riser Systems. *Int. J. Multiphase Flow* (submitted December, 2011).

Mokhatab, S., Towler, B., and Purewal, S. 2007. A review of current technologies for severe slugging remediation. *Petroleum Science & Tech. J.* **25**(10): 1235-1245. doi: 10.1080/10916460500423320.

Petalas, N., and Aziz, K. 2000. A mechanistic model for multiphase flow in pipes. *J. of Canadian Petroleum Technology* **39**(6): 43-55.

Pots, B., Bromilow, I., and Konijn, M. 1987. Severe slug flow in offshore flowline/riser systems. *SPE Prod Eng* **2**(4): 319-324. SPE-13723-PA. doi: 10.2118/13723-PA.

Santana, B.W., Fetzner, D.J., Edwards, N.W., and Haupt, R.W. 1993. Program for Improving Multiphase Flow Slug Force Resistance at Kuparuk River Unit Processing Facilities. Paper SPE 26104 presented at the SPE Western Regional Meeting, Anchorage, Alaska, 26-28 May. doi: 10.2118/26104-MS.

Sarica, C., and Shoham, O. 1991. A simplified transient model for pipeline-riser systems. *Chemical Engineering Science* **46**(9): 2167-2179. doi: 10.1016/0009-2509(91)85118-H.

Schmidt, Z., Doty, D.R., and Dutta-Roy, K. 1985. Severe Slugging in Offshore Pipeline-Riser Pipe Systems. *SPE J.* **25**(1): 27-38. SPE-12334-PA. doi: 10.2118/12334-PA.

Schmidt, Z., Brill, J., and Beggs, H. 1980. Experimental study of severe slugging in a two-phase-flow pipeline-riser pipe system. *SPE J.* **20**(5): 407-414. SPE-8306-PA. doi: 10.2118/8306-PA.

Shoham, O. 2006. *Mechanistic Modeling of Gas-Liquid Two-Phase Flow in Pipes.* Richardson, Texas, SPE.

Taitel, Y. 1986. Stability of severe slugging. *Int. J. Multiphase Flow* **12**(2): 203-217. doi: 10.1016/0301-9322(86)90026-1.

Taitel, Y., Vierkandt, S., Shoham, O., and Brill, J. 1990. Severe slugging in a riser system: experiments and modeling. *Int. J. Multiphase Flow* **16**(1): 57-68. doi: 10.1016/0301-9322(90)90037-J.

Tengesdal, J., Sarica, C., and Thompson, L. 2003. Severe slugging attenuation for deepwater multiphase pipeline and riser systems. *SPE Prod & Fac* **18**(4): 269-279. SPE-87089-PA. doi: 10.2118/87089-PA.

Yocum, B. 1973. Offshore Riser Slug Flow Avoidance: Mathematical Models for Design and Optimization. Paper SPE 4312 presented at the SPE European Meeting, London, United Kingdom, 2-3 April. doi: 10.2118/4312-MS.

Zhang, H.-Q., Al-Safran, E.M., Jayawardena, S.S., Redus, C.L., Sarica, C., and Brill, J.P. 2003. Modeling of Slug Dissipation and Generation in Gas-Liquid Hilly-Terrain Pipe Flow. *ASME J. Energy Resour. Technol.* **125**(3): 161-168. doi: 10.1151/1.1580847.

Reza Malekzadeh (MSc) is currently a PhD student in the Department of Multi-Scale Physics, Delft University of Technology. E-mail: rezamalekzadeh@gmail.com. Reza received his MSc in petroleum engineering from Delft University of Technology in 2005. He worked with National Iranian Oil Company as a senior reservoir engineer before pursuing his PhD in 2008. **Ruud A. W. M. Henkes** (PhD) is a professor of multiphase flow in the Department of Multi-Scale Physics, Delft University of Technology. He also is the principal technical expert of fluid flow at Shell Technology Centre Amsterdam. **Robert F. Mudde** (PhD) is a professor of multiphase flow and the head of the Department of Multi-Scale Physics, Delft University of Technology.

Chapter 11

Epilogue

The purpose of this chapter is to focus more on practical applications by putting some of our main findings and their implications in a broader perspective, and is not just to provide a summary of the conclusions of the preceding chapters.

11.1 Sand production

In Chapter 5, we have shown that severe slugging may occur at the bottom of an extended reach well and would cause a large-amplitude flowing bottom hole pressure fluctuations. The drawdown pressure, i.e. the difference between the volumetric-average reservoir pressure and the flowing pressure at the bottom of the well, induces rock failure near the well region and can cause sand production[1,2].

Sand production may cause pipelines and surface equipment such as separators to be easily eroded and worn out in a relatively short period of time and would results in expensive repair costs[2]. Furthermore, sand deposition in pipelines and separators often leads to excessive operating costs and well suspension[3].

One strategy in the sand control and management is to evaluate the critical drawdown pressure below which sands would not produce[2,4,5]. However, in the process of severe slugging, during the gas blowdown stage, the flowing bottom hole pressure reaches its minimum leading to a large drawdown pressure. As a result, the drawdown pressure may exceed the critical drawdown pressure and can cause sand production. Therefore, accurate prediction of the severe slugging characteristics at the bottom of the well, especially the flowing bottom hole pressure, is crucial in the sand control and management strategy.

11.2   Gannet field data

In Chapter 6, we have presented a transient drift flux model to predict the severe slugging characteristics in a pipeline-riser system. The model was tested against experimental data of air-water two-phase flow in a laboratory scale pipeline-riser system and predicted all the major features of the data. We now show that the slip model published by Shi et al. [6], which was implemented in our drift flux model, can also be used to simulate the severe slugging phenomenon in a real offshore oil and gas pipeline-riser system.

We have also implemented the slip model published by Shi et al. [6] in Compas (Shell's in-house transient one-dimensional drift flux model). Compas is a drift flux model which uses a different set of slip models taking into account the different flow regimes. Thus, during the simulation, the flow regime should be delineated in advance, thereafter, the slip model associated with the predicted flow regime is used for the calculations of the flow variables.

Here, we compare the predictions of modified Compas, all the built-in flow-regime-dependent slip models were replaced by the slip model published by Shi et al. [6], with the available filed data for the Shell Gannet pipeline-riser system in the North Sea (see Seim et al. [7]). It comprises an undulating near-horizontal subsea pipeline of about 15 km in length, followed by a 119 m high vertical riser, see Fig. 11.1. The internal diameter of the pipe is 0.1012 m. The pressure at the top of the riser is 19 bara. The conditions and geometry data used in the simulations, are given in Table 11.1.
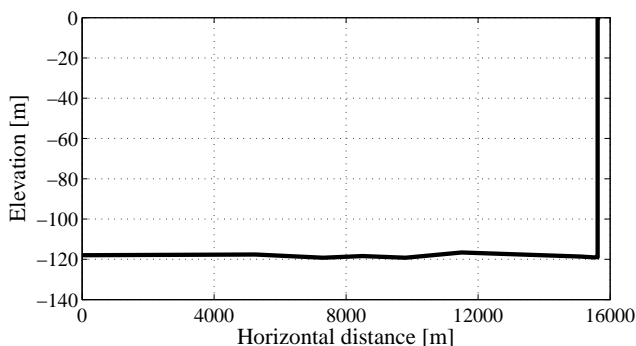
Figure 11.1: *Geometry description of the Shell Gannet pipeline-riser system. x=0 corresponds to the inlet of the system.*

Fig. 11.2 shows the comparison between the modified Compas and OLGA in predicting the measured pressure at the inlet of the pipeline. Results for the oil outflow rate at the top of the riser is shown in Fig. 11.3. As can be seen, both models predict the periodic flow behaviour associated with the process of severe slugging. Fig. 11.3 depicts that there are periods of no oil outflow at the riser

Table 11.1: *Definition of Gannet field data*

Pipe geometry	Configuration	Near-horizontal and vertical
	Length	15 km (near-h.) and 119 m (v.)
	Diameter	0.1012 m
Transient scenario	Inlet gas flowrate	0.077813 kg/s
	Inlet liquid flowrate	0.954187 kg/s
	Outlet pressure	19 bar
Fluid properties at 19 bara & 21°C	Composition	Oil and gas
	Gas density	17.2 kg/m^3
	Liquid density	719.9 kg/m^3
	Gas viscosity	1.2 10^{-5} Pa.s
	Liquid viscosity	61.2 10^{-3} Pa.s
	Surface tension	0.0205 N/m

top (production starvation) followed by large peaks of oil outflow. Therefore, this is severe slugging of type 1. The produced slug volume is about 8 m^3, which corresponds to the produced slug length of about 1 km.

The measured time period of a cycle is about 1.9 hours. The OLGA model gives a slightly higher value of about 2.5 hours, whereas the modified Compas predicts a slightly lower value of about 1.6 hours, which is reasonably close to the measured value in comparison with the OLGA predictions.
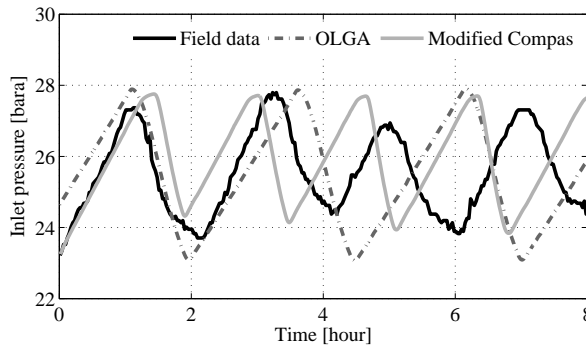
Figure 11.2: *Measured and predicted inlet pressure during the process of severe slugging in the Gannet pipeline-riser system in the North Sea.*

11.3   Final remarks

In Chapter 7, we have presented a modified stability criterion for the prediction of the flow behaviour in the pipeline-riser system. This criterion can be used as a
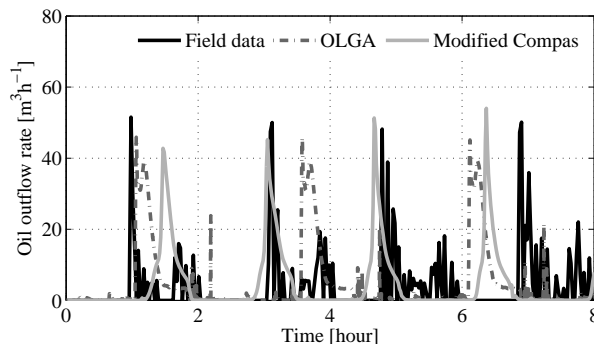
Figure 11.3: *Measured and predicted oil outflow rate during the process of severe slugging in the Gannet pipeline-riser system in the North Sea.*

check in the early design phase of the pipeline-riser systems. However, a transient multiphase flow simulator is recommended in the detailed design phase.

It would be interesting to further test the performance of the modified stability criterion against experimental data for severe slugging in pipeline-riser systems equipped with a choke at the riser top.

In Chapters 7-10, we have shown that the occurrence of severe slugging is not limited to a downward inclined pipeline-riser system, and it may even in a horizontal pipeline-riser system. However, a downward inclined section upstream of the riser base is necessary for the formation of severe slugging of type 1. In the design of a pipeline-riser system, one should know that preventing a low spot in the pipeline by removing the hilly-terrain units or downward inclined sections in the pipeline may alleviate severe slugging but does not guarantee that severe slugging does not occur in the horizontal pipeline-riser system.

Furthermore, a new class of severe slugging was found and referred to as dual-frequency severe slugging, which exhibits flow instability with two distinctly different frequencies. Knowing that the low-frequency oscillations associated with dual-frequency severe slugging is related to the dynamics of gas-liquid flow in the pipeline-riser system, would help operators of an offshore oil and gas production facility to realize that this instability may not be related to the inflow of oil and gas from the reservoir into the wellbore, and consequently would prevent unnecessary production tests.

It would be interesting to further study the physics behind the dual-frequency severe slugging. Applying a sophisticated numerical simulation method, e.g. the volume of fluid method, might be beneficial.

References

[1] L.Y. Chin and G.G. Ramos. Predicting Volumetric Sand Production in Weak Reservoirs. Paper SPE/ISRM 78169 presented at the SPE/ISRM Rock Mechanics Conference, Irving, Texas, 20 - 23 October 2002.

[2] T. Oshita, S. Hirokawa, A. Aziz, and Y. Rammah. Integrated Approach for Sand Management: Field Application to an Offshore Oil Field. Paper SPE 37767 presented at the SPE Middle East Oil Show and Conference, Bahrain, 15 - 18 March 1997.

[3] G. E. Smith. Fluid Flow and Sand Production in Heavy-Oil Reservoirs Under Solution-Gas Drive. *SPE Production Eng. J.*, 3(2):169-180, 1988.

[4] S. Ong, R. Ramos, and Z. Zheng. Sand Production Prediction in High Rate, Perforated and Open-hole Gas Wells. Paper SPE 58721 presented at the SPE International Symposium on Formation Damage Control, Lafayette, Louisiana, 23 - 24 February 2000.

[5] J. Bellarby. *Well completion design*, volume 56 of *Development in petroleum science*. Elsevier B.V., Amsterdam, The Netherlands, 2009.

[6] H. Shi, J. Holmes, L. Durlofsky, K. Aziz, L. Diaz, B. Alkaya, and G. Oddie. Drift-flux modeling of two-phase flow in wellbores. *SPE J.*, 10(1):24-33, 2005.

[7] J.E. Seim, V.L. van Beusekom, R.A.W.M. Henkes, and O.J. Nydal. Experiments and modelling for the control of riser instabilities with gas lift. Presented at 15th International Conference on Multiphase Production Technology, Cannes, France, 15-17 June, 2011.

List of publications

Papers

[1] R. Malekzadeh, S.P.C. Belfroid and R.F. Mudde. Transient drift flux modelling of severe slugging in pipeline-riser systems. *International Journal of Multiphase Flow*, 46(C):32-37, 2012, doi: 10.1016/j.ijmultiphaseflow.2012.06.005.

[2] R. Malekzadeh, R.A.W.M. Henkes and R.F. Mudde. Severe slugging in a long pipeline-riser system: Experiments and predictions. *International Journal of Multiphase Flow*, 46(C):9-21, 2012, doi: 10.1016/j.ijmultiphaseflow.2012.06.004.

[3] R. Malekzadeh, R.F. Mudde and R.A.W.M. Henkes. Experimental and Numerical Investigation of Severe Slugging in Horizontal Pipeline-Riser Systems. *International Journal of Multiphase Flow*, submitted.

[4] R. Malekzadeh, R.F. Mudde and R.A.W.M. Henkes. Dual-Frequency Severe Slugging in Horizontal Pipeline-Riser Systems. *Journal of Fluids Engineering-Transactions of the ASME*, submitted.

[5] R. Malekzadeh, R.A.W.M. Henkes and R.F. Mudde. Experimental Study of Flow Instabilities in a Hilly-Terrain Pipeline-Riser System. *SPE Journal*, Accepted.

Proceedings

[1] R. Malekzadeh, R.A.W.M. Henkes and R.F. Mudde. Dependence of Severe Slugging on the Orientation Angle of the Pipeline Upstream of the Riser

Base. Presented at 8th North American Conference on Multiphase Techno-logy, Banff, Canada, 20 - 22 June 2012.

[2] R. Malekzadeh and R.F. Mudde. A Modelling Study of Severe Slugging in Wellbore. Paper SPE 150364 presented at the SPE North Africa Technical Conference and Exhibition, Cairo, Egypt, 20 - 22 February 2012, doi: 10.2118/150364-MS.

[3] R. Malekzadeh, R.F. Mudde, S. Belfroid and W. Schiferli. Transient Drift Flux Modeling of Severe Slugging in Pipeline-Riser Systems. Presented at 7th International Conference on Multiphase Flow, ICMF 2010, Tampa, FL, May 30 - June 4, 2010.

Acknowledgements

I would like to express my appreciation to the members of the dissertation committee: Prof. ir. K.C.A.M. Luyben, chairman; Prof. dr. R.F. Mudde; Prof. dr. ir. R.A.W.M. Henkes; Prof. dr. B.J. Azzopardi; Prof. dr. O.J. Nydal; Prof. dr. ir. J.D. Jansen; Prof. dr. ir. H.W.M. Hoeijmakers; Prof. dr. ir. H.E.A. van den Akker; and Prof. dr. ir. C.R. Kleijn.

My deep and endless gratitude goes to my supervisors: Rob and Ruud. Rob, I am really in debt to you for having me as your student at the Department of Multi-Scale Physics, which unfortunately does not exist anymore. You made me to grow as a scientist. You are a life teacher in addition to being a supervisor. Your lessons: way of dealing with people, and how to be a goal-oriented person were extremely beneficial and will not be forgotten. Moreover, I admire your constructive way of criticizing my presentations and papers. The lessons are well learned and are clearly visible. Ruud, you are truly a sustainable source of energy and drive, continuous help and encouragement. I have been fortunate to get you involved in my research. I am also extremely thankful to you for inviting me as a research intern at Shell Technology Centre Amsterdam to use the experimental flow facility to conduct the experiments. I am also thankful to Jan Dirk Jansen for his involvement in the early stage of this project. His cooperation and recommendations are deeply appreciated.

Thanks are due to Vincent van Beusekom for the operator training with the experimental flow facility, to Daniele Baroni for his help in the modification of the test loop and dealing with technicians, to Rutger Ijzermans and Sebastiaan Olijerhoek for their helps in the numerical simulations with Compas and programming in C++, and to the rest of the multiphase flow team of Shell for the open and inspiring working environment.

I am thankful to Stefan Belfroid, Garrelt Alberts and Wouter Schiferli from TNO for their insightful ideas and valuable feedbacks on the numerical modelling.

I would like to thank Scandpower Petroleum Technology and in particular,

Curriculum Vitae

Reza Malekzadeh was born in September 26, 1979 in Ghaemshahr, Iran. In 2002 he obtained the B.Sc. degree in Mining Engineering at Isfahan University of Technology in Iran. Reza received his M.Sc. degree in Petroleum Engineering from the Faculty of Civil Engineering and Geosciences, Delft University of technology, The Netherlands in 2005. He worked with National Iranian Oil Company as a senior reservoir engineer before pursuing his Ph.D. in July 2008 at the Department of Multi-Scale Physics, Faculty of Applied Sciences, Delft University of Technology.